

Synaptic Plasticity and Behavior Profiles of Ventral Tegmental Area Inhibitory Circuits

by

Robyn M. St. Laurent

B.A. Colby College, 2012

A dissertation submitted in partial fulfillment of the requirements for the Degree of Doctor of
Philosophy in the Department of Neuroscience at Brown University

Providence, Rhode Island
May 2019

© 2019 by Robyn M. St. Laurent

This dissertation by Robyn M. St. Laurent is accepted in its present form by the Department of Neuroscience as satisfying the dissertation requirement for the degree of Doctor of Philosophy.

Date _____
_____ Dr. Julie Kauer, Advisor

Recommended to the Graduate Council

Date _____
_____ Dr. Barry Connors, Reader

Date _____
_____ Dr. Christopher Moore, Reader

Date _____
_____ Dr. Christopher McBain, Reader

Approved by the Graduate Council

Date _____
_____ Dr. Andrew G. Campbell
Dean of the Graduate School
Brown University

CURRICULUM VITAE

EDUCATION

Neuroscience Graduate Program, Brown University (Providence, RI)

Doctor of Philosophy expected May 2019

Advisor: Julie Kauer

Colby College (Waterville, ME)

Bachelor of Arts – May 2012

GPA: 3.69, *cum laude*, distinction in the major: Psychology - Neuroscience concentration

PUBLICATIONS

[in preparation] **St. Laurent R.** & Kauer, J.A. *Synaptic plasticity at inhibitory synapses in the ventral tegmental area depends upon stimulation site*

[in revision] **St. Laurent R.**, Tsuda A.C., Kauer J.A. *Periaqueductal gray and rostromedial tegmental inhibitory afferents to the ventral tegmental area have distinct plasticity and opiate sensitivity*

Pradier, B., Shin, H. B., Kim, D. S., **St. Laurent, R.**, Lipscombe, D., & Kauer, J. A. (2018). Long-term depression induced by optogenetically driven nociceptive inputs to trigeminal nucleus caudalis or headache triggers. Journal of Neuroscience, 38(34), 7529-7540. doi:10.1523/jneurosci.3032-17.2018

Bossert JM, Adhikary S, **St. Laurent R**, Marchant NJ, Wang HL, Morales M, Shaham Y. (2016) Role of projections from ventral subiculum to nucleus accumbens shell in context-induced reinstatement of heroin seeking in rats. Psychopharmacology (Berl) 233(10): 1991-2004. PMID 26344108

Micioni Di B mV, Ciccocioppo R, Romano A, Bossert JM, Rice KC, Ubaldia M, **St. Laurent R**, Gaetani S, Massi M, Shaham Y, Cifani C (2014) Role of BNST CRF receptors in tantalization stress-induced binge-like palatable food consumption in female rats with a history of food restriction. Journal of Neuroscience 34(34):11316-24. PMID 25143612

LaRoche DP, Marques NR, Shumila HN, Logan CR, **St. Laurent R**, Gonçalves M (2014) Excess body weight and gait influence energy cost of walking in older adults. Medicine & Science in Sports & Exercise: PMID 25202852.

St Laurent R, O'Brien LM, Ahmad ST (2013) Sodium butyrate improves locomotor impairment and early mortality in a rotenone-induced *Drosophila* model of Parkinson's disease. Neuroscience 246:382-390. PMID 23623990

St Laurent R, Helm SR, Glenn MJ (2013) Reduced cocaine-seeking behavior in heterozygous BDNF knockout rats. Neuroscience Letters 544:94-99. PMID 23583595

Theberge FR, Li A, Kambhampati S, Pickens, CL, **St Laurent R**, Bossert JM, Baumann MH, Hutchinson MR, Rice RC, Watkins LR, Shaham Y (2013) Effect of chronic delivery of the Toll-like receptor 4 antagonist (+)-Naltrexone on incubation of heroin craving. Biological Psychiatry 73:729-737. PMID 23384483

HONORS & AWARDS

Graduate:

Brown University Chapter of the Society of Sigma Xi, Full Member 2018-present
Winter Conference on Brain Research Travel Fellow 2018
Best Graduate student poster at Winter Conference on Brain Research 2018
Ruth L. Kirschstein National Research Service Award: F31DA045419
 "Novel Opioid-Sensitive Inhibitory Long-Term Potentiation"
Honorable mention 2015 National Science Foundation Graduate Research Fellowship Program
Honorable mention 2014 National Science Foundation Graduate Research Fellowship Program
Sidney Frank Fellowship (2014) awarded by Division of Biology & Medicine at Brown University

Postbaccalaureate and Undergraduate:

Outstanding poster award at 2014 NIH Post-Baccalaureate Poster Day
Outstanding poster award at 2014 NIDA Poster and Mentoring Awards Day
William D. Adams Presidential Scholar at Colby College (2008-2012)
2009 NEIAAA Track & Field All New England Team
2009 Track & Field All New England Team Division III
New England Small College Athletic Conference All-Academic Team: 2010, 2011, 2012

PRIOR RESEARCH EXPERIENCE

Postbaccalaureate Intramural Research Training Award
National Institute on Drug Abuse (NIDA), Baltimore, MD Oct. 2012 – June 2014
Mapped neurocircuitry involved in context-induced relapse in rodent models of heroin seeking under the mentorship of Dr. Jennifer Bossert and Dr. Yavin Shaham

Collaborative Research in Neural Plasticity & Behavior, *Colby College* ... Sept. 2011 – May 2012
Investigated the role of brain-derived neurotrophic factor (BDNF) in cocaine addiction and relapse in rats using a conditioned place preference paradigm, immunohistochemistry, and ELISAs with Dr. Melissa Glenn

Independent Neurobiology Research, *Colby College* Sept. 2011 – May 2012
Completed a project regarding the efficacy of sodium butyrate treatment in a toxin-induced *Drosophila* model of Parkinson's disease with Dr. Tariq Ahmad

Research Assistant, *Durham, NH* 2010 & 2011
Measured the phenomenon of unintentional synchronization of stride rate to a metronome beat during human running

Independent Psychology Research, *Colby College* Spring 2010
Explored the effects of auditory stimulation on unintentional synchronization in distance runners
Presented results to faculty and peers at the Undergraduate Research Symposium at Colby College

Volunteer Research Assistant, *University of New Hampshire, Durham, NH* Summer 2011
Worked closely with members of the exercise science department in data collection for procedures examining how body mass and age affect gait, walking performance, and energetic costs of normal walking

POSTERS & CONFERENCE ATTENDANCE

St Laurent R, Tsuda A & Kauer J. SfN 2018 Annual Meeting
Low frequency stimulation has a bidirectional effect on plasticity in periaqueductal gray and rostromedial tegmental nucleus GABAergic synapses in the ventral tegmental area

St Laurent R & Kauer J. Winter Conference on Brain Research 2018
Novel LTP at an opioid-sensitive GABAergic synapse in the VTA

St Laurent R & Kauer J. SfN 2017 Annual Meeting
Novel LTP at an opioid-sensitive GABAergic synapse in the VTA

St Laurent R, Moore C, Hochgeschwender U, Connors B, Lipscombe D, Kauer J.
SfN 2016 Annual Meeting Bioluminescent control of optogenetics in acute brain slices

St Laurent R, Moore C, Hochgeschwender U, Connors B, Lipscombe D, Kauer J.
Gordon 2016: Optogenetic Approaches to Understanding Neural Circuits & Behavior
Bioluminescent control of optogenetics in dopamine neurons

St Laurent R, Wang H, Morales M, Shaham Y, Bossert JM. SfN 2013 Annual Meeting
Context-induced relapse after suppression of heroin seeking by adverse consequences and an alternative palatable food reward

St Laurent R, Wang H, Morales M, Shaham Y, Bossert JM. Gordon Research Conference: Catecholamines 2013
Context-induced relapse after suppression of heroin seeking by adverse consequences and an alternative palatable food reward

St Laurent R, Wang H, Morales M, Shaham Y, Bossert JM. Annual NIDA Fellows Poster Day 2013
Context-induced relapse after suppression of heroin seeking by adverse consequences and an alternative palatable food reward

St Laurent R, Ahmad ST. Annual Drosophila Research Conference by The Genetics Society of America 2012
Sodium Butyrate Improves Motor Impairment in a Rotenone-Induced *Drosophila* Model of Parkinson's Disease

St Laurent R, Helm S, Glenn MJ. 3rd Annual Mainely Data, Some Theory Conference 2012
Reduced cocaine-seeking behavior in female BDNF^{+/-} rats

(Conference attendance only) SfN 2015 Annual Meeting

(Conference attendance only) Gordon 2015: Excitatory Synapses & Brain Function

(Conference attendance only) SfN 2014 Annual Meeting

INVITED TALKS

Panel speaker and co-chair at Winter Conference on Brain Research 2018
"Hitting the brakes: Mechanisms of inhibitory control of dopaminergic signaling in the VTA"

Invited speaker at NIDA monthly seminar series: Science for Nonscientists 2013
"Consequences of being a party animal: How to model relapse in rats"

Invited speaker at 3rd Annual Mainely Data, Some Theory Conference 2012
"Reduced cocaine-seeking behavior in female BDNF^{+/-} rats"

OTHER ACTIVITIES

Founder of “brainSTEM”: community outreach (2014-2016) - Science, Technology, Engineering, and Mathematics career talks and mentoring at Newmarket High School (NH) in a rural community

SAAC (Student Athletic Advisory Committee; 2010-2012) – Coach-selected panel for improving/advertising athletics at Colby College

Colby College Women’s Cross Country (2008-2011) – Elected varsity captain 2011

Colby College Women’s Indoor Track (2008-2012) – Elected varsity captain 2011/2012

Colby College Women’s Outdoor Track (2009-2012) – Elected varsity captain 2012

The International Honor Society in Psychology, Psi Chi, Secretary of Colby College chapter (2011-2012)

PREFACE & ACKNOWLEDGEMENTS

When I joined the Kauer lab, I was really interested in understanding how synaptic plasticity altered the activity of midbrain dopamine cells. I first started this thesis project in the beginning of my 3rd year with some “exploration” experiments within the rostromedial tegmental nucleus (RMTg) where I recorded from cells and tried applying various agonists that we had around the lab to see what would happen. I was hoping to find something – besides opioids - that depressed the RMTg cells that robustly inhibit the dopamine cells in the VTA. That desire led to the experiments in Chapter 3 where I placed a stimulating electrode caudal to the VTA, where I thought RMTg axons might be, and stimulated at a low frequency. What resulted from that first experiment was really unexpected: I saw very robust long term potentiation of the inhibitory inputs to about 400% of the original amplitude. After establishing that low frequency stimulation surprisingly led to strengthening of some synapses in the VTA, I was faced with a choice of follow-up experiments: try to determine the underlying mechanism or try to find the presynaptic source of the input. I stubbornly refused to choose, and instead, ambitiously tried to do both at the same time. Luckily for me, I did not fail at both courses of action and was able to identify that the periaqueductal gray (PAG) projection to the VTA expressed this unique form of long term potentiation induced with low frequency stimulation. Along the way, I also found that the RMTg depressed with the same stimulus pattern. The divergence of synaptic plasticity at VTA afferents made me extremely curious to find out what behaviors those synapses regulated. I found that behavior regulated by synapses in the VTA was also completely different between the two afferent populations. The RMTg elicited aversion and the PAG elicited immobility. Behavior elicited by the PAG to be particularly interesting because this input to the VTA had thus far been completely ignored. Even more intriguing was that the behavior was completely blocked when the mice had morphine in their system. In the end, this dissertation increased our knowledge of synaptic plasticity, opioid effects, and behaviors regulated in the VTA.

I would like to thank my advisor – Dr. Julie Kauer, who graciously gave me the freedom to roam about the brain and come up with my own project for my PhD. I recognize how unique of an experience this is and I am grateful that she was on board with and supported so many of my crazy ideas. I also would like to thank her for her patience in helping me to improve my writing skills over the years; I knew it was a weakness of mine and having a writing role model and mentor was essential for improving this career skill.

I am thankful for the comraderie of the past members of the Kauer lab, particularly Dr. Abigail Polter, who continues to be both a friend and mentor. I would like to thank the BL-OG working group for being like my second lab. I learned so much from every member of this group and cannot wait to see the incredible discoveries to come; I will definitely miss those meetings.

I am also incredibly grateful for my thesis committee members for guiding me along the years through not only the project written here, but the several others that did not quite pan out. Specifically, Dr. Barry Connors was incredibly helpful in asking the tough questions on my electrophysiology data and also always giving key suggestions at just the right time. Dr. Chris Moore pushed me to think about my data in ways that I did not always expect, eagerly jumped in to help interpret my behavioral data, and always was there to encourage me in my professional goals. I would also like to thank Dr. Chris McBain, for taking time out of a packed schedule and agreeing to be my outside reader.

I would like to thank the entire NSGP community and my 2014 cohort for making my experience at “small town, Brown” an incredible one. A special shout out to Valerie Estela for our absolutely critical coffee dates.

Last, but not least, I would like to thank my friends and family for being my unbreakable support system. Especially to Ben, my soon-to-be husband, who provided endless puppy videos, support houseplants, words of encouragement, and a relentless belief that I was better at this science

thing than I could even imagine. To my mom and dad – I cannot express in words how much your love and support is fundamental to each and every one of my accomplishments. Your unwavering confidence in me, whether I want to be an ice cream truck driver or neuroscientist, allows me to go after any ambition that I can dream up and actually believe that I can achieve it.

TABLE OF CONTENTS

Chapter 1. General Introduction	1
1.1 Cellular Heterogeneity of the Ventral Tegmental Area	3
1.1.1 Dopamine	3
1.1.2 GABA	4
1.1.3 Glutamate	4
1.2 Circuit Architecture of the VTA	5
1.2.1 Excitatory Afferents	5
1.2.2 Inhibitory Afferents	5
1.3 Behaviors Regulated by the VTA	6
1.4 Opioids and the VTA	7
1.5 Synaptic Plasticity in the VTA	9
1.6 Summary	11
Chapter 2. Methods	13
Chapter 3. Synaptic Plasticity at Inhibitory Synapses in the VTA Depends Upon Stimulation Site	23
3.1 Introduction	24
3.2 Results	25
3.2.1 Location of electrical stimulation determines expression of synaptic plasticity	25
3.2.2 Low frequency stimulation potentiates caudal-evoked inhibitory inputs	26
3.2.3 LFS of optically-evoked inhibitory inputs in the VTA does not induce plasticity	26
3.2.4 Forskolin potentiation does not occlude LFS-induced LTP	27
3.2.5 LFS-induced LTP does not require postsynaptic GPCR signaling or increased postsynaptic calcium	28
3.3 Discussion	29
Chapter 4. RMTg and PAG Inhibitory Afferents to the VTA	44
4.1 Introduction	45
4.2 Results	47
4.2.1 Long-term depression of RMTg _{GABA} →VTA synapses with LFS	47
4.2.2 Electrical HFS of caudal placed electrode with RMTg _{GABA} →VTA synapses	47
4.2.3 VTA-projecting vPAG GABA cells are candidates for expressing LFS-LTP	48
4.2.4 vPAG _{GABA} →VTA synapses display an unusual form of LTP with LFS	49
4.2.5 Possible mechanisms of LTP of vPAG _{GABA} →VTA synapses	50
4.2.6 vPAG _{GABA} →VTA synapses attenuate dopamine cell firing	51
4.2.7 Opioids depress vPAG _{GABA} →VTA more than RMTg _{GABA} →VTA synapses	52
4.2.8 vPAG _{GABA} →VTA are smaller in amplitude than RMTg _{GABA} →VTA synapses	53
4.3 Discussion	54
Chapter 5. Distinct Behavioral Profiles of Activating RMTg and PAG Inhibitory Afferents to the VTA	76
5.1 Introduction	77

5.1.1 Rostromedial tegmental nucleus.....	77
5.1.2 Periaqueductal gray	78
5.2 Results	79
5.2.1 Activating RMTg _{GABA} →VTA synapses is aversive	79
5.2.2 Activating vPAG _{GABA} →VTA synapses induces a quiescent phenotype	80
5.2.3 Morphine blocks vPAG _{GABA} →VTA stimulation-induced quiescent behavior	83
5.2.4 RMTg _{GABA} →VTA or vPAG _{GABA} →VTA does not disrupt consumption of palatable food....	85
5.3 Discussion	86
Chapter 6. Discussion	104
References	113

List of Illustrations

FIGURE 3-1. Electrical stimulation in horizontal midbrain slices.....	32
FIGURE 3-2. Location of electrical stimulation determines expression of synaptic plasticity.....	34
FIGURE 3-3. Low frequency stimulation of caudal electrode induces LTP.....	36
FIGURE 3-4. No effect with low frequency optical stimulation of VGAT+ synapses.....	38
FIGURE 3-5. Forskolin potentiation does not occlude LFS-induced LTP.....	40
FIGURE 3-6. LFS-induced LTP does not require postsynaptic GPCRs or increased calcium ..	42
FIGURE 4-1. RMTg _{GABA} →VTA synapses exhibit LTD with LFS	58
FIGURE 4-2. Forskolin, but not HFS of caudal placed electrode potentiates RMTg _{GABA} →VTA synapses	60
FIGURE 4-3. VTA-projecting GABAergic cells in the vPAG are sensitive to opioids.....	62
FIGURE 4-4. PAG _{GABA} →VTA synapses display an unusual form of LTP after LFS.....	64
FIGURE 4-5. Potentiation of vPAG _{GABA} →VTA synapses requires postsynaptic depolarization, but not neurotensin receptor activation	66
FIGURE 4-6. Possible mechanisms of LFS-induced LTP at PAG GABA synapses.....	68
FIGURE 4-7. vPAG _{GABA} →VTA synapses can inhibit dopamine cell firing.....	70
FIGURE 4-8. A μ-opioid receptor agonist depresses vPAG _{GABA} →VTA synapses more than RMTg _{GABA} →VTA synapses	72
FIGURE 4-9. Strength of inhibition differs between RMTg and PAG originating synapses	74
FIGURE 5-1. In vivo stimulation of RMTg _{GABA} →VTA synapses is aversive	90
FIGURE 5-2. In vivo stimulation of vPAG _{GABA} →VTA synapses induces quiescence	92
FIGURE 5-3. Effect of test order with LFS preconditioning before RTPP	94
FIGURE 5-4. Optogenetically driven quiescent behavior is blocked by systemic morphine	96
FIGURE 5-5. Time course of immobility during light tests	98
FIGURE 5-6. RMTg _{GABA} →VTA or vPAG _{GABA} →VTA does not disrupt rotarod performance	100
FIGURE 5-7. RMTg _{GABA} →VTA, but not vPAG _{GABA} →VTA, photoactivation slightly disrupts palatable food consumption	102
FIGURE 6-1. Exceptionally large amplitude inhibitory currents	111
FIGURE 6-2. Summary	112

CHAPTER 1

GENERAL INTRODUCTION

For organisms to survive in a world filled with potential danger means that they must continually balance actions that avoid danger with those that facilitate survival, such as finding food, water, shelter, and mates. Accordingly, the brain has adapted circuits to respond to stimuli in the environment that signal both positive and negative situations. However, in humans, some of these circuits become maladaptive, leading to behavior that is detrimental to the individual. One strong example of this issue is when people are exposed to exogenous opioids, such as morphine, heroin, or fentanyl. The brain has its own substances that normally act on opioid receptors: enkephalins and endorphins. Exogenous opioids also bind to these receptors and affect pathways in the brain that normally function to respond to rewarding or aversive stimuli. These modifications lead to long-lasting changes in circuit function that may underlie motivational disorders, such as addiction. This is a major health concern and economic burden on society with overdose deaths in the past decade on the rise. In particular, overdose deaths from opiate abuse have risen dramatically over the last decade (CDC, 2015). Decades of research have been focused on the cellular adaptations in regions of the reward pathway that may precede the transition to addiction (Hyman et al., 2006). Many changes occur in the ventral tegmental area (VTA), yet not every adaptation at the cellular, synaptic, circuit, and behavioral level has been explored. These unknowns could be key players in causing some of the maladaptive behavior seen in drug abuse. All drugs of abuse increase dopamine concentration in VTA projection regions and within the VTA (Di Chiara and Imperato, 1988). A common adaptation seen after exposure to nearly all drugs of abuse is an increase in synaptic strength at excitatory synapses on dopamine cells in the VTA (Saal *et al*, 2003; Ungless *et al*, 2001). Our current understanding of changes in excitatory transmission in the VTA has prompted possible intervention strategies for treatment of addiction (Pascoli et al., 2015, Terraneo et al., 2016). These strategies focus mainly on excitatory synapses on VTA dopamine cells, however, opioids dramatically impact another important component of VTA regulation: inhibition. Inhibition functions as a strong “brake” for VTA dopamine cells and therefore is well poised as a candidate therapeutic target for addiction. There is evidence that

opioids increase excitability of VTA dopamine cells via disinhibition (Johnson and North, 1992) and that morphine alters synaptic plasticity at inhibitory synapses in the VTA (Dacher and Nugent, 2011, Nugent et al., 2007). Activating inhibitory terminals in the VTA of rodents is sufficient to interfere with reward behavior (Tan et al., 2012, Van Zessen et al., 2012). Gaining a more complete understanding of opioid regulation of inhibition, inhibitory synaptic plasticity, and inhibitory circuits in the VTA and the behaviors that they regulate is of utmost importance for future efforts focused on treating addiction.

1.1 Cellular Heterogeneity of the Ventral Tegmental Area

1.1.1 Dopamine

The VTA is best known for its dopaminergic cell population but it also contains inhibitory interneurons and projection cells, as well as a small population of glutamatergic cells. The VTA is approximately 60% dopaminergic. Dopamine cells in the VTA exhibit pacemaking and fire spontaneously in the range of 0.5-5 Hz (Khaliq and Bean, 2008). There are two components responsible for pacemaking in VTA dopamine cells; a voltage-insensitive sodium current (leak) that is active at membrane potentials more depolarized than -55 mV and voltage-gated sodium channels that are activated between -55 mV and threshold (Khaliq and Bean, 2010). Dopamine cells can also fire in bursts in the range of 14-30 Hz (Grace and Bunney, 1984, Schultz, 1986, Hollerman and Schultz, 1998, Hyland et al., 2002) and can be triggered by activation of NMDA receptors (Overton and Clark, 1992, Chergui et al., 1993, Deister et al., 2009). Bursting is required for reinforcement learning (Schultz, 1997).

Dopamine cells are a heterogeneous population and several groups have categorized subpopulations of the VTA cells by their targets, intrinsic receptors and ion channels, or afferent inputs (Ford et al., 2006, Margolis et al., 2006a, Margolis et al., 2008, Lammel et al., 2008, Watabe-Uchida et al., 2012, Ekstrand et al., 2014). The main projection targets of VTA dopamine cells include the nucleus accumbens, amygdala, medial prefrontal cortex, and hippocampus and

these different regions regulate different behaviors. Circuits involving VTA dopamine cells play a critical role in learning, motivation, and motor processes.

1.1.2 GABA

Ultrastructural evidence and numerous electrophysiological studies show VTA GABA interneurons synapse onto and exert inhibitory control over dopamine cells (Omelchenko and Sesack, 2009; Matsui and Williams, 2011; Tan et al., 2012; van Zessen et al., 2012; Bocklisch et al., 2013; Matsui et al., 2014; Simmons et al., 2017; Polter et al., 2018). However, the precise connectivity of local interneurons with their neighboring dopamine cells remains an open question. There is preliminary evidence that different subpopulations of VTA dopamine cells may receive different local inhibition based on the dopamine projection target (Yang et al., 2018). Unlike in the forebrain, canonical markers of interneuron cell types do not translate well to VTA GABA cells. Instead, some evidence suggests that subpopulations could be distinguished by their responsiveness to dopamine D2 or mu opioid receptors (Margolis et al., 2012). However, there is still a need for further identification of subclasses of inhibitory interneurons in the VTA.

1.1.3 Glutamate

Glutamatergic cells in the VTA are by far the least studied of all the cell types. Recently, a small population of glutamatergic cells in the VTA were reported to exist. They express the vesicular glutamate transporter (VGLUT2) and project to the nucleus accumbens, lateral habenula, ventral pallidum, and amygdala (Hnasko et al., 2012). Stimulation of VGLUT2-positive cells in the VTA is rewarding but there are nuanced differences in the behavioral outcome based on projection target (Yoo et al., 2016). Notably, some of these glutamatergic VTA cells co-release dopamine (Hnasko et al., 2012) or GABA (Yoo et al., 2016). Glutamatergic cells that co-release neurotransmitters are likely to have distinct functions as well as control over specific behaviors that are different from cells that only release glutamate.

1.2 Circuit Architecture of the VTA

1.2.1 Excitatory Afferents

Many regions send excitatory projections to the VTA, including the cortex, the bed nucleus of stria terminalis (BNST), central amygdala, pedunculo pontine tegmental nucleus, and laterodorsal tegmentum (LDT) (Forster and Blaha, 2000, Gariano and Groves, 1988, Geisler and Zahm, 2005, Georges and Aston-Jones, 2001, Georges and Aston-Jones, 2002, Gonzales and Chesselet, 1990, Lodge and Grace, 2006, Oakman et al., 1995). Glutamatergic and cholinergic pedunculo pontine tegmental nucleus (PPTg) inputs to the VTA increase VTA dopamine cell bursting and dopamine release in the nucleus accumbens (Floresco et al., 2003). Burst firing may be critical for modulation of behaviors, such as reward-seeking, and promote maladaptive responses to previously neutral situations or items, such as drug-associated cues (Adamantidis et al., 2011). Modification of the strength of excitatory VTA synapses is therefore going to have a significant effect on activity in downstream regions. Excitatory synapses undergo synaptic plasticity, some forms of which are sensitive to drug exposure (Saal et al. 2003). These adaptations have been described in depth elsewhere (Kauer, 2004). However, most synapses in the VTA are inhibitory and also deserve equal attention.

1.2.2 Inhibitory Afferents

Dopamine cells receive inhibition from local interneurons and afferent inhibitory inputs. The NAc sends GABAergic projections to the VTA (Rahman and McBride, 2000, Matsui et al., 2014, Edwards et al., 2017). Parvalbumin-positive cells in the pallidum target dopamine cells in the VTA (Faget et al., 2016). The BNST has GABAergic synapses in the VTA (Kudo et al., 2014, Kudo et al., 2012) and approximately half of LDT synapses on VTA cells are inhibitory (Omelchenko and Sesack, 2005). Another midbrain region, the rostromedial tegmental nucleus (RMTg) forms inhibitory synapses primarily on dopaminergic dendrites in the VTA (Balcita-Pedicino et al., 2011).

Other regions that have GABAergic input to the VTA include the dorsal raphe (Beier et al., 2015, Faget et al., 2016) and periaqueductal gray (PAG) (Omelchenko and Sesack, 2010, Ntamati et al., 2018). Out of all of these, afferents that are especially sensitive to opioids, such as the RMTg and the PAG are of particular interest for opioid research and are discussed in depth in Chapters 4 and 5.

1.3 Behaviors Regulated by the VTA

Optogenetic activation of dopamine cells in the VTA promotes reward behavior. Rodents will self-stimulate VTA dopamine cells expressing an excitatory opsin by nose-poking (Kim *et al*, 2012). Photostimulation of dopamine cells in the VTA also induces conditioned place preference, a behavioral measure of reward one compartment of an apparatus is paired with an experience, such as drug exposure, and the subject's time spent in that compartment vs. a non-drug-paired compartment is compared (Tsai et al., 2009, Witten et al., 2012). It also increases food-seeking operant behavior and reactivates extinguished food seeking (Adamantidis et al., 2011). Conversely, inhibiting firing of VTA dopamine cells using inhibitory opsins, such as halorhodopsin, produces operant place avoidance (Ilango et al., 2014). Inhibiting GABAergic VTA cells using halorhodopsin increases VTA dopamine cell firing whereas activating NAc GABAergic inputs using channelrhodopsin disinhibits VTA dopamine cells (Bocklisch et al., 2013). Photostimulation of VTA GABA cells strongly inhibits dopamine neuron firing *in vivo* and *in vitro*, induces conditioned place aversion, and decreases sucrose consumption (Tan et al., 2012, Van Zessen et al., 2012). Activation of archaerhodopsin, another inhibitory opsin, expressed in VTA terminals in the NAc was able to block cocaine- or cue- induced reinstatement of lever pressing in rats (Stefanik et al., 2013). Although most of these reports support the idea that increasing dopamine release is rewarding, while decreasing release is aversive. However, given the heterogeneity of

VTA subpopulations, studies that isolate specific afferents or subpopulations reveal more complexity of this generalized view.

Optogenetic circuit-cracking has been useful to probe the function of many pathways, including those involving the VTA. For instance, photostimulation of lateral habenula excites VTA dopamine cells projecting to the prefrontal cortex and produces conditioned place aversion; conversely, photostimulation of LDT excited VTA dopamine cells projecting to the NAc and produced conditioned place preference (Lammel et al., 2012). The RMTg is innervated by lateral habenula (LHb) glutamatergic projections (Gonçalves et al., 2012, Jhou et al., 2009b) and is activated by aversive stimuli (Jhou et al., 2009a) such as footshock (Stamatakis and Stuber, 2012). The VTA is involved in fear, anxiety, stress, and other aversive behaviors and it appears that the LHb→RMTg→VTA circuit is mediating those emotional states and their corresponding behaviors. However, the direct activation of RMTg terminals in the VTA has not been verified to induce place aversion, instead, the role of this specific afferent has been inferred from activation or inhibition of the entire region. Other afferents have not been investigated at all. For instance, the PAG has a distinct role in many fear and pain behaviors, yet the consequences of its GABAergic projections to the VTA have never been probed for behavioral output. In Chapter 5, I will discuss some of the behavioral implications of activating two inhibitory afferents to the VTA originating in the RMTg and the PAG. Interestingly, activation of these two afferents results in different behavioral outputs, despite both being sources of inhibition. I also found that both are highly sensitive to opioids. It is possible that separate afferent populations could underlie different facets of opioid abuse.

1.4 Opioids and the VTA

Opioids increase the firing rate of VTA dopamine cells *in vitro* (Johnson and North, 1992, de Guglielmo et al., 2014) by binding to endogenous opioid receptors (Raynor et al., 1994) and inhibiting GABA release, leading to disinhibition of VTA dopamine cells (Johnson and North, 1992,

Steffensen et al., 2006). Opioids bind to the 3 known types of opioid peptide receptors: μ , κ , and δ (MOR, KOR, DOR; respectively). They are G-protein coupled receptors (GPCRs) that signal via heterotrimeric G proteins to modulate cation channels and inhibit adenylyl cyclase (Williams and Grudt, 1995). Differences in receptor subtype expression can influence the effect of opioid exposure within a brain region. In the VTA, MOR are located on dopamine cells, GABAergic interneurons, and on GABAergic axons whose cell bodies originate outside of the VTA. MOR may also inhibit neurotransmitter release by acting on voltage-gated calcium channels and release proteins such as SNAP-25, resulting in increased VTA dopamine activity (Blackmer et al., 2005, Gerachshenko et al., 2005). It should be noted that since dopamine cells can also express opioid receptors, some opioid effects are likely a consequence of direct MOR activation (Margolis et al., 2014).

Activation of MOR in the VTA is rewarding (Zangen et al., 2002a). On the other hand, activation of KOR is aversive and involved in stress (Graziane et al., 2013, Land et al., 2008, Polter et al., 2014) and DOR are widely expressed in the brain and may have a more complex role in pain, drug reward, and emotional processing (Chu Sin Chung and Kieffer, 2013). Drugs with a high likelihood of abuse, such as morphine or fentanyl, have high affinity for MOR but not KOR or DOR (Raynor et al., 1994). Even acute administration of opioids, such as morphine, cause long-lasting changes in the VTA. Normally, GPCRs undergo desensitization via β -arrestin recruitment which leads to receptor internalization. However, MOR do not appear to undergo G-protein uncoupling through this process when activated by morphine (Whistler and von Zastrow, 1998). Therefore, morphine may set off intracellular signaling cascades via MOR without eventual receptor endocytosis (Keith et al., 1996), which may account for the long term changes seen with morphine but not endogenous agonists of MOR.

Several behavioral and electrophysiological reports show that MOR are critical for opioid reward. For example, systemic morphine induces conditioned place preference (Vezina and Stewart,

1987). Rodents will self-administer morphine or other MOR agonists directly into the VTA (Bozarth and Wise, 1981, Zangen et al., 2002b). Systemic or direct injection of morphine into the VTA increases dopamine release in the nucleus accumbens (Di Chiara and Imperato, 1988, Leone et al., 1991) and an intact VTA is necessary for expression of conditioned place preference to morphine (Olmstead and Franklin, 1997). Because of the substantial expression of MOR on inhibitory VTA afferents, these synapses are likely major sites of action for the euphoric and reinforcing properties of opioids.

Administering morphine directly into the RMTg - a strong inhibitory afferent - increases dopamine cell firing in the VTA (Lecca et al., 2012a). The robust projection from the RMTg (also sometimes referred to as the tail of the VTA) synapses on NAc-projecting VTA dopamine cells and exerts strong inhibitory control through a high spontaneous firing rate (Jhou et al., 2009a, Jhou et al., 2009b, Barrot et al., 2012, Matsui et al., 2014). Morphine hyperpolarizes RMTg cells, reducing their spontaneous firing and thereby disinhibiting VTA dopamine cells (Lecca et al., 2011). If the inhibition by the RMTg is taken away by inactivating that region, the effect of morphine on increasing the firing of VTA dopamine cells *in vivo* is lost (Jalabert et al., 2011). This is one example showing how the removal of a source of inhibition has a strong effect on the function of VTA dopamine cells. Synaptic plasticity is another way that the strength of any particular synapse can be up- or down-regulated. Measuring synaptic plasticity is therefore also critical to understanding the function of the VTA.

1.5 Synaptic Plasticity in the VTA

One type of synaptic plasticity, long-term depression (LTD), leads to a persistent down-regulation of strength at GABAergic synapses on VTA dopamine cells. Endocannabinoid signaling with CB1 receptor activation can depress GABAergic inputs onto VTA dopamine cells (Pan et al., 2008). LTD can also be induced by low frequency afferent stimulation (Dacher and Nugent, 2011, Dacher

et al., 2013) or precise temporal spiking of pre- and post-synaptic cells induces Hebbian spike timing dependent plasticity (Kodangattil et al., 2013). Furthermore, modulation of inhibitory synapses in the VTA is bidirectional and there are many reports of long-term potentiation (LTP) in addition to LTD at GABAergic inputs in the VTA.

Spike timing dependent plasticity can also induce LTP at inhibitory synapses (Kodangattil et al., 2013, Langlois et al., 2018). Our lab previously found that high frequency stimulation (HFS) of GABA_A receptor-mediated currents onto VTA dopamine cells induces long-term potentiation (LTP_{GABA}) by releasing nitric oxide from the postsynaptic cell. Calcium-dependent processes in the postsynaptic cell led to production and release of nitric oxide, a soluble gas, that can cross the cellular membrane and travel to the presynaptic terminal. In the presynaptic terminal, nitric oxide acts on the guanylate cyclase pathway to increase cyclic GMP and leads to increased GABA release. NMDAR antagonists or MOR agonists were able to block LTP_{GABA} because they prevented calcium entry into the postsynaptic cell (Nugent et al., 2007). Another report described how blockade of D1 receptors prevented HFS-induced potentiation of NAc inputs onto VTA dopamine cells (Bocklisch et al., 2013).

A common adaptation seen with nearly all drugs of abuse is an increase in synaptic strength at excitatory synapses on dopamine cells in the VTA (Ungless et al., 2001, Saal et al., 2003, Faleiro et al., 2004) and drug exposure also blocks LTP at inhibitory synapses (Laviolette et al., 2004, Niehaus et al., 2010, Nugent et al., 2007). The net result of these drug-induced changes in synaptic strength is to increase dopamine cell firing. Loss of LTP_{GABA} occurs also occurs after a single exposure to morphine, cocaine, ethanol, nicotine, and stress (Nugent et al., 2007, Niehaus et al., 2010, Guan and Ye, 2010). Resveratrol, a natural phytoalexin that is commonly found in wine, blocks endocannabinoid-mediated inhibitory LTD and induced LTP of GABAergic inputs to VTA dopamine cells via a cyclic AMP-mediated mechanism (Li et al., 2017). Drugs can also induce plasticity; for example, repeated cocaine injections *in vivo* caused LTP at NAc_{GABA}→VTA

GABA cells which in turn disinhibited VTA dopamine cells (Bocklisch et al., 2013) and a MOR agonist potentiated IPSCs in VTA slices taken from chronic morphine treated mice (Madhavan et al., 2010). The studies mentioned above are evidence that environmental factors (i.e. drugs of abuse or stress) interact with synaptic plasticity. However, these reports did not address the possibility that there is variability across afferent inputs. Subcircuits are likely to vary in susceptibility to environmental insults and different protein expression or other cellular differences may dictate which synapses are pushed to the point of becoming dysfunctional.

Several of the studies mentioned above preceded the invention of circuit-cracking tools such as optogenetics and instead used local electrical stimulation. For example, our lab first described LTP_{GABA} with electrical stimulation (Nugent et al., 2007), however, when isolating specific populations using optogenetics, our lab and others found that presence of LTP_{GABA} varied depending on presynaptic source (Simmons et al., 2017, Polter et al., 2018). LTP_{GABA} is expressed at NAc and VTA GABA synapses, but not RMTg-originating VTA synapses. It is likely that other forms of plasticity that have been described in the VTA also have input-specific expression. I will introduce a previously undescribed form of inhibitory LTP in the VTA using electrical stimulation in Chapter 3 that I will show has input-specific expression using optogenetics in Chapter 4.

1.6 Summary

The VTA encodes information about both rewarding and aversive stimuli and is required for the addictive properties of drugs of abuse (Nestler, 2004, Jones and Bonci, 2005, Mazei-Robison and Nestler, 2012). The VTA receives inhibitory input from local interneurons, but also from numerous extrinsic brain areas. Opiate drugs inhibit GABAergic cells that normally regulate dopamine cell firing, increasing their firing rate (Johnson and North, 1992, Gysling and Wang, 1983, Steffensen et al., 2006, Ford et al., 2006, Matsui and Williams, 2011). Despite this common denominator, deciphering the effect of opioids in the VTA is a complex task because the relative suppression

by opioids differs among GABAergic sources (Matsui et al., 2014). This is further complicated by the divergent roles that VTA dopamine cells themselves have in regulating reward or aversion (Lammel et al., 2011). To place the relative contribution of opioid effects into context, it is essential to understand the heterogeneous properties of different VTA afferents using genetic and anatomical isolation of afferent populations (Lammel et al., 2014, Pathan and Williams, 2012). The following chapters will address the hypothesis that not all possible mechanisms of inhibitory synaptic plasticity in the VTA have been established as evidenced by two novel ways of inducing inhibitory LTP (Chapter 3), compare and contrast plasticity and opioid-sensitivity of RMTg and PAG afferents (Chapter 4), and profile behaviors that are regulated by RMTg→VTA and PAG→VTA inhibitory afferents (Chapter 5).

CHAPTER 2

Methods

2.1 Animals

All procedures were carried out in accordance with the guidelines of the National Institutes of Health for animal care and use and were approved by the Brown University Institutional Animal Care and Use Committee. Mice were maintained on a 12-h light/dark cycle and provided food and water ad libitum.

Experiments in Chapter 3 used VGAT::IRES-Cre (Jackson Laboratory, stock number: 028862, strain code: B6J.129S6(FVB)-Slc32a1^{tm2(cre)Lowl}), DAT::IRES-Cre (Jackson Laboratory, stock number:006660, strain code: B6.SJL-Slc6a3^{tm1.1(cre)Bkmn/J}) (Zhuang et al., 2005) Ai14 Cre reporter mice (Jackson Laboratory, stock number: 007908, strain code: B6;129S6-Gt(ROSA)26Sor^{tm14(CAG-tdTomato)Hze/J}), VGAT-ChR2(H134R)-EYFP (stock number: 014548, strain code: B6.Cg-Tg(Slc32a1-COP4*H134R/EYFP)8Gfng/J) (Zhao et al., 2011), and C57BL/6 male and female mice bred in-house.

Experiments in Chapter 4 used VGAT::IRES-Cre (Jackson Laboratory, stock number: 028862, strain code: B6J.129S6(FVB)-Slc32a1^{tm2(cre)Lowl}), DAT::IRES-Cre (Jackson Laboratory, stock number:006660, strain code: B6.SJL-Slc6a3^{tm1.1(cre)Bkmn/J}), Ai14 Cre reporter mice (Jackson Laboratory, stock number: 007908, strain code: B6;129S6-Gt(ROSA)26Sor^{tm14(CAG-tdTomato)Hze/J}), Pitx-GFP (TG(PITX3EGFP)), and C57BL/6 male and female mice bred in-house.

Experiments in Chapter 5 used VGAT::IRES-Cre (Jackson Laboratory, stock number: 028862, strain code: B6J.129S6(FVB)-Slc32a1^{tm2(cre)Lowl}) male and female mice bred in-house.

2.2 Stereotaxic Injections

Stereotaxic surgeries were performed on male and female mice between postnatal days 25-35. For RMTg injections, VGAT::IRES-Cre mice were deeply anesthetized with ketamine and dexdomitor and 200-300 nL of AAV2-EF1a-DIO-hChR2(H134R)-EYFP or AAV2-EF1a-DIO-hChR2(H134R)-mCherry (UNC vector core) was bilaterally injected into the RMTg (AP: -2.5, ML: ± 0.5, DV: -4.4). Horizontal slices containing the VTA were prepared 3-6 weeks after surgery. For

PAG experiments, VGAT::IRES-Cre mice were deeply anesthetized with ketamine and dexdomitor and 200-300 nL of AAV2/9-hsyn-ChR2-EYFP, AAV5- EF1a-DIO-hChR2(H134R)-mCherry or AAV-DJ-DIO-ChETA-EYFP were injected unilaterally into the PAG (AP: -3.7, ML: 0.4, DV: -2.6). Horizontal slices containing the VTA were prepared 5-9 weeks after surgery. For some PAG injections, C57BL/6 or DAT x tdTomato mice were injected unilaterally with AAV2/9-hsyn-ChR2-eYFP (AP: -3.7, ML: 0.4, DV: -2.6). Slices were prepared 2-9 weeks after surgery and GABAergic inputs were isolated using pharmacological methods (1 μ M strychnine, 10 μ M DNQX). For experiments involving retrograde labeling of PAG cells, 200-300 nL of Retrobeads™ from Lumafluor were injected unilaterally into the VTA of VGAT x tdTomato mice. Slices from injection regions were prepared to confirm their locations; data from mice with mistargeted injection sites of virus or of retrobeads were discarded.

2.3 Preparation of brain slices

Horizontal brain slices (220 μ m) were prepared as previously described from deeply anesthetized mice (Polter et al., 2018). Briefly, anesthetized mice were perfused with ice-cold oxygenated artificial cerebrospinal fluid (ACSF) (in mM): 126 NaCl, 21.4 NaHCO₃, 2.5 KCl, 1.2 NaH₂PO₄, 2.4 CaCl₂, 1.0 MgSO₄, 11.1 glucose, 5 sodium ascorbate. Following perfusion, the brain was rapidly dissected and horizontal slices (220 μ m) were prepared using a vibratome. Slices recovered for 1 h at 34°C in oxygenated HEPES holding solution (in mM): 86 NaCl, 2.5 KCl, 1.2 NaH₂PO₄, 35 NaHCO₃, 20 HEPES, 25 glucose, 5 sodium ascorbate, 2 thiourea, 3 sodium pyruvate, 1 MgSO₄·7H₂O, 2 CaCl₂·2H₂O, and then were held in the same HEPES solution at room temperature until use. Slices were then transferred to a recording chamber where they were submerged in ACSF without sodium ascorbate.

2.4 Electrophysiology

Electrophysiological experiments were performed as described previously (Nugent et al., 2007, Graziane et al., 2013). Horizontal midbrain slices were continuously perfused with ACSF

containing 10 μM 6,7-dinitroquinoxaline- 2,3-dione (DNQX) and 1 μM strychnine, AMPA and glycine receptor antagonists, respectively. Except where noted, recordings also included the NMDA receptor antagonist APV (50 or 100 μM). Whole-cell recordings were performed with KCl pipette solution and voltage-clamped at -70mV. Patch pipettes were filled with (in mM): 125 KCl, 2.8 NaCl, 2 MgCl_2 , 2 ATP- Na^+ , 0.3 GTP- Na^+ , 0.6 EGTA, and 10 HEPES. In some experiments EGTA was increased to 15 mM, or GDP- β -S (1 mM) was included in the pipette solution as noted. For experiments using outward oIPSCs, patch pipettes were filled with (in mM): 117 K-gluconate, 2.8 NaCl, 5 MgCl_2 , 0.2 CaCl_2 , 2 ATP- Na^+ , 0.3 GTP- Na^+ , 0.6 EGTA, and 10 HEPES. Presence of a large hyperpolarization current was used to select postsynaptic cells for recording. If the steady-state h-current was greater than 25 pA during a step from -50 mV to -100 mV, the cell was included in analyses. In a subset of cells, dopamine cells were also identified via fluorescent labeling in a DATxTdTomato line.

It is difficult to differentiate dopamine cells from other neurotransmitter cell types in acute brain slices. Therefore, the subject of dopamine cell identity is one that has become a point of debate in the field. Historically, presence of a large hyperpolarization-induced current (I_h) was used to identify dopamine cells. However, this method was based on characteristics of dopamine cells in the substantia nigra, where the distinction between dopamine and GABA cells appears to be less of a gray area. In the VTA, there are dopamine cells that do not express I_h and there are GABA cells that do express I_h . Therefore, this measure cannot be used to determine if a cell is positive for tyrosine hydroxylase (TH), the rate limiting enzyme in dopamine synthesis (Margolis et al., 2006b). Fortunately, there are genetic markers of dopamine cell identity that can now be used to circumvent this issue, such as dopamine transporter (DAT) and tyrosine hydroxylase (TH) cre recombinase or Pitx-GFP mouse lines.

For electrical stimulation, a bipolar stainless steel stimulating electrode was placed caudal to the VTA (except where noted) to stimulate inhibitory post synaptic currents (IPSCs) at 0.1 Hz.

Channelrhodopsin- or ChETA-induced synaptic currents were evoked through the microscope objective using 0.1-10 ms full-field light pulses from a white LED (Mightex) controlled by driver (ThorLabs) and reflected through a 40x water immersion lens (Polter et al., 2018). Pairs or trains of light-evoked IPSCs were separated by 30s to avoid desensitization of the opsin. When feasible, oIPSCs were shown to be GABA_A receptor-mediated by bath application of 10 μ M bicuculline at the end of recordings. The series resistance was monitored continuously during the experiment and cells were discarded for deviations >15%.

2.5 Electrical Stimulation Protocols

1 Hz LFS: For LFS experiments, after a stable 10 min baseline, stimulation was delivered at 1 Hz while depolarizing the postsynaptic cell to -40 mV for 6 min.

100 Hz HFS: While voltage-clamped at -70mV, two 1 s tetani of 100 Hz were delivered across 40 s. For all stimulus frequencies, intensity remains constant throughout the experiment.

2.6 Optogenetic Stimulation Protocols

For optical LFS experiments, after a stable 10 min baseline, stimulation was delivered at 1 Hz while voltage-clamping the postsynaptic cell to -40 mV for 6 min. Experiments using LFS without postsynaptic cell depolarization maintained -70 mV voltage clamp during LFS. For a subset of experiments, a bipolar stimulating electrode was placed 200 microns caudal to the VTA in a horizontal slice and used to stimulate IPSCs. For electrical HFS, IPSCs were stimulated for 1 second at 100 Hz twice, separated by 40 seconds. The postsynaptic cell remained in voltage clamp at -70 mV for the duration of HFS. For all stimulus frequencies, intensity remains constant throughout the experiment.

2.7 Immunohistochemistry and Imaging

For imaging experiments, mice were deeply anesthetized with ketamine (75 mg/kg) and dexmedetomidine (0.25mg/kg) i.p. and transcardially perfused with 50 mL of PBS followed by 50 mL of 4% PFA. Whole brains were dissected out and post-fixed overnight, then transferred to 30% sucrose in PBS for 48 hours until sunk. Brains were embedded in 3% agarose and cut to 50 μ m thickness on a Vibratome ® 1000 plus Sectioning System and stored in PBS. For virus and optic fiber implant verification, slices were mounted on slides with VectaShield mounting medium (Vector Laboratories, Inc.). For immunostaining, free floating slices were washed three times (10 min) in PBS, three times (10 min) in warmed PBS containing 5% Triton-X 100 (PBS-T) and blocked in 5% normal donkey serum (NDS) and 5% bovine serum albumin (BSA) in PBS at room temperature for 1 hour. Sections were then incubated in primary antibody against TH (rabbit anti-TH, 1:1000 Millipore AB152) or FoxP1 (rabbit anti-FoxP1, 1:20,000 Abcam ab16645) in 0.1% PBS-T at 4°C for 96 hours or overnight, respectively. Sections were washed three times (10 min) in PBS, blocked in 5% NDS in 0.25% PBS-T for three washes (10 min), then incubated in secondary antibodies (donkey anti-rabbit conjugated to Alexa-594 or Alexa-405 fluorescent dyes, 2mg/ml ThermoFisher) for 3 hours at room temperature. Slices were rinsed five times (10 min) in PBS and then mounted on slides with Fluoromount-G mounting medium (Southern Biotech). Imaging of immunofluorescence, retrobeads, and virally expressed fluorescent proteins was performed using a Zeiss LSM 800 using the 10x, 20x and 40x (water immersion) objectives. EYFP was imaged using a 488 nm diode laser; Alexa594 and mCherry were imaged using a 561 nm diode laser; and Alexa 405 was imaged using the 405 diode laser. Images were processed and analyzed using Zeiss Zen Blue software and Adobe Illustrator CC 2017.

2.8 Optic Fiber Implantation

Stereotaxic surgeries were performed on male and female mice between postnatal days 25-35. For RMTg injections, VGAT::IRES-Cre mice were deeply anesthetized with ketamine and dexdomitor and 200-300 nL (of AAV2-EF1a-DIO-hChR2(H134R)-EYFP or AAV2-EF1a-DIO-hChR2(H134R)-mCherry (UNC vector core) was unilaterally injected into the RMTg (AP: -2.5, ML: \pm 0.5, DV: -4.4). For vPAG experiments, AAV5-DIO-hChR2(H134R)-mCherry, AAV5-DIO-mCherry, (AddGene) or AAV-DJ-DIO-ChETA-EYFP (Stanford Vector Core) were injected unilaterally into the vPAG (AP: -3.7, ML: 0.4, DV: -2.6). During the same surgery, a ceramic ferrule with a 200 μ M light fiber (ThorLabs) was implanted over the VTA on the same hemisphere and affixed to the skull with Metabond and dental acrylic. Light output for all ferrules was in the range of 4 – 10 mW at the tip measured using an optical power meter (ThorLabs). The exposed end of the ferrule was protected with a dust cap except when the mouse was tethered to the LED cable. All behavioral assays were performed between 4 and 9 weeks after surgery to allow for adequate viral expression. Behavioral data from mice where the virus or implant site was not in the correct region were excluded from analysis.

2.9 Real Time Place Preference (RTPP) Procedure

RTPP experiments were conducted in custom-made, two-chamber behavioral arenas (35 x 30 x 30 cm). For all tests, mice were assigned one counterbalanced side of the arena as the light stimulation side and each test lasted for a total duration of 10 min. At the onset of the test, mice were placed in the center of the arena between the two chambers and the 10 min test was immediately started. For tests where light stimulation was present, light was triggered by entry into the designated light-paired chamber and delivered constantly at the appropriate frequency until the mouse crossed into the non-stimulation side. Behavioral data was monitored and light stimulation was triggered via a CCD camera interfaced with Ethovision software (Noldus

Information Technologies). Light stimulation was triggered by 10 ms TTL pulses generated by a Master-8 connected to an LED driver (Plexon LD-1). For RMTg experiments, mice underwent 3 test sessions each separated by 24 h: pretest, 60 Hz light stimulation, and posttest. For vPAG experiments, mice underwent 4 test sessions each separated by 24 h: pretest, 20 Hz light stimulation, LFS preconditioning & 20 Hz light stimulation, and posttest. Days 2 and 3 were counterbalanced. Mice were connected to the optic fiber cable on all testing days and light was only delivered on days 2 and 3. One outlier was excluded from the vPAG experiments, defined as being > 2 standard deviations from the mean.

Another cohort of vPAG mice (n = 8 fluorophore, n = 13 ChR2) were used for the morphine RTPP procedure. The morphine RTPP procedure used the same behavioral apparatus as the RTPP procedure. Two days prior to testing, all mice received a single intraperitoneal injection of saline in their home cage in the animal care facility. One day prior to testing, all mice were transported to the testing room where they were again injected with saline for habituation purposes. On day one, all groups of mice were injected with saline 30 min prior to being tested in the RTPP apparatus; on day 2, mice received a single i.p. injection of morphine (3 mg/kg at 1 mg/ml) or saline 30 min prior to being tested. On day 3, all groups were injected with saline 30 min prior to being returned to the apparatus for a posttest. Mice were connected to the optic fiber cable on all testing days and light was only delivered on day 2. For all sessions (pretests, light tests, posttests), mice were connected to a light fiber with black tubing covering the ferrule connector to reduce the amount of light visible from the head cap.

2.10 Rotarod

A subset of mice (n = 5 vPAG fluorophore, n = 5 vPAG opsin, n = 6 RMTg fluorophore, n = 5 RMTg opsin) used for behavioral assays were tested on a rotarod. First, mice were placed on a

5 lane rotarod for mice (Med Associates) at a starting speed of 4 rpm. After a brief session where the mouse learned to walk forward to avoid falling off, mice learned to walk at 20 rpm by gradually accelerating the speed until the mouse was able to maintain 20 rpm. After a period of rest, the mouse was attached to a fiber optic cable and returned to the rotarod. After a stable 1 min baseline period at 20 rpm to acclimate to the fiber optic cable, light stimulation was turned on for 1 min (20 or 60 Hz for vPAG and RMTg mice, respectively). Light stimulation was followed by 1 min of light off. Number of falls or complete inversions on the rotarod per minute were compared between light on and light off conditions.

2.11 Statistical analysis

Results are expressed as mean \pm S.E.M. Significance was determined using a Student's t-test or one-way ANOVA with significance level of $p < 0.05$. LTP or LTD values are reported as averaged IPSC amplitudes for 10 min just before LTP or LTD induction compared with averaged IPSC amplitudes during the 10-min period from 10–20 min after manipulation. Paired-pulse ratios (50 ms interstimulus interval) and coefficient of variation were measured over 10 min epochs of 10-30 IPSCs each. The paired pulse ratio was calculated using the average value for all IPSC2 amplitudes was divided by the average value for the corresponding IPSC1 amplitudes and reported as the mean paired pulse ratio for that epoch. $1/CV^2$ was determined by dividing the mean amplitude of IPSCs squared recorded over 10 minute epochs by the mean variance of these IPSCs.

For RTPP and suppression of feeding tasks: time spent in each chamber, number of visits to each chamber, time spent immobile, number of immobile episodes, distance traveled, and velocity were compared across experimental groups. Trials were recorded and scored using EthoVision Software and test values were normalized to pretest values for each mouse. Data were analyzed in GRAPHPAD Prism using one-way or two-way analysis of variance (ANOVA) with differences

between groups determined by post-hoc analysis of significant F values using Sidak's test or Bonferroni test to correct for multiple comparisons. P values less than 0.05 were considered significant.

2.12 Materials

6 β -naltrexol and 6,7-Dinitroquinoxaline-2,3[1H,4H]-dione (DNQX) were obtained from Sigma-Aldrich. D-2-Amino-5-phosphonopentanoic acid (APV), bicuculline, SR48692, [D-Ala², NMe-Phe⁴, Gly-ol⁵]-enkephalin (DAMGO), forskolin, and naloxone were obtained from Tocris. Strychnine was obtained from Tocris or Abcam.

CHAPTER 3

Synaptic Plasticity at Inhibitory Synapses in the VTA Depends Upon Stimulation Site

3.1 INTRODUCTION

The VTA contains dopaminergic cells that receive inhibition from GABAergic cell bodies originating within the VTA and from many other brain regions (Watabe-Uchida et al., 2012, Beier et al., 2015). Despite a wealth of anatomical and behavioral studies investigating the diversity of VTA afferents (Beier et al., 2015), historically, plasticity at inhibitory synapses was described without identification of the presynaptic partner. The idea that plasticity is segregated to specific populations is not a new one, and in fact, many reports segregate experiments by postsynaptic cell identity. For example, long-term depression (LTD) induced by low frequency afferent stimulation is only expressed in putative dopamine cells in the VTA that express large H currents (I_h) (Dacher and Nugent, 2011). With local electrical stimulation in acute slices, identity based on neurotransmitter content is usually easier to manipulate than circuit identity. Although the location of the postsynaptic VTA cell (e.g. medial vs. lateral VTA) can sometimes predict output site, inputs from over 20 brain regions contact dopamine cells in all VTA subregions (Beier et al., 2015). It is also possible that there are other plasticity mechanisms that have yet to be uncovered because their expression is limited to a subset of inputs, and therefore not apparent with global activation of all inputs. Here I use different electrical stimulation sites, and report two ways of inducing LTP at inhibitory synapses in the VTA with a mechanism(s) that is non-overlapping with that of LTP_{GABA} or other known forms of LTP at inhibitory synapses in the VTA.

3.2 RESULTS

3.2.1 Location of electrical stimulation determines expression of synaptic plasticity

Most reports examining synaptic plasticity in the VTA use a stimulating electrode placed within the VTA rostral to the recorded cell in a horizontal slice (Figure 1A). This approach has been assumed to randomly sample the synaptic inputs onto cells within the VTA. I hypothesized that stimulating caudal to and outside of the VTA might bias the inputs differently than with a rostral placement (Figure 1A). I refer to this as “caudal” stimulation. I recorded IPSCs in putative dopamine cells identified by a large I_h and compared synaptic properties using either caudal or rostral electrical stimulation. I did not detect any differences in the onset delay, rise slope, or time of peak amplitude of IPSCs between rostral and caudal stimulation (Figure 1B-D; rostral vs. caudal onset delay: $p = 0.82$; rise slope: $p = 0.74$; time of peak: $p = 0.98$; rostral: $n = 15$ cells, caudal: $n = 18$ cells). Opioids depress GABAergic inhibition in the VTA, therefore I compared the opioid-sensitivity of caudal and rostral-stimulated IPSCs. IPSCs from both stimulating locations were depressed by $1 \mu\text{M}$ [D-Ala², N-MePhe⁴, Gly-o]-enkephalin (DAMGO) to the same degree (data not shown; rostral = $42.9 \pm 9.2\%$ of baseline, $n = 6$ cells; caudal = $42.2 \pm 9.4\%$ of baseline, $n = 13$ cells; $p = 0.96$). Thus, synaptic properties were similar when stimulating either the rostral or caudal site.

I then used a stimulation protocol known to induce the nitric oxide-dependent LTP_{GABA} : high frequency stimulation (HFS) consisting of two 100 Hz tetani separated by 10 seconds. LTP_{GABA} is dependent on NMDA receptor (NMDAR) activation that leads to the release of nitric oxide and activation of a signaling cascade that increases presynaptic GABA release (Nugent et al., 2007). When stimulating caudally, HFS resulted in LTP with $100 \mu\text{M}$ NMDAR antagonist, APV, in the bath solution (Figure 2A,C-D; $p < 0.05$, $n = 17$ cells). Conversely and consistent with prior results, the same tetanus of a rostrally-placed electrode did not potentiate IPSCs in APV (Figure 2B-D; $p = 0.79$, $n = 5$ cells). Potentiation after HFS of the caudally-stimulated electrode was correlated

with a decrease in paired pulse ratio and an increase in normalized $1/CV^2$ values (Figure 2E,F; $p < 0.05$, $n = 12$ cells and $p < 0.05$, $n = 11$ cells, respectively). This finding supported my hypothesis that electrode placement may activate different subsets of synapses and lead to a different outcome when performing protocols to induce synaptic plasticity.

3.2.2 Low frequency stimulation potentiates caudal-evoked inhibitory inputs

Inhibitory synapses can be regulated bidirectionally by different afferent stimulation patterns. In an earlier study, low frequency stimulation (LFS) of afferents by a stimulating electrode placed rostral to the VTA cell being recorded was used to elicit LTD of inhibitory synapses in the VTA. LTD was induced by an LFS protocol that consisted of 6 minutes of 1 Hz afferent stimulation while voltage clamping the postsynaptic cell at -40 mV (Dacher and Nugent, 2011). LFS-induced LTD occurs independently of NMDAR activation and is partially blocked by a dopamine D2 receptor antagonist (Dacher and Nugent, 2011). Given the surprising result with HFS of a caudally-placed electrode, I asked whether LFS of a caudally-placed stimulating electrode would induce LTD. Instead, LFS of caudally-evoked IPSCs triggered LTP, both in the absence or presence of APV (Figure 3A-D; $p < 0.05$, $n = 38$ cells). PPR was not significantly altered in cells potentiating after LFS (Figure 3E; $p = 0.06$, $n = 22$ cells) and neither were the normalized $1/CV^2$ values (Figure 3F; $p = 0.09$, $n = 19$ cells). This surprising finding led me to believe that, as with HFS-induced LTP, previous observations of LTD following LFS were dependent upon activation of a subset of VTA afferents.

3.2.3 LFS of optically-evoked inhibitory inputs in the VTA does not induce plasticity

This observation brought up the question – is LTD the predominant outcome when performing LFS at GABAergic synapses in the VTA? One way to probe this question would be to use a

technique that activates GABAergic synapses concurrently, such as with genetic expression of an activating opsin in VGAT-positive synapses such as the BAC transgenic mouse line, VGAT-ChR2(H134R)-EYFP (Zhao et al., 2011). When using optogenetics to activate GABAergic inputs, LFS could result in a net effect of LTD, LTP, or no plasticity. For these experiments, whole field LED illumination of the slice was used to activate inhibitory inputs. After generating a stable 10 minute baseline of light-evoked IPSCs, optical LFS was paired with depolarization to -40 mV of the postsynaptic cell. The mean light-evoked IPSC amplitude was unchanged after optical LFS (Figure 4A-C; $p = 0.83$, $n = 7$ cells). PPR was not significantly altered after LFS (data not shown; $p = 0.97$, $n = 7$ cells) and neither were the normalized $1/CV^2$ values (data not shown; $p = 0.95$, $n = 7$ cells).

3.2.4 Forskolin potentiation does not occlude LFS-induced LTP

Another report of synaptic plasticity in the VTA was described using forskolin, an activator of adenylyl cyclase. Forskolin potentiates GABAergic synapses in the VTA (Melis et al., 2002, Nugent et al., 2009) as well as at many excitatory and inhibitory synapses throughout the CNS (Briggs et al., 1988, Greengard et al., 1991, Cameron and Williams, 1993, Chavez-Noriega and Stevens, 1994, Huang and Kandel, 1994, Weisskopf et al., 1994, Bonci and Williams, 1996, Salin et al., 1996, Bonci and Williams, 1997, Huang and Kandel, 1998, Castro-Alamancos and Calcagnotto, 1999, Linden and Ahn, 1999, Mellor et al., 2002). Both prior reports looking at forskolin when stimulating GABAergic VTA afferents used rostral electrical stimulation. I tested whether forskolin would also potentiate inputs evoked with caudal afferent stimulation or if these synapses would again be distinct from other VTA synapses. I found that 10 μ M forskolin potentiates IPSCs stimulated with a caudally-placed electrode (Figure 5A-C; $p < 0.05$, $n = 14$ cells), although PPR was not significantly altered after forskolin (data not shown; $p = 0.64$, $n = 13$ cells). Forskolin-induced potentiation occludes NMDAR-dependent LTP_{GABA} (Nugent et al.,

2009). Therefore, I performed occlusion experiments to ask if forskolin potentiation occludes caudal LFS-induced LTP. However, forskolin-induced potentiation did not occlude further potentiation by LFS (Figure 5E-F; $p < 0.05$, $n = 10$ cells). This suggests that the mechanism underlying LFS-induced LTP is distinct from that of forskolin potentiation.

3.2.5 LFS-induced LTP does not require postsynaptic GPCR signaling or increased postsynaptic calcium

Potentiation after LFS was not associated with a significant change in the paired pulse ratio or coefficient of variation, suggesting that the mechanism may reflect an increase in GABAergic signaling in the postsynaptic cells. Many, even most, forms of potentiation are triggered by increases in calcium concentration in the postsynaptic cell, and so I tested whether LFS-LTP required a rise in postsynaptic calcium. When the concentration of the calcium buffer, EGTA, was raised to 15mM in the patch pipette, LFS still potentiated caudally-evoked IPSCs (Figure 6A-C; $n = 5$ cells). An alternative postsynaptic mechanism might require activation of receptors on the postsynaptic cell other than GABA_A receptors. For example, the report of LFS-LTD found that depression was partially dependent upon dopamine D2 receptors, which are coupled to the G_i subtype of GPCRs. When I included an inhibitor of GPCR activity (1 mM GDP- β -S) in the patch pipette to inhibit all postsynaptic GPCR signaling, LFS still potentiated caudally-evoked IPSCs (Figure 6D-F; $n = 4$ cells).

3.3 DISCUSSION

Most reports describing synaptic plasticity in the VTA used electrical stimulation that does not address the possibility of circuit-specificity that can now be probed using optogenetic tools. The data above provide evidence that electrical stimulation in horizontal midbrain slices preferentially activates subsets of inputs rather than sampling the entire population randomly. Furthermore, some inhibitory synapses in the VTA have different requirements for inducing LTP depending on the placement of the stimulating electrode. Specifically, I found that using a caudal stimulation site with either low or high frequency stimulation induces LTP independently of NMDAR activation.

Synaptic plasticity induction

Using the same stimulation protocol but with the electrode at a site that deviated from the common placement I serendipitously discovered that I could induce NMDAR-independent LTP using either HFS or LFS. Pairing postsynaptic cell depolarization with afferent stimulation, to substitute for a strong tetanus, is a classic approach used to induce LTP in the hippocampus (Nicoll, 2017). However, this method for inducing LTP is generally due to NMDAR activation. Conversely, robust LFS-induced LTP in the VTA was induced in the presence of an NMDAR antagonist. Previously described LFS-LTD in the VTA is also NMDAR-independent (Dacher and Nugent, 2011). The biggest question that arises from these results is how the same patterning of afferent stimulation results in opposite synaptic plasticity outcomes. One likely explanation is that different electrode locations preferentially activate different subsets of synapses in the VTA. The VTA dopamine cells are innervated by both local GABA neurons and GABA projections originating in regions throughout the brain that may differ in protein expression leading to different forms of synaptic plasticity. Another possibility is that the timing of inputs differs when using the two stimulating electrode locations; however, I did not observe a significant difference in onset delay, rise slope, or time of peak amplitude of IPSCs from caudal vs. rostral.

Low frequency stimulation and synaptic plasticity

With electrical stimulation protocols, the resulting effect on synapses is generally unidirectional (either LTP or LTD), although there are exceptions to every rule, for example, HFS of mossy fiber synapses varies outcome depending on postsynaptic cell type and prior activation of metabotropic glutamate receptor 7 (Pelkey et al., 2005). While numerous studies have shown that LFS induced LTD (Bear and Malenka, 1994, Gutlerner et al., 2002), there are fewer instances where LFS induced LTP and these generally required pairing with strong depolarization to activate NMDAR (Bonci and Malenka, 1999, Lante et al., 2006). Here, I found that LFS potentiates VTA GABA synapses with mild depolarization and LFS that did not require NMDAR activation. This seems to be a rare mechanism at CNS synapses. One other example is at the excitatory synapse from lateral perforant path to dentate gyrus cells, where LFS also potentiates synapses independently of NMDAR activation (Gonzalez et al., 2014). However, to my knowledge, mine is the first report of LTP at GABAergic synapses elicited by LFS.

Afferent sources to the VTA

Exposure to drugs of abuse causes LTP at excitatory synapses (Ungless et al., 2001, Saal et al., 2003) and blocks LTP_{GABA} in the VTA (Nugent et al., 2007, Niehaus et al., 2010) and the net result of these drug-induced changes is thought to be increased dopamine cell firing via enhanced excitatory drive and disinhibition. However, if more types of synaptic plasticity exist than these previously suspected, the effects of drugs of abuse on VTA afferents probably have a more intricate effect on dopamine cell firing. LTP_{GABA} is expressed at VTA_{GABA}→VTA but not at RMTg_{GABA}→VTA synapses and it is likely that HFS- and LFS- induced LTP are only expressed at a subset of inputs. In addition to the RMTg, the dorsal raphe, PAG, pedunculo pontine nucleus,

and LDT send inhibitory projections and are located caudal to the VTA (Beier et al., 2015, Faget et al., 2016, Omelchenko and Sesack, 2010, Ntamati et al., 2018). Given the placement of the caudal electrode in my experiments, it is possible that the synapses from these experiments in Chapter 3 are from one of these caudal brain regions, although it is alternatively possible that regions located elsewhere in the brain send projections that pass through the caudal stimulation location. In the next chapter, I will try to identify the region(s) that expresses LFS-LTP. Based on my results, I hypothesized that the RMTg was the main source of potentiating inputs.

FIGURE 3-1. Electrical stimulation in horizontal midbrain slices

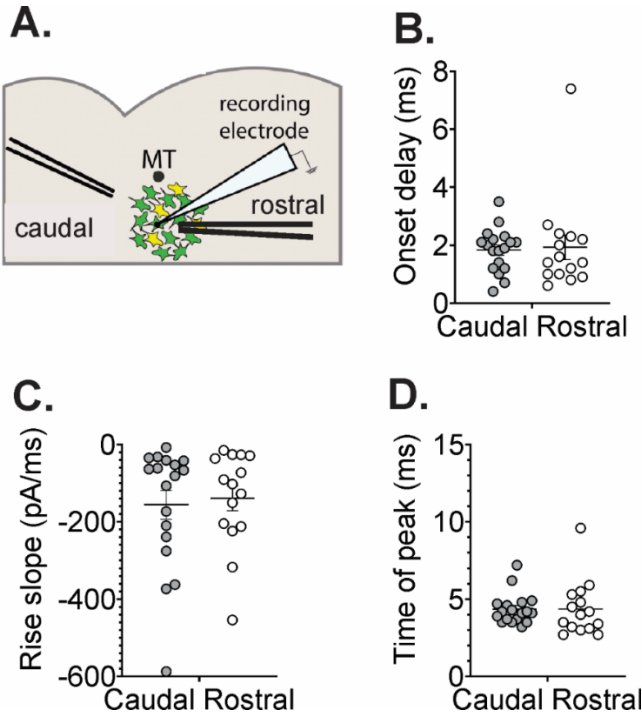


FIGURE 3-1. Electrical stimulation in horizontal midbrain slices

A. Recording setup using “caudal” or “rostral” placements of a bipolar stimulating electrode. **B.** Analysis of caudal vs. rostral IPSC onset delay, **C.** rise slope, and **D.** time of peak amplitude.

Error bars represent standard error of the mean (S.E.M)

34FIGURE 3-2. Location of electrical stimulation determines expression of synaptic plasticity

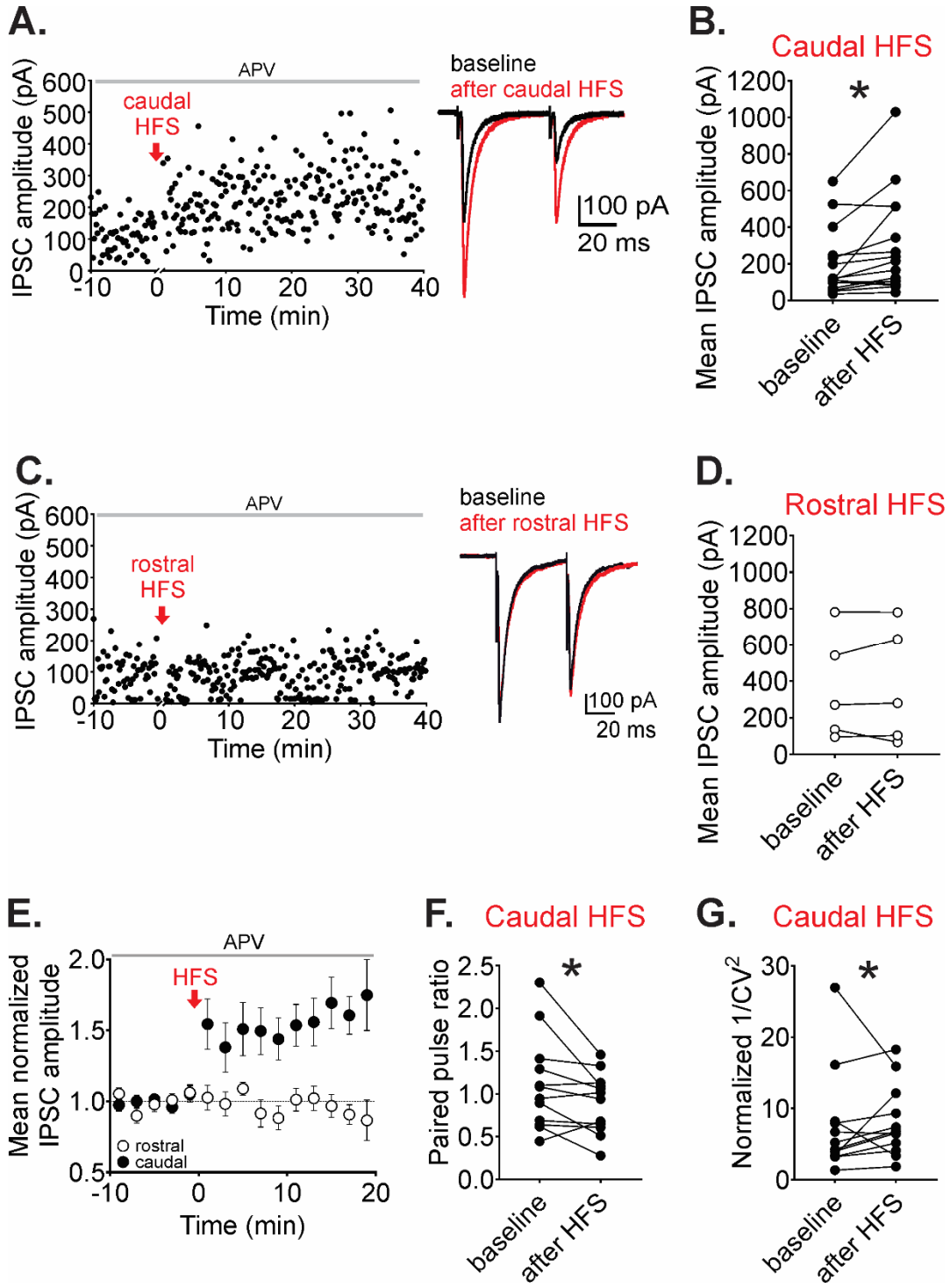


FIGURE 3-2. Location of electrical stimulation determines expression of synaptic plasticity

A. Representative experiment with HFS of a caudal electrode. Inset: baseline (black traces) and 10-20 min after HFS (red traces). **B.** Mean IPSC amplitudes from a 10 min baseline to 10-20 min after caudal HFS (n = 5 cells). **C.** Representative experiment with HFS of a rostral electrode. Inset: baseline (black traces) and 10-20 min after HFS (red traces). **D.** Mean IPSC amplitudes from a 10 min baseline to 10-20 min after rostral HFS (n = 17 cells). **E.** Time course of averaged IPSC amplitudes before and after HFS. **F.** Paired pulse ratios before and after caudal HFS from each cell that potentiated >10% of basal values (n = 12 cells). **G.** Normalized $1/CV^2$ values before and after caudal HFS from each cell that potentiated >10% of basal values (n = 11 cells).

**p < .05, paired t-test of amplitude of 10 min baseline vs. 10-20 min after HFS.*

Error bars represent S.E.M

FIGURE 3-3. Low frequency stimulation of caudal electrode induces LTP

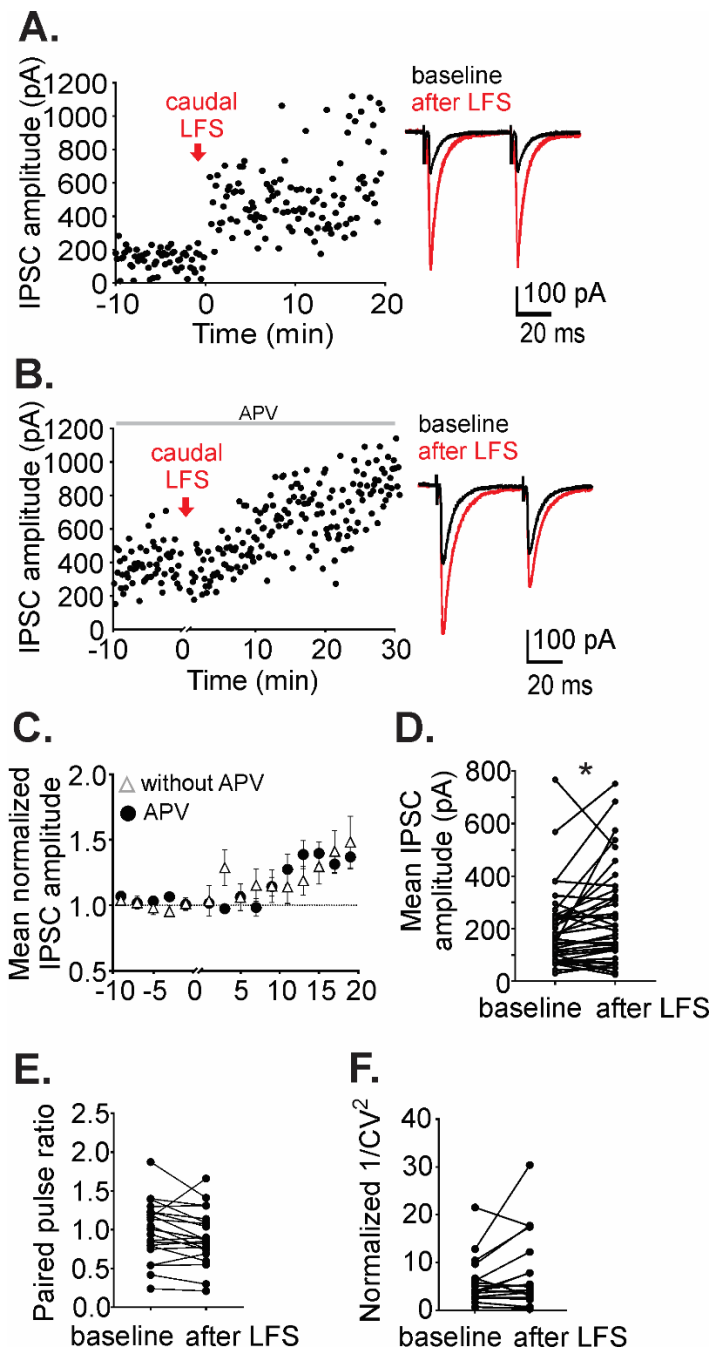


FIGURE 3-3. Low frequency stimulation of caudal electrode induces LTP

A. Representative experiment with LFS of a caudal electrode without APV or **B.** with APV. Inset: baseline (black traces) and 10-20 min after LFS (red traces). **C.** Time course of averaged IPSC amplitudes before and after LFS. **D.** Mean IPSC amplitudes from a 10 min baseline to 10-20 min after caudal LFS (n = 38 cells). **E.** Paired pulse ratios before and after caudal LFS from each cell that potentiated >10% of basal values (n = 22 cells). **F.** Normalized $1/CV^2$ values before and after caudal LFS from each cell that potentiated >10% of basal values (n = 19 cells).

**p < .05, paired t-test of amplitude of 10 min baseline vs. 10-20 min after LFS.*

Error bars represent S.E.M

FIGURE 3-4. No effect with low frequency optical stimulation of VGAT⁺ synapses

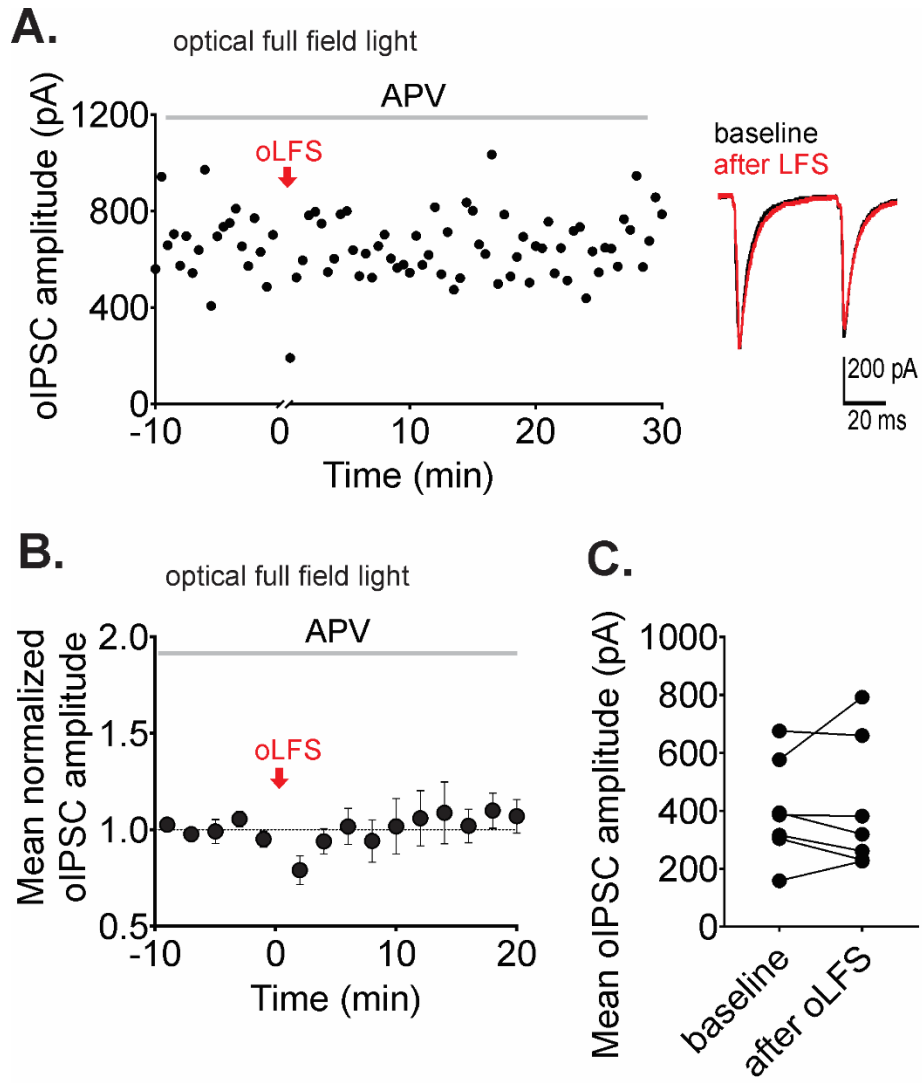


FIGURE 3-4. No effect with low frequency optical stimulation of VGAT⁺ synapses

A. Representative experiment with optical LFS. Inset: baseline (black traces) and 10-20 min after LFS (red traces). **B.** Time course of averaged IPSC amplitudes before and after LFS. **C.** Mean IPSC amplitudes from a 10 min baseline to 10-20 min after optical LFS (n = 7 cells).

Error bars represent S.E.M

FIGURE 3-5. Forskolin potentiation does not occlude LFS-induced LTP

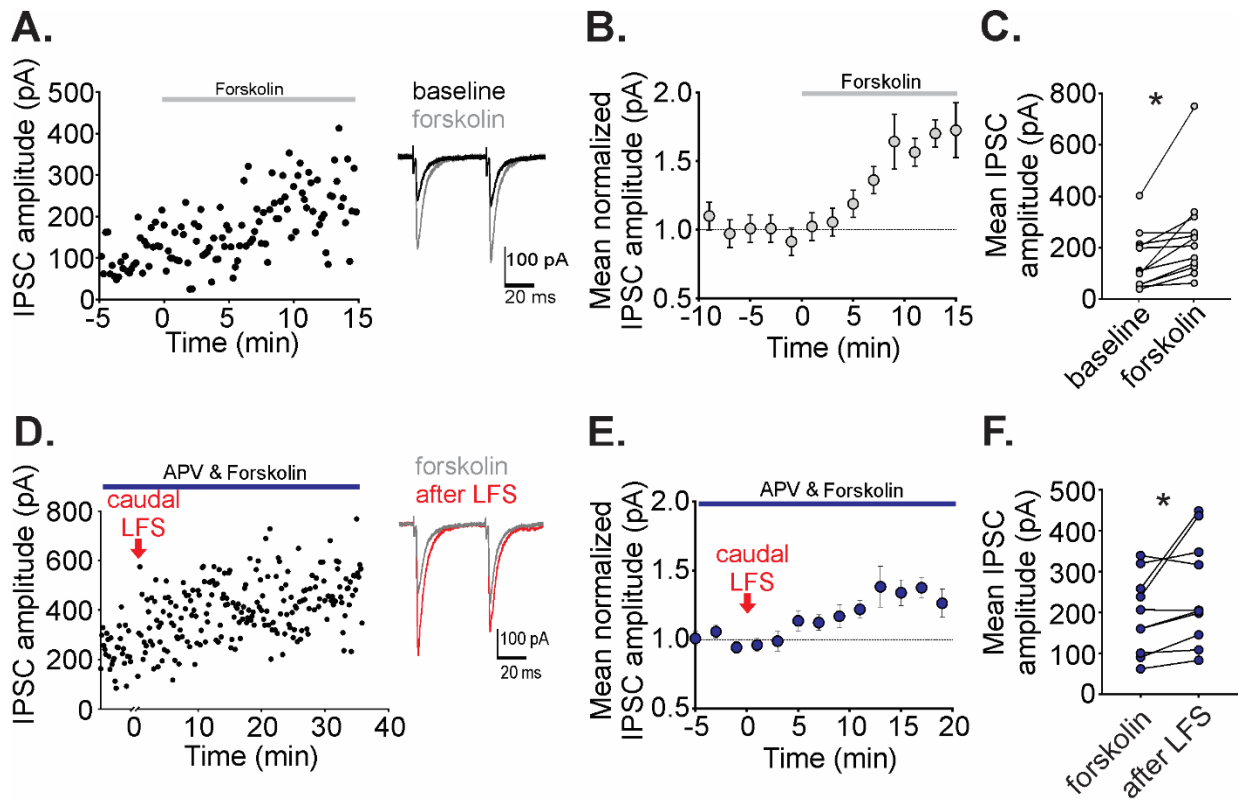


FIGURE 3-5. Forskolin potentiation does not occlude LFS-induced LTP

A. Representative experiment with 10 μ M forskolin. Inset: baseline (black traces) and in forskolin (gray traces). **B.** Time course of averaged IPSC amplitudes before and after forskolin. **C.** Mean IPSC amplitudes from a 10 min baseline to 10-20 min after forskolin (n = 14 cells). **D.** Representative experiment with caudal LFS in the presence of 10 μ M forskolin. Inset: baseline in forskolin (gray traces) and 10-20 min after LFS (red traces). **E.** Time course of averaged IPSC amplitudes before and after caudal LFS in forskolin. **F.** Mean IPSC amplitudes from a 10 min baseline to 10-20 min after forskolin (n = 10 cells).

**p < .05, paired t-test of amplitude of 10 min baseline vs. 10-20 min after forskolin or LFS.*

Error bars represent S.E.M

FIGURE 3-6. LFS-induced LTP does not require postsynaptic GPCRs or increased calcium

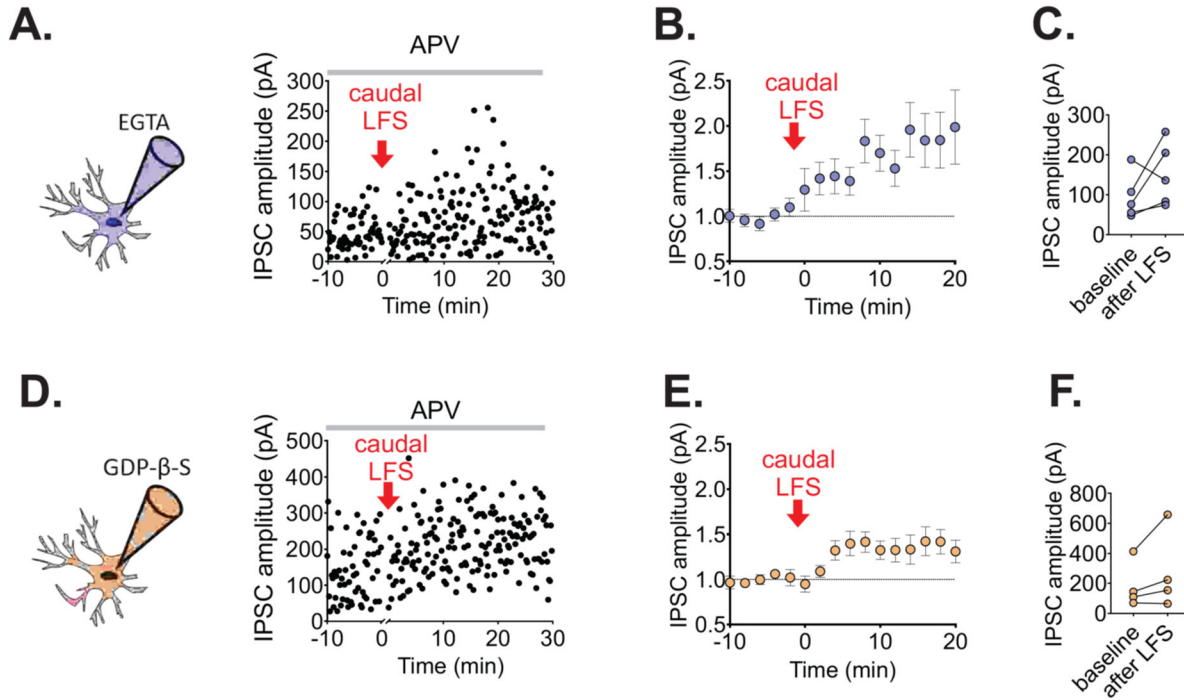


FIGURE 3-6. LFS-induced LTP does not require postsynaptic GPCRs or increased calcium

A. Representative experiment with caudal LFS when EGTA concentration was raised to 15 mM in the patch pipette intracellular solution. **B.** Time course of averaged IPSC amplitudes before and after caudal LFS with 15 mM EGTA. **C.** Mean IPSC amplitudes from a 10 min baseline to 10-20 min after caudal LFS with 15 mM EGTA (n = 5 cells). **D.** Representative experiment with caudal LFS when 1 mM GDP- β -S was included in the patch pipette intracellular solution. **E.** Time course of averaged IPSC amplitudes before and after caudal LFS with 1 mM GDP- β -S. **F.** Mean IPSC amplitudes from a 10 min baseline to 10-20 min after LFS with 1 mM GDP- β -S (n = 4 cells).

**p < .05, paired t-test of amplitude of 10 min baseline vs. 10-20 min after LFS.*

Error bars represent S.E.M

CHAPTER 4

RMTG AND PAG INHIBITORY AFFERENTS TO THE VTA

4.1 INTRODUCTION

The unusual finding of LTP with LFS was particularly interesting to me because it suggested that afferent inputs are differentially altered by the same stimulation pattern, specifically, when afferent firing is reduced to very low rates. Opioids greatly reduce GABA cell firing to a range that could possibly be sufficient to trigger this form of synaptic plasticity. Therefore, I wanted to know which afferent inputs are potentiating with LFS, as this may reflect what naturally happens in the presence of opioids.

One major source of GABAergic inhibition to the VTA originates in a neighboring midbrain region, the RMTg (Jhou et al., 2009b). The RMTg extends dorso-caudally from the VTA and because of this location, I first thought that fibers being stimulated with the caudal electrode location might originate in the RMTg. In addition, another group used a very similar electrode location to study putative RMTg IPSCs in VTA dopamine cells in horizontal brain slices (Lecca et al., 2012b). Several groups have documented how the RMTg receives excitatory glutamatergic projections from the lateral habenula that are required for behavioral responses reflecting strong aversion, including passive, active and conditioned avoidance (Stamatakis and Stuber, 2012, Jhou et al., 2009a). The aversive nature of this stimulation results in part from inhibition by the RMTg cells of the VTA dopamine cells they innervate (Jhou et al., 2009a, Hong et al., 2011). A defining feature of RMTg_{GABA}→VTA synapses is that they are robustly depressed by mu opioid receptor (MOR) activation (Matsui and Williams, 2011, Matsui et al., 2014), more than other sources of GABAergic inhibition in the VTA, including local VTA interneurons and nucleus accumbens projections (Matsui et al., 2014), and strongly regulate VTA dopamine cell firing (Jalabert et al., 2011). Surprisingly, these synapses do not express LTP_{GABA} (Simmons et al., 2017, Polter et al., 2018), a form of potentiation that is blocked by morphine (Nugent et al., 2007) even though the RMTg is a robust, opioid-sensitive connection to the VTA. It is also unknown whether RMTg_{GABA}→VTA

synapses can express other forms of synaptic plasticity, such as LTD (Dacher and Nugent, 2011, Dacher et al., 2013). Here I used an optogenetic approach to assess the effect that LFS has on $RMT_{GABA} \rightarrow VTA$ synapses and find that, surprisingly, they do not potentiate, suggesting that they are not the input being stimulated by the caudal electrode. Instead, I find that the GABAergic input from the ventral PAG (vPAG) potentiates with LFS.

4.2 RESULTS

4.2.1 Long-term depression of RMTg_{GABA}→VTA synapses with LFS

I hypothesized that RMTg synapses exhibit LTP after LFS based on my findings with caudal stimulation. I used a viral-targeting strategy with optogenetics to selectively drive RMTg afferents in acute midbrain slices, injecting an adeno-associated virus into the RMTg of a VGAT-IRES-Cre mouse to express channelrhodopsin (AAV2-DIO-ChR2-mCherry). To validate that the viral injections selectively targeted RMTg GABAergic cells, I used FoxP1 immunostaining (Lahti et al., 2016) and saw strong co-expression of FoxP1 with the virally-induced fluorescent reporter (Figure 1A). Several weeks after viral injection, I prepared acute midbrain slices. For all LFS experiments I targeted cells identified by a large I_h (Ungless and Grace, 2012, Baimel et al., 2017, Edwards et al., 2017). Recording from dopamine cells while blocking AMPA and glycine receptors, ChR2-mediated IPSCs (oIPSCs) were evoked using brief LED pulses. After establishing a stable baseline of oIPSCs, delivery of optical low-frequency stimulation (oLFS: 1 Hz, 6 minutes during depolarization to -40 mV) modestly depressed RMTg GABAergic oIPSCs (Baseline 353.6 ± 59.3 pA, 10-20 min after oLFS 294.8 ± 68.7 pA; $t = 2.673$, $p = 0.018$, $n = 15$ cells; Figure 1B-E). Depression after oLFS did not affect the paired pulse ratio (Baseline 0.9 ± 0.1 , 10-20 min after oLFS 1.1 ± 0.1 ; $t = 2.078$ $df=10$, $p = 0.064$ $n = 11$ cells, Figure 1F). Furthermore, this LTD occurred independently of NMDAR activation (Figure 1B-C), similarly to the previously reported LFS-LTD_{GABA} (Dacher and Nugent, 2011). Therefore, these data do not support my original hypothesis that the RMTg fibers potentiate with LFS, as did IPSCs evoked caudally.

4.2.2 Electrical HFS of caudal placed electrode with RMTg_{GABA}→VTA synapses

In the previous chapter, I also demonstrated that HFS of caudal electrode potentiated inhibitory inputs in an NMDAR-independent manner. The frequency of HFS (100 Hz), however, is higher

than most opsins can reliably evoke action potentials. Therefore, I combined light-induced activation of isolated RMTg inputs with electrically-induced unidentified IPSCs using a caudally-placed electrode in the same whole-cell recording. IPSCs and oIPSCs were evoked in an alternating fashion with 15 seconds separating each IPSC and oIPSC. After generating a stable baseline of the RMTg oIPSCs, I performed HFS of the electrically evoked IPSCs (eHFS). This resulted in a trending nonsignificant increase of RMTg oIPSCs (Figure 2A-D; baseline 373 ± 81 pA, 10-20 min after eHFS 463 ± 110 pA; $t = 2.18$, $p = 0.065$, $n = 8$ cells). A tetanus of 10Hz light stimulation with equal number of pulses as eHFS had no effect on RMTg oIPSCs (forskolin data not shown, $p = 0.55$, $n = 10$ cells). RMTg synapses were capable of potentiating with bath application of forskolin (Figure 2E-F, baseline 586 ± 151 pA, 10-20 min after $10 \mu\text{M}$ forskolin 894 ± 261 pA, $p = 0.044$, $n = 6$ cells), as previously reported (Simmons et al., 2017).

4.2.3 VTA-projecting vPAG GABA cells are candidates for expressing LFS-LTP

After finding that RMTg synapses appear to express the canonical LFS-LTD rather than LTP, I identified other candidate regions that could express the unusual LTP that I found with LFS as discussed in Chapter 3. In order to identify afferent regions that express LFS-LTP, I first used a sledgehammer approach with optogenetics to target several caudal afferent regions in the same brain. With these experiments, channelrhodopsin was expressed pan-neuronally using the human synapsin (hsyn) promoter and injected in three regions spanning the ventral-dorsal axis about 1 mm caudal to the VTA. When I prepared brain slices from these mice and performed oLFS of light-evoked IPSCs, I occasionally saw LTP (data not shown). Experiments in which I saw LTP tended to include strong viral expression in the PAG, and those that did not have LTP sometimes did not include the PAG. Therefore, I hypothesized that the PAG may be one afferent region that expressed LFS-LTP.

The PAG sends both glutamatergic and GABAergic projections to the VTA (Omelchenko and Sesack, 2010, Ntamati et al., 2018, Faget et al., 2016). The PAG is required for diverse opiate

actions, as morphine administration into the PAG produces analgesia (Jensen and Yaksh, 1989, Lewis and Gebhart, 1977, Mayer et al., 1971), opioid receptor antagonists in the PAG precipitate morphine withdrawal (Laschka and Herz, 1977), and microinjections of morphine into either the PAG or the VTA are sufficient to induce conditioned place preference (Olmstead and Franklin, 1997). Analgesia is most profound when morphine is locally targeted to the caudal portion of the ventrolateral region (Yaksh et al., 1976). Because of this involvement of the PAG in opioid-related behaviors, a link between the PAG and VTA is of great interest as a potential locus for persistent changes induced by opioids, however, very little is known about these projections. PAG innervation of the VTA corresponds with the columnar organization of the PAG; dorsal PAG has very sparse, if any, VTA projections compared to ventral subdivisions (Ntamati et al., 2018). Therefore, I first investigated some of the basic properties of GABAergic VTA-projecting vPAG cells. I injected green retrobeads unilaterally into the VTA of a VGAT-cre;Tdtomato mouse and several weeks later prepared coronal sections containing the vPAG. I recorded from retrobead- and VGAT-positive cells in the vPAG (Figure 3A). I found that VGAT⁺ cells in PAG slices fired spontaneously in vitro (8.1 ± 1.1 Hz, $n = 3$ cells, data not shown) in a range similar to that reported in vivo (Tovote et al., 2016). VTA-projecting vPAG_{GABA} cells fired action potentials in response to trains of current stimulation at 20 and 40 Hz and went into depolarization block at 60 Hz (Figure 3B). In one cell, I found that saw that bath application of 1 μ M DAMGO hyperpolarized and halted spontaneous firing (Figure 3C).

4.2.4 vPAG_{GABA}→VTA synapses display an unusual form of LTP with LFS

To study synaptic inputs from the vPAG to the VTA, I injected AAV2/9-hsyn-ChR2-EYFP (AAV-hsyn-ChR2) unilaterally into the vPAG of wildtype or DATxtdTomato mice to infect all PAG neuronal cell types (Figure 4A,L). I noted both glutamatergic and GABAergic-mediated currents were present in VTA dopamine cells, as described previously (Ntamati et al., 2018). For plasticity

experiments, GABA-mediated currents were pharmacologically isolated with DNQX, APV, and strychnine during afferent stimulation in VTA dopamine cells in response to LED light pulses. These oIPSCs were abolished with bath application of the GABA receptor antagonist, bicuculline ($p = 0.028$, $n = 3$ cells; Figure 4B). I used the same oLFS protocol used to induce LTD in RMTg inputs to determine if vPAG_{GABA} terminals in the VTA express LFS-LTP_{GABA}. Optical LFS of vPAG GABAergic oIPSCs triggered robust LTP (baseline 382.9 ± 58.2 pA, 10-20 min after oLFS 572.8 ± 115.5 pA; $t = 2.545$, $p = 0.023$, $n = 15$ cells; Figure 4C-E), in direct contrast to the LTD observed after oLFS at RMTg_{GABA}→VTA synapses and instead fitting with the experiments using a caudal electrode. I also noted a marked reduction of the vPAG→VTA oIPSC upon exposure to a MOR agonist [D-Ala², N-MePhe⁴, Gly-ol]-enkephalin (1 μ M DAMGO; Figure 4C, see also Figure 8). Potentiation after oLFS was correlated with a significant decrease in the paired pulse ratio (baseline: 1.3 ± 0.2 , 10-20 min after oLFS 1.0 ± 0.1 , $t = 2.48$, $p = 0.0325$, $n = 11$ cells; Figure 4F). Therefore, I next tried to understand the underlying mechanism that was responsible for LFS-LTP of vPAG_{GABA}→VTA synapses.

4.2.5 Possible mechanisms of LTP of vPAG_{GABA}→VTA synapses

GABAergic inputs onto dopamine cells in the neighboring substantia nigra pars compacta undergo LTP in the presence of the neuropeptide, neurotensin and induction is prevented in the presence of neurotensin 1 receptor antagonist, SR48692 (Tschumi and Beckstead, 2018). The PAG contains large dense core vesicles, indicating the presence of peptides (Omelchenko and Sesack, 2010) and there is immunohistochemical evidence for the existence of neurotensin in PAG cells that project to the raphe magnus (Beitz et al., 1983). Therefore, I tested the hypothesis that LFS-LTP of vPAG_{GABA}→VTA synapses is a result of neurotensin receptor 1 activation in the VTA. When I included 10 μ M SR48692 in the bath solution for the duration of the experiment, oLFS still resulted in LTP of oIPSCs (baseline: 311 ± 104 pA, 10-20 min after oLFS 464 ± 115 pA, $n = 6$ cells; Figure 5A-C). Potentiation after oLFS was correlated with a trending decrease in the

paired pulse ratio (baseline: 1.12 ± 0.10 , 10-20 min after oLFS 0.98 ± 0.08 , $t = 2.1$, $p = 0.1$, $n = 5$ cells; Figure 5D). Therefore, neurotensin receptor 1 activation was not required for induction of LTP. The potentiation here and in Figure 4 occurred in the presence of 100 μ M APV, indicating no requirement for NMDARs in LTP induction, however, postsynaptic cell depolarization was needed to induce LTP because oLFS failed to induce LTP when the cell was voltage clamped at -70 mV (Baseline 259.3 ± 122.3 pA, 10-20 min after oLFS 255.2 ± 122.7 pA, $t = 0.5382$, $p = 0.614$, $n = 6$ cells; Figure 5E-G).

The viral strategy used thus far for the PAG inputs, hsyn-ChR2, was different from that used for RMTg experiments. To test if the viral strategy was responsible for the differences between RMTg and PAG with LFS, I used genetic targeting of ChR2 to VGAT⁺ cells in VGAT-cre mice. With oLFS of VGAT⁺ oIPSCs recorded in VTA dopamine cells, LTP was still induced (Baseline 229 ± 32 pA, 10-20 min after oLFS 297 ± 53 pA, $t = 2.23$, $p = 0.053$, $n = 10$ cells; Figure 5H-J). In comparing the normalized magnitude of LTP after oLFS, the only experimental condition that is significantly non-potentiated compared to the original experiment (oLFS with depolarization in hsyn-ChR2 viral-injected mice) is the group without depolarization (Figure 6A). When looking for other determinants of LTP, I found that neither I_h amplitude nor the baseline oIPSC amplitude was predictive of LTP after oLFS (I_h : $p = 0.757$, amplitude: $p = 0.919$, $n = 15$ cells; Figure 6B-C).

4.2.6 vPAG_{GABA}→VTA synapses attenuate dopamine cell firing

My finding of LFS-induced LTP along with prior studies on anatomical and physiological properties of the PAG projection suggests that this VTA afferent is functionally different than the RMTg projection. For example, the PAG sends glutamatergic and GABAergic projections to the VTA where they form synapses on both dopaminergic and GABAergic cells (Omelchenko and Sesack, 2010, Ntamati et al., 2018), while in contrast, the RMTg sends primarily GABAergic afferents that synapse preferentially on dopaminergic cells (Jhou et al., 2009a, Balcita-Pedicino et al., 2011). RMTg synapses inhibit dopamine cell firing, yet the consequence of PAG inhibition on VTA

dopamine cell firing is unknown. Here, I assessed the physiological properties of vPAG GABAergic cells and their influence on VTA dopamine cells. When I expressed the fast channelrhodopsin variant, ChETA, using AAV-DJ-DIO-ChETA-EYFP (AAV-DIO-ChETA) in the vPAG of VGAT-tdTomato mice (Figure 7A) and recorded from VGAT⁺ and ChETA⁺ cells in the vPAG, 20 Hz trains of light caused the cell to depolarize and fire action potentials but action potential fidelity dropped off after 40 Hz stimulation (Figure 7B). In acute midbrain slices, ChETA⁺ terminals could be detected in the VTA adjacent to cells expressing the rate-limiting enzyme of catecholamine biosynthesis, tyrosine hydroxylase (TH) (Figure 7C). I expressed AAV-DIO-ChETA or AAV5-DIO-ChR2 in the vPAG of VGAT-cre mice and recorded from VTA cells in midbrain horizontal slices (ChR2 experiments only, Figure 6D). Ramps of current induced action potential firing in dopamine cells and when alternating ramps with and without a 20 Hz train of LED pulses in the same cell; photostimulation robustly inhibited dopamine cell firing (Figure 7E). Light-evoked inputs originating from the vPAG were comprised of GABA_AR-mediated currents, as evidenced by total blockade of current in the presence of bicuculline (Figure 7E, right panel). Therefore, vPAG_{GABA}→VTA synapses decrease the firing rate of dopamine cells.

4.2.7 Opioids depress vPAG_{GABA}→VTA more than RMTg_{GABA}→VTA synapses

Both the PAG and RMTg are major sites of action for opioids. RMTg cells hyperpolarize in the presence of DAMGO (Matsui and Williams, 2011) and RMTg synapses in the VTA are robustly depressed by opioid receptor activation (Matsui et al., 2014). GABAergic cells in the PAG are also robustly hyperpolarized by opioid receptor activation (Vaughan et al., 2003), however, the effect of opioids on vPAG synapses in the VTA is unknown. I compared the relative suppression of oIPSCs from RMTg or vPAG afferents in VTA dopamine cells by measuring their amplitudes before and after bath application of 1 μM DAMGO (Figure 8A-B). DAMGO potently depressed synapses from both afferents and depression was reversed by 2 μM naloxone. DAMGO depressed vPAG oIPSCs more than RMTg oIPSCs (PAG 12.9 ± 2% of baseline amplitude, n = 6

cells, RMTg $28.7 \pm 5\%$, $n = 7$ cells; $t = 2.67$, $p = 0.022$; Figure 8C-D). DAMGO did not significantly alter the paired pulse ratio for both PAG and RMTg (PAG: baseline = 0.93, DAMGO = 1.07, $p = 0.23$; RMTg: baseline = 0.91, DAMGO = 1.18, $p = 0.29$; Figure 8E). As noted in the synaptic plasticity experiments above, initially, different viral strategies were used to isolate PAG and RMTg inputs for DAMGO experiments and it was possible that this could affect the results. However, when the PAG experiments were repeated with a matching viral strategy (AAV-DIO-ChR2), the PAG values were not significantly different from each other (PAG hsyn vs. PAG VGAT, PAG hsyn: $12.9 \pm 2.5\%$; PAG VGAT: Mean: $20.7 \pm 5.2\%$; $p = 0.17$; Figure 8G). Additionally, a dose response curve using only AAV-DIO-ChR2 data indicated that PAG inputs are more sensitive to DAMGO (Figure 8H).

4.2.8 vPAG_{GABA}→VTA are smaller in amplitude than RMTg_{GABA}→VTA synapses

In addition to the differences in synaptic plasticity and opioid responses, I noticed that the amplitude of oIPSCs from RMTg experiments tended to be larger than those from PAG experiments. Basal synaptic strength is another parameter that will determine the relative ability of a given afferent to modulate VTA cells. Interestingly, our lab previously found that optogenetic stimulation of the RMTg led to very large light-evoked IPSCs, which may mean that it is robustly synapsing on VTA dopamine cells (Polter et al., 2018). One caveat is that large light-evoked responses are not *necessarily* indicative of the strength of the input and could alternatively be explained by tropism for the RMTg regarding channelrhodopsin expression. Comparing the amount of current generated by photostimulation demonstrated that RMTg oIPSCs were significantly larger than vPAG oIPSCs (Kolmogorov-Smirnov test, $p < 0.0001$; RMTg $n = 222$ data points from 28 cells, vPAG $n = 230$ data points from 41 cells; Figure 9). The RMTg oIPSC values are similar to those reported previously (Polter et al., 2018).

4.3 DISCUSSION

Here I report notable differences between RMTg and PAG inhibitory VTA afferents. First, opposing persistent effects on synaptic strength were triggered by LFS of RMTg vs. PAG GABAergic synapses in the VTA. Unexpectedly, LFS of PAG inputs but not RMTg inputs resulted in robust LTP. This is the first report of LTD at RMTg synapses, a prominent source of inhibition for VTA dopamine cells that is implicated in many reward and aversion-related behaviors. This is also the first report of synaptic plasticity at inhibitory PAG→VTA synapses, and the finding of LTP after LFS is highly unusual and one of only a handful of examples of LTP after LFS. I also found that vPAG synapses were depressed more by a MOR agonist than RMTg synapses, making it the most opioid vulnerable inhibitory VTA afferent described to date.

Synapses from the RMTg to the VTA exhibit LTD after low frequency stimulation

As described above, the RMTg input to VTA dopamine cells is a powerful one, producing larger IPSCs on average than comparable optogenetic activation of local GABAergic interneurons in the VTA (Polter et al., 2018) or PAG (Figure 9). Optogenetic targeting of PAG afferents in other studies produces IPSCs in approximately 30% of dopamine cells (Ntamati et al., 2018); I observed responses in about half of my similar recordings. In contrast, optogenetic targeting of RMTg afferents produce more reliable synaptic contacts onto dopamine cells in the VTA (Polter et al., 2018). RMTg cells fire spontaneously at relatively high rates (15-30 Hz; (Jhou et al., 2009a, Hong et al., 2011, Jalabert et al., 2011, Lecca et al., 2011) and changes in synaptic strength at their VTA synapses could therefore powerfully regulate the excitability of dopamine cells. Previous work demonstrated that neither high-frequency afferent stimulation nor a nitric oxide donor applied to optogenetically activated RMTg_{GABA}→VTA synapses elicits LTP, as these stimuli do at other GABAergic VTA synapses (Nugent et al., 2007, Polter et al., 2018, Simmons et al., 2017). Although forskolin can potentiate these synapses (Simmons et al., 2017), other, more

physiological triggers have not been found to increase synaptic strength. A strong inhibitory input like that from RMTg→VTA may not require a large upward dynamic range, and this might account for the absence of available LTP mechanisms at this synapse. My data demonstrate that these synapses can undergo modest LTD after LFS (1 Hz). Furthermore, the strong reduction of this afferent input by DAMGO indicates that in the presence of opioid drugs, RMTg→VTA IPSCs will be decreased, even to levels mimicking the 1 Hz LTD induction protocol, further and more persistently weakening RMTg synapses on dopamine cells. In support of this idea, local delivery of morphine into the RMTg in vivo reduced firing rates in some cells to as low as 1 Hz (Jalabert et al., 2011). There is some evidence to suggest that CB1 receptor activation can also depress RMTg inputs in the VTA, although the duration of the depression beyond 20 minutes is not yet known (Lecca et al., 2012a).

Unique LTP of synapses from the PAG to the VTA after low frequency stimulation

After finding that LFS weakly depressed RMTg_{GABA}→VTA synapses, I discovered that the same protocol instead potentiated vPAG_{GABA}→VTA synapses. This divergence highlights how vital it is to address circuit-specific elements when measuring plasticity. It also provides a likely explanation for my findings in Chapter 3, suggesting that location of electrode placement in a midbrain slice results in biased selection of inputs. To my knowledge, this is the first report of LTP at GABAergic synapses elicited by LFS and suggests that there are still plasticity mechanisms in the VTA that have not yet been identified. As mentioned above, at least with virus-mediated optogenetic activation, the vPAG→VTA afferents do not appear to target every dopamine cell in lateral VTA, and the IPSCs are smaller than those evoked from RMTg. LFS-LTP_{GABA} of vPAG→VTA synapses could upregulate a relatively weak signal to sharply increase its importance in the circuit. Moreover, opiate drugs reduce the firing rate of vPAG cells, normally around 8 Hz, and might reduce the firing rate of these cells into the frequency range that will trigger LTP at their synapses in the VTA.

Differential regulation of inhibition by opioids in the VTA

Opioids do not uniformly depress sources of inhibition, for instance, mu opioid receptor activation has more robust inhibition of RMTg GABAergic synapses than of local VTA interneurons (Matsui et al., 2014). Furthermore, morphine tolerance is afferent-specific, occurring at RMTg→VTA synapses but not VTA or NAc synapses (Matsui et al., 2014). Opioid receptors are widely expressed in the brain and there is plenty of evidence that specific regions contain dense expression compared to others. For example, the PAG is a major site of opioid action, yet even within this structure, the analgesic effects of opioids are limited to the ventrolateral portion. Within the VTA, microinfusion of morphine is rewarding when targeted to the posterior VTA (now known to likely include the RMTg) versus the anterior VTA (Zangen et al., 2002a). The rewarding effects are dependent on MOR activation and can be blocked by concurrent presence of naloxone, a MOR antagonist. The RMTg was reported to be the most opioid-sensitive of VTA GABAergic afferents (Matsui et al., 2014). Here, I found that isolated PAG_{GABA}→VTA synapses were more strongly depressed in the presence of a MOR agonist than isolated RMTg_{GABA}→VTA synapses. While somewhat unsurprising given the literature on opioid responses within the PAG itself, this finding suggests that the PAG to VTA pathway may be important for some opioid-induced changes that lead to maladaptive behavior. Additionally, the heterogeneity of opioid-sensitivity of VTA afferents could indicate that subcircuits are differentially regulated by opioid exposure in a meaningful way. The specific role of the PAG_{GABA}→VTA in mediating aspects of opioid adaptations is one that should be further characterized.

Summary

The ventral tegmental area (VTA) is a major target of addictive drugs, including opiates. Here I investigated the control of VTA dopamine cells by two GABAergic inputs to the VTA, the rostromedial tegmental nucleus (RMTg) and the periaqueductal gray (PAG). I found that when

isolating GABAergic RMTg terminals in the VTA, low frequency stimulation induces long term depression in vitro. Conversely, low frequency stimulation unexpectedly caused long term potentiation of GABAergic PAG terminals in the VTA. PAG inhibitory synapses were profoundly depressed by opioid receptor activation, making the PAG GABAergic cells perhaps the most opioid vulnerable synaptic population innervating the VTA described to date.

FIGURE 4-1. RMTg_{GABA}→VTA synapses exhibit LTD

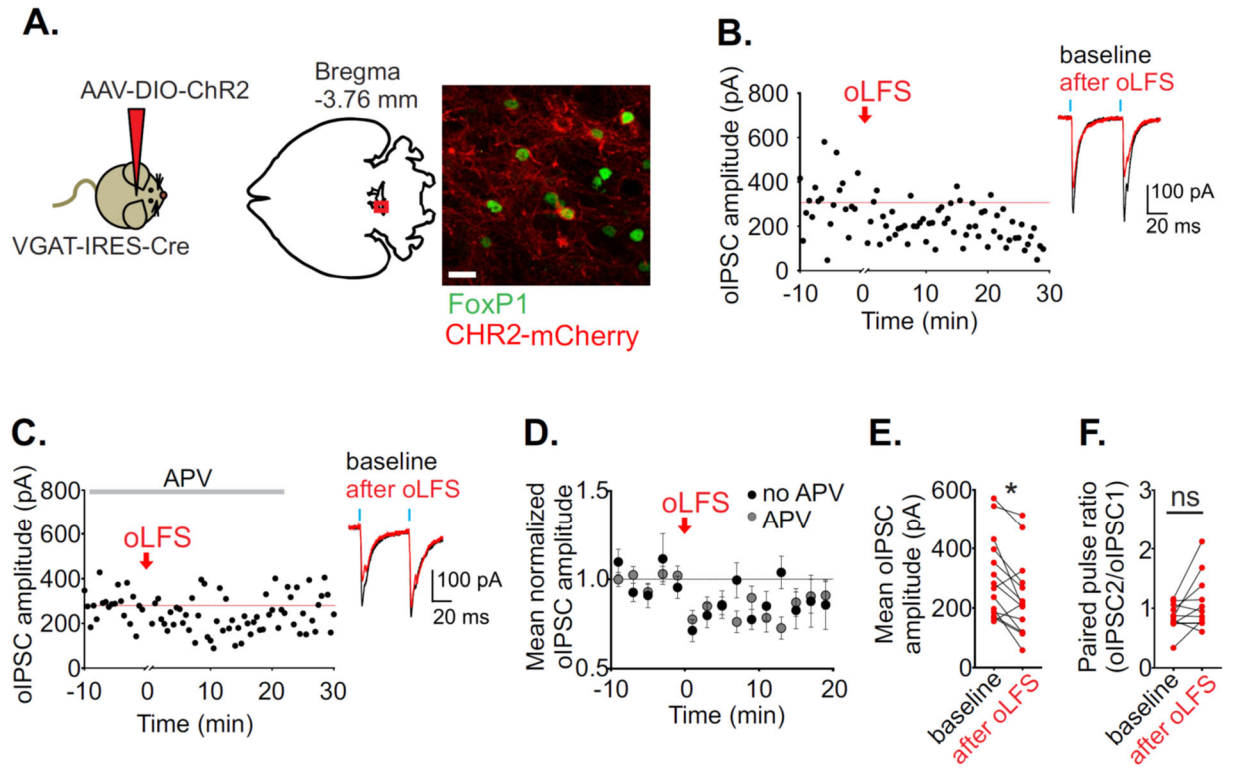


FIGURE 4-1. RMTg_{GABA}→VTA synapses exhibit LTD with LFS

A. Schematic of viral injection (left panel) and representative image of ChR2-mCherry expression in the RMTg overlapped with FoxP1 immunostaining (right panel). Scale bar = 20 μm. Red arrow indicates time of oLFS. **B.** Representative experiment showing LTD after oLFS of RMTg GABAergic oIPSCs recorded in a VTA dopamine cell and **C.** in the presence of the NMDAR antagonist, d-APV. Insets: oIPSCs during baseline (black) and 10-20 min after oLFS (red). **D.** Time course of average oIPSC amplitude before and after oLFS (n = 14 cells). **E.** Mean oIPSC amplitudes shown for each cell recorded during a 10 min baseline decrease 10-20 min after oLFS. **F.** Paired pulse ratios before and after oLFS of cells depressed <10% of baseline (n = 11 cells).

Red arrow indicates time of oLFS

**p < .05, paired t-test of amplitude of 10 min baseline vs. 10-20 min after oLFS.*

FIGURE 4-2. Forskolin, but not HFS of caudal placed electrode, potentiates

RMT_{GABA}→VTA synapses

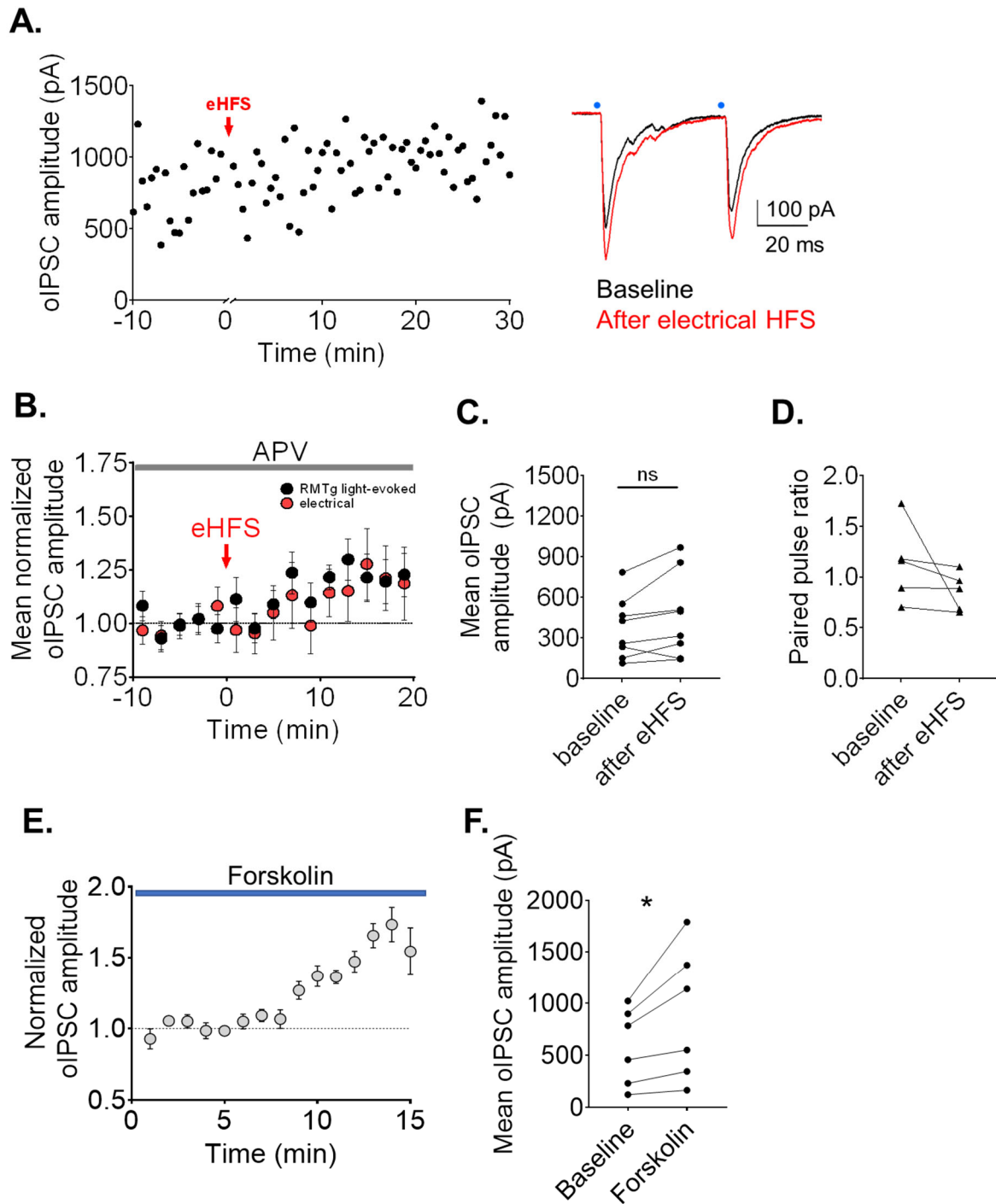


FIGURE 4-2. HFS of caudal placed electrode does not potentiate RMTg_{GABA}→VTA synapses

A. Representative experiment showing electrical HFS of a caudally placed electrode with light-evoked RMTg GABAergic oIPSCs recorded in a VTA dopamine cell in the presence of APV. Insets: oIPSCs during baseline (black) and 10-20 min after eHFS (red). **B.** Time course of average RMTg oIPSC amplitude (black) and electrical IPSCs (red) before and after eHFS (n = 8 cells). **C.** Mean oIPSC amplitudes from a 10 min baseline to 10-20 min after eHFS. **D.** Paired pulse ratios before and after eHFS for RMTg oIPSCs that potentiated > 20% (n = 5 cells). **E.** Time course of average RMTg oIPSC amplitude with bath application of 10 μM forskolin (n = 6 cells). **F.** Mean oIPSC amplitudes from a 10 min baseline to 10-20 min after forskolin (n = 6 cells).

Red arrow indicates time of eHFS.

**p < .05, paired t-test of amplitude of 10 min baseline vs. 10-20 min after eHFS.*

FIGURE 4-3. VTA-projecting GABAergic cells in the vPAG are sensitive to opioids

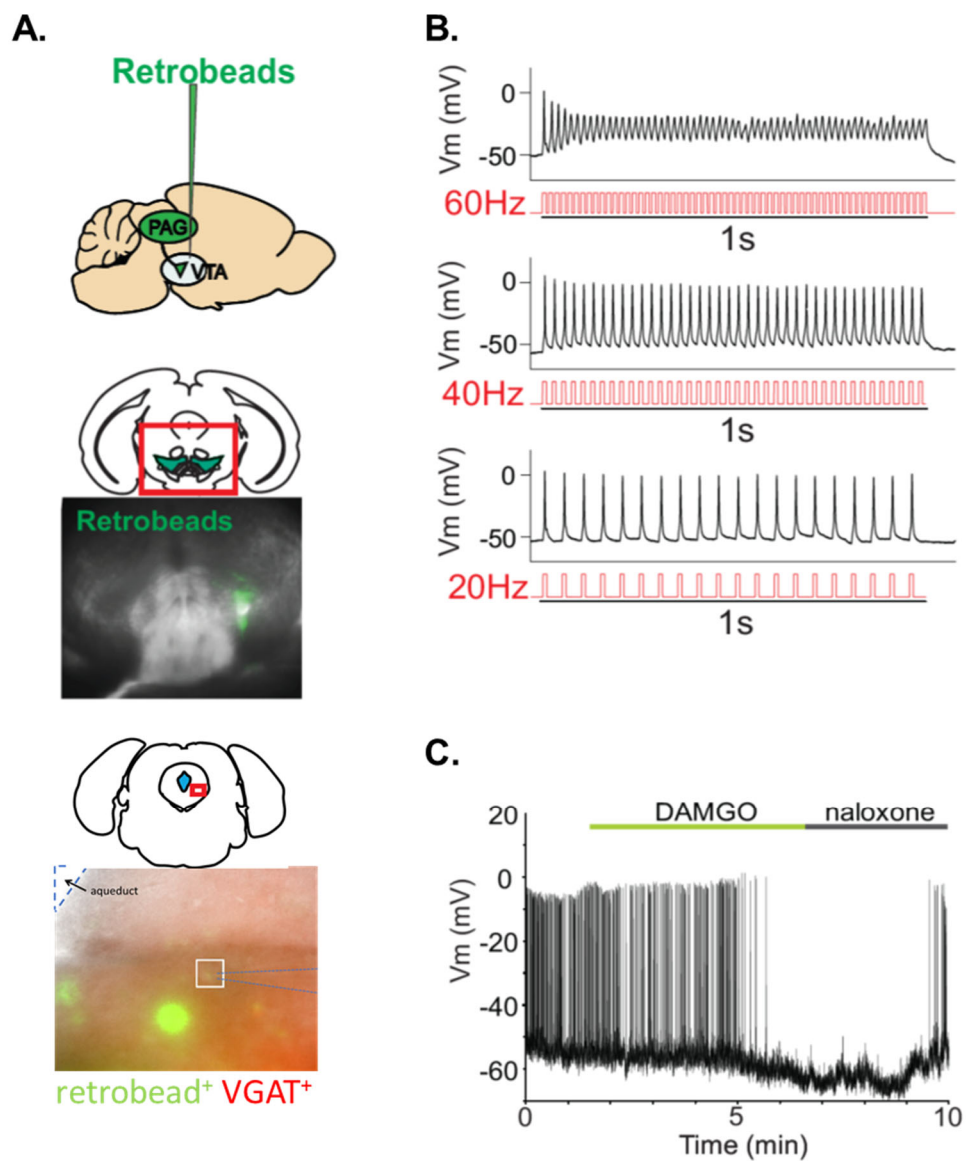


FIGURE 4-3. VTA-projecting GABAergic cells in the vPAG are sensitive to opioids

A. Unilateral injection of green retrobeads into the VTA of a VGAT-cre;Tdtomato mouse (top panel). Location of retrobead fluorescence in a coronal brain section containing the VTA (middle panel). Image of a retrobead- and VGAT-positive whole-cell recording in the vPAG (bottom panel). **B.** Current clamp recording of trains of current injections and **C.** bath application of 1 μ M DAMGO in a retrobead- and VGAT-positive ventral PAG cell.

FIGURE 4-4. PAG_{GABA}→VTA synapses display an unusual form of LTP after LFS

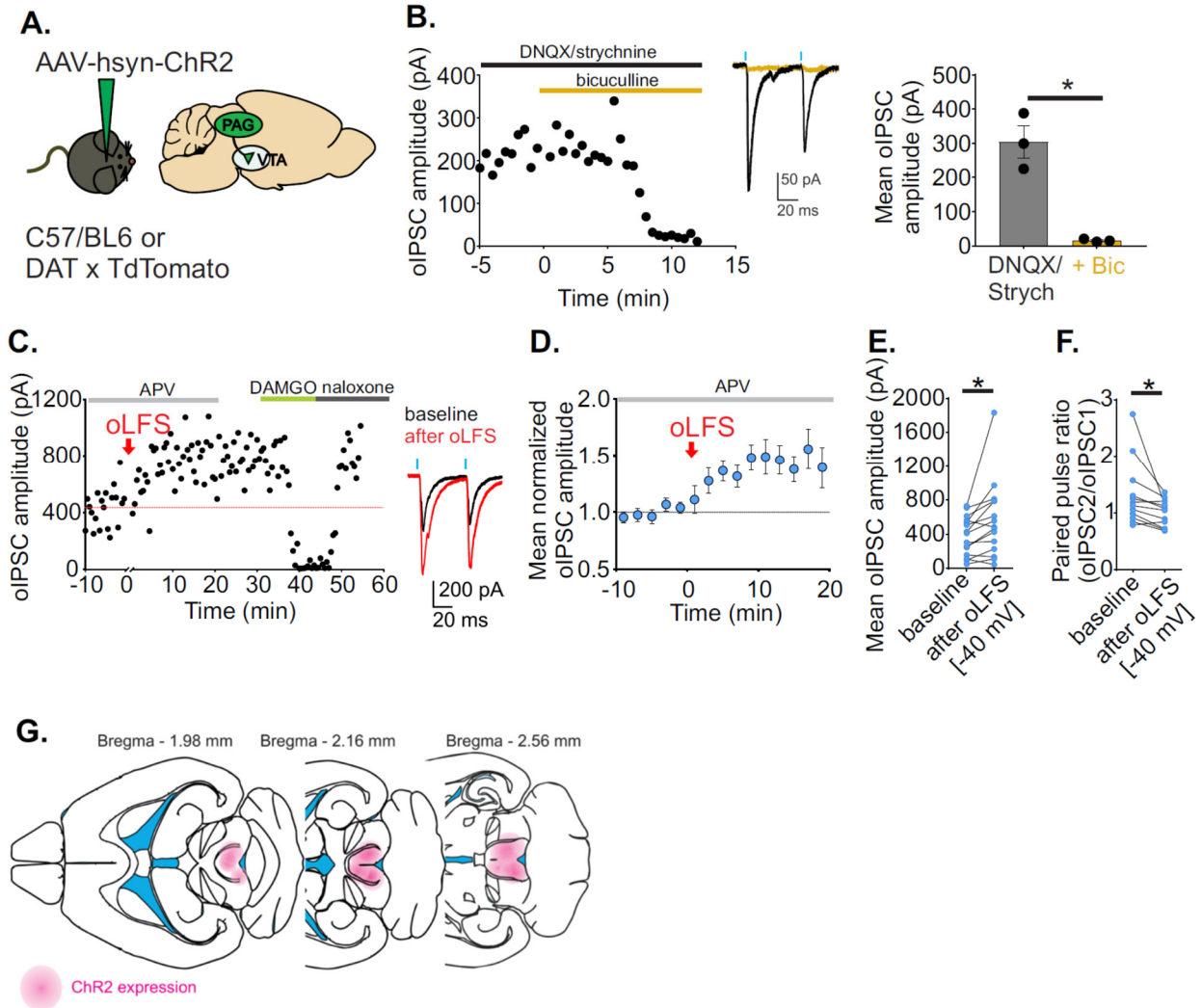


FIGURE 4-4. PAG_{GABA}→VTA synapses display an unusual form of LTP after LFS

A. Schematic of viral injection into the vPAG of C57/BL6 or DAT-cre x TdTomato mice. **B.** Voltage-clamp recording from a VTA dopamine cell of PAG oIPSCs in DNQX/strychnine before and after bath application of bicuculline (left panel) and average amplitudes in similar experiments (n = 3 cells, right panel). **C.** Example experiment showing LTP after oLFS + depolarization to -40 mV of PAG oIPSCs recorded in a VTA dopamine cell in the presence of APV. Application of DAMGO depresses the oIPSC and naloxone reverses this. Red arrow indicates time of oLFS. Inset: oIPSCs during baseline (black trace) and 10-20 min after oLFS (red trace). **D.** Time course of averaged oIPSC amplitudes before and after oLFS (n = 15 cells). **E.** Mean oIPSC amplitude for each cell during baseline and 10-20 min after oLFS. **F.** Paired pulse ratios before and after oLFS from each cell that potentiated >10% of basal values (n = 11 cells). **G.** Map of ChR2 expression in the vPAG for in vitro plasticity experiments. Horizontal sections adapted from (Franklin, 2013).

Red arrow indicates time of oLFS

**p < .05, paired t-test comparing amplitudes during 10 min baseline vs. 10-20 min after oLFS.*

FIGURE 4-5. Potentiation of vPAG_{GABA}→VTA synapses requires postsynaptic depolarization, but not neurotensin receptor activation

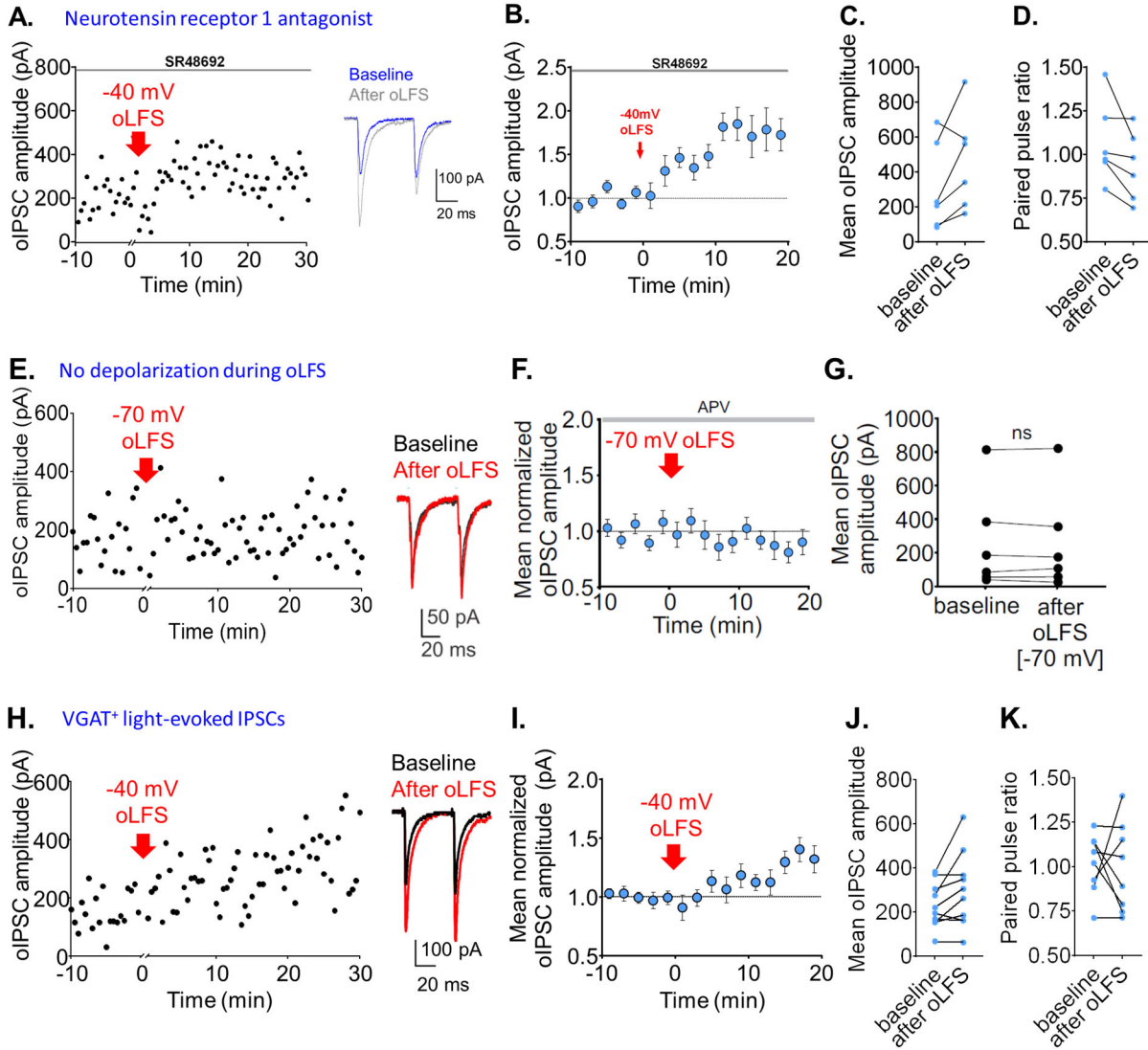


FIGURE 4-5. Potentiation of vPAG_{GABA}→VTA synapses requires postsynaptic depolarization, but not neurotensin receptor activation

A. Representative experiment showing LTP after oLFS + depolarization to -40 mV of PAG oIPSCs recorded in a VTA dopamine cell in the presence of APV and SR48692. Inset: oIPSCs during baseline (blue trace) and 10-20 min after oLFS (gray trace). **B.** Time course of averaged oIPSC amplitudes before and after oLFS (n = 6 cells). **C.** Mean oIPSC amplitude for each cell during baseline and 10-20 min after oLFS. **D.** Paired pulse ratio before and after oLFS.

E. Representative experiment after oLFS without depolarization showing PAG oIPSCs recorded in a VTA dopamine cell in the presence of APV (left). Inset: oIPSCs during baseline (black trace) and 10-20 min after oLFS (red trace). **F.** Time course of averaged oIPSC amplitudes before and after oLFS without depolarization (n = 6 cells). **G.** Mean oIPSC amplitudes are shown for each cell before and after oLFS. **H.** Representative experiment showing LTP after oLFS + depolarization to -40 mV of VGAT⁺ PAG oIPSCs recorded in a VTA dopamine cell in the presence of APV. Inset: oIPSCs during baseline (blue trace) and 10-20 min after oLFS (gray trace). **I.** Time course of averaged oIPSC amplitudes before and after oLFS (n = 10 cells). **J.** Mean oIPSC amplitude for each cell during baseline and 10-20 min after oLFS. **K.** Paired pulse ratio before and after oLFS.

Red arrow indicates time of oLFS.

FIGURE 4-6. Possible mechanisms of LFS-induced LTP at PAG GABA synapses

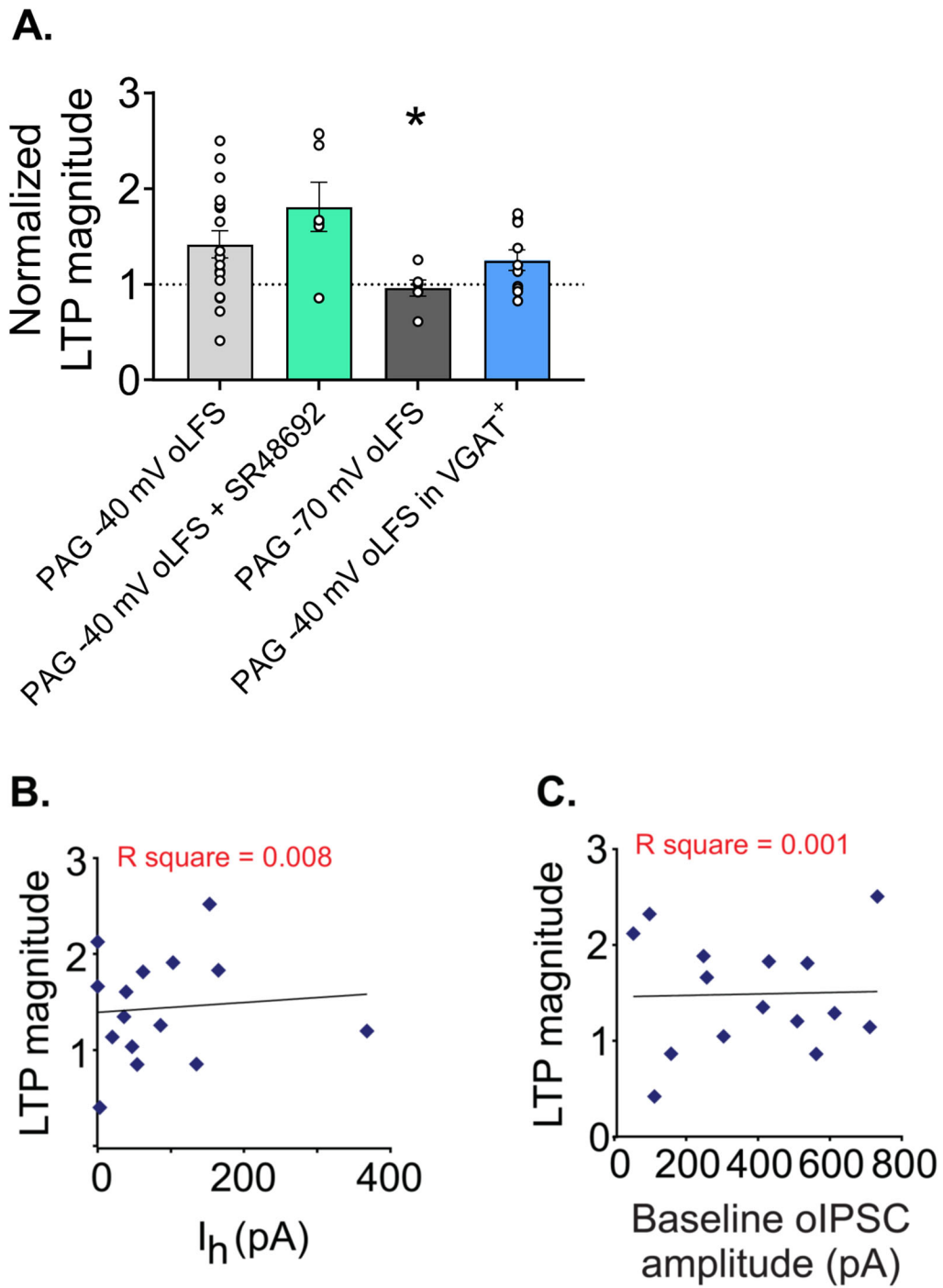


FIGURE 4-6. Possible mechanisms of LFS-induced LTP at PAG GABA synapses

A. LFS induced LTP in all experimental conditions tested except for when it was not paired with mild depolarization (dark gray bar). **B.** Magnitude of LTP after oLFS vs. H-current. **C.** Magnitude of LTP after oLFS vs. baseline oIPSC amplitude.

**p < .05, Brown-Forsythe and Welch ANOVA tests comparing each test to PAG -40 mV oLFS*

FIGURE 4-7. vPAG_{GABA}→VTA synapses can inhibit dopamine cell firing

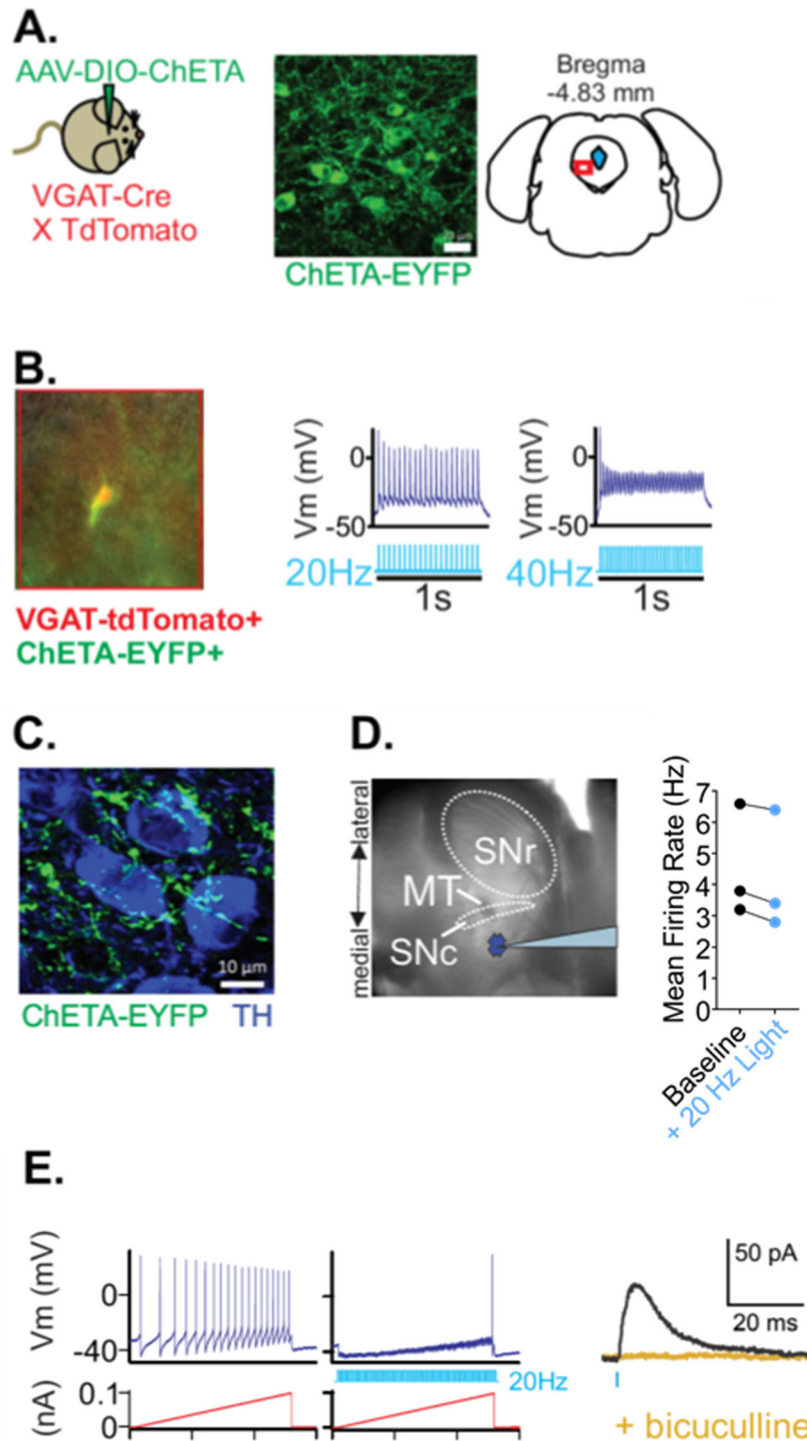


FIGURE 4-7. vPAG_{GABA}→VTA synapses can inhibit dopamine cell firing

A. Schematic of viral injection in the vPAG (left) and image of ChETA-EYFP viral expression in the PAG (right). Scale bar = 20 μ M **B.** Representative action potential firing of a PAG VGAT⁺, ChETA⁺ PAG cell (middle panel) in response to 20 or 40 Hz trains of LED pulses (right). **C.** ChETA⁺ terminals (green) in the VTA are seen adjacent to TH⁺ cells (blue). Scale bar = 10 μ M. **D.** Horizontal slice containing the VTA and location of recording electrode (left) and effect of 20 Hz light stimulation (ChR2 experiments only) on evoked VTA dopamine cell firing (right). **E.** Representative current clamp recording of alternating ramps of current injection without light stimulation (left panel) and with concurrent 20 Hz light stimulation (ChETA) of PAG oIPSCs (middle panel). Voltage clamp recording of oIPSCs from the same cell using K gluconate pipette solution are blocked with GABA_AR antagonist, bicuculline (right panel).

FIGURE 4-8. A μ -opioid receptor agonist depresses vPAG_{GABA}→VTA synapses more than RMTg_{GABA}→VTA synapses

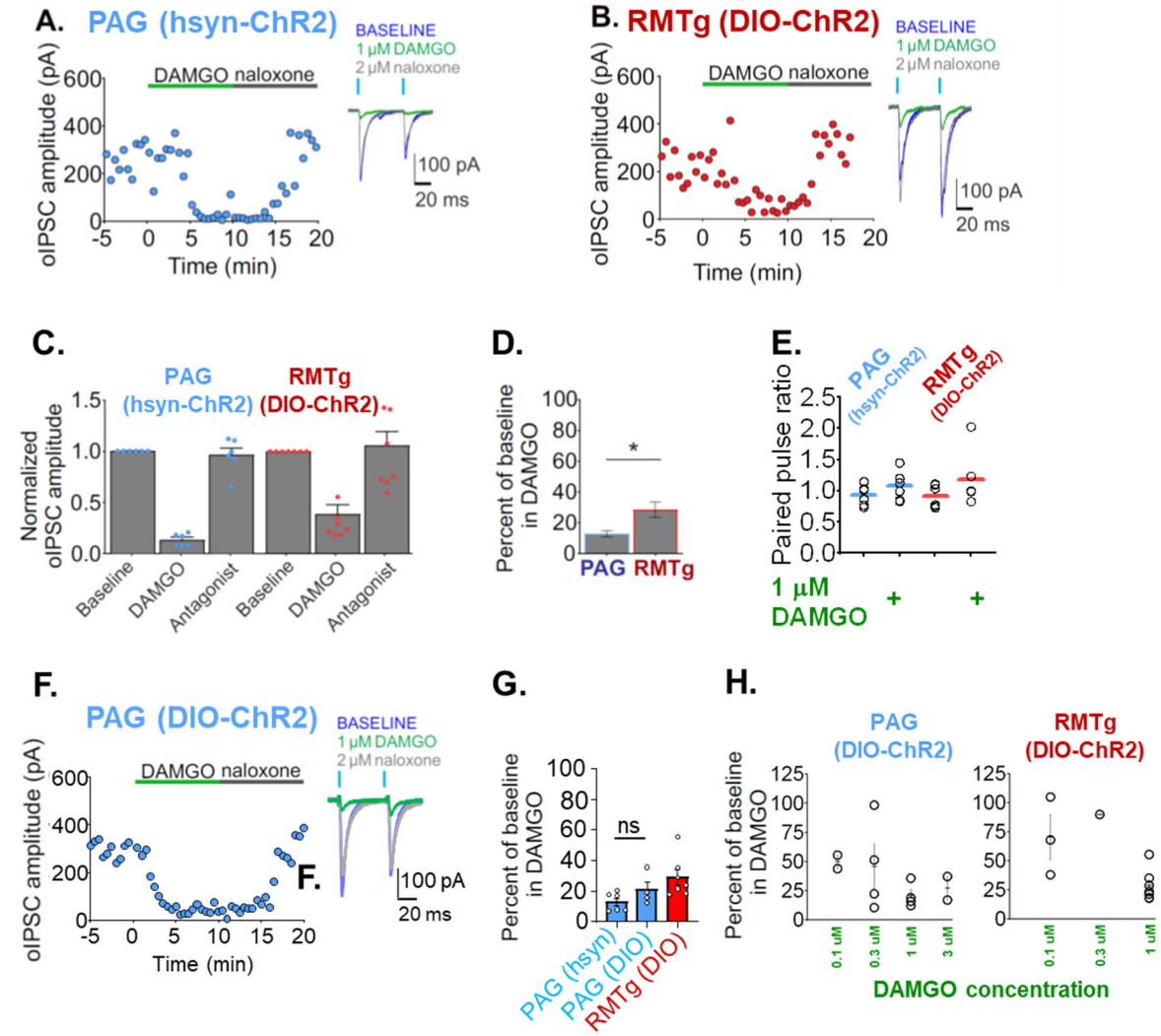


FIGURE 4-8. A μ -opioid receptor agonist depresses vPAG_{GABA}→VTA synapses more than RMTg_{GABA}→VTA synapses

A. Representative voltage clamp recordings of vPAG oIPSCs or **B.** RMTg oIPSCs with bath application of the MOR agonist, DAMGO, and antagonist, naloxone. Insets: oIPSCs during baseline (blue), DAMGO (1 μ M, green), and naloxone (2 μ M, gray). **C.** Mean oIPSC amplitudes of vPAG or RMTg oIPSCs, normalized to basal values. **D.** PAG oIPSCs are depressed significantly more than RMTg oIPSCs by DAMGO (n = 6 PAG, n = 7 RMTg). **E.** Paired pulse ratio analyses of values during baseline vs. DAMGO. **F.** Representative voltage clamp recordings in brain slices from VGAT-cre mice injected with floxed ChR2. Timecourse of vPAG oIPSCs with bath application of DAMGO and naloxone. Insets: oIPSCs during baseline (blue), DAMGO (1 μ M, green), and naloxone (2 μ M, gray). **G.** Comparison of PAG oIPSCs using hsyn-ChR2 (n = 6 cells) or DIO-ChR2 (n = 4 cells) and RMTg oIPSCs using DIO-ChR2 (Mean: $28.7 \pm 5.0\%$, n = 7 cells). **H.** Dose response curves to DAMGO for PAG and RMTg oIPSCs using DIO-ChR2.

**p < .05, paired t-test comparing amplitudes during 10 min baseline vs. 10-20 min after DAMGO is added to the bath solution*

FIGURE 4-9. Strength of inhibition differs between RMTg and PAG originating synapses

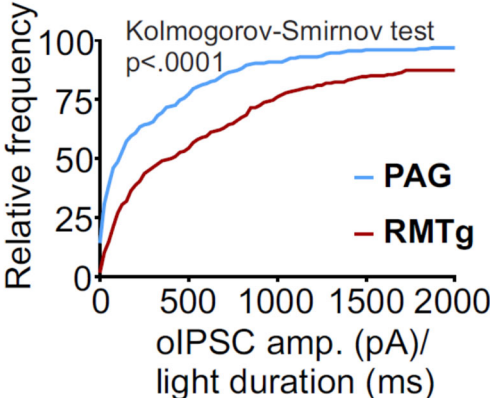


FIGURE 4-9. Strength of inhibition differs between RMTg and PAG originating synapses

RMTg oIPSCs (red) were of greater amplitude per millisecond light stimulation than vPAG oIPSCs (blue).

Kolmogorov-Smirnov test, $p < 0.0001$

CHAPTER 5

DISTINCT BEHAVIORAL PROFILES OF ACTIVATING

RMTG AND PAG AFFERENTS TO THE VTA

5.1 INTRODUCTION

The VTA encodes information about both rewarding and aversive stimuli and is required for the addictive properties of drugs of abuse. There is a great deal of heterogeneity of innervation in the VTA, in part because it receives inhibitory input from local interneurons and numerous extrinsic brain areas. Characterization of the heterogeneous properties of different VTA circuits will place opioid effects into context for future studies involving therapeutic intervention for disorders involving the reward pathway. The RMTg and PAG are two inhibitory afferents that are known for their interaction with opioids but require more careful dissection of their roles in VTA circuits. Here, I used several behavioral assays to probe the function of two inhibitory afferents to the VTA. Activating the RMTg and vPAG GABAergic afferents in vivo produced distinct behavioral profiles: activating RMTg_{GABA}→VTA synapses was aversive, but these effects were not seen upon activation of vPAG_{GABA}→VTA synapses. Instead, activating vPAG_{GABA}→VTA synapses increased immobility and that increase was blocked in the presence of morphine.

5.1.1 Rostromedial tegmental nucleus

The RMTg is a major node in circuits that regulate aversion. Once thought of as an extension of the VTA, the RMTg has more recently been characterized as a separate region based on distinct cell identities with genetic markers, a lack of dopaminergic cells, and functional differences, e.g. increases in immediate early gene reactivity to psychostimulants (Kaufling et al., 2010). It is perfectly situated as a relay between the lateral habenula and the VTA; when the lateral habenula is activated, RMTg cells increase their firing rate, leading to inhibition of VTA dopamine cells (Jalabert et al., 2011). The photoactivation of glutamatergic terminals in the RMTg at 60 Hz, a rate higher than baseline firing rate, produces profound behavioral correlates of aversion: mice in a real time place preference procedure (RTPP) will robustly avoid the stimulation-paired chamber and exhibit escape behavior (Stamatakis and Stuber, 2012). Furthermore, a memory of that

aversive experience is stored and 24 hours later, in the absence of stimulation, mice will continue to avoid the stimulation-paired chamber. Additionally, lesions of the RMTg are sufficient to block conditioned place aversion to a variety of aversive stimuli, suggesting that an intact RMTg is required for behavioral responding to aversive stimuli (Li et al., 2019). RMTg cells respond to a variety of aversive stimuli including footshock, loud tones, bright lights, lithium chloride, restraint stress, and cocaine (Li et al., 2019) and conditioned taste aversion to ethanol (Glover et al., 2016). Decreased dopamine tone, through direct RMTg stimulation or an aversive stimulus, is thought to mediate the aversive nature of RMTg stimulation. Somewhat surprisingly, however, the behavioral response of directly manipulating RMTg terminals in the VTA in RTPP has not been explored. The VTA is not the only output pathway of the RMTg - it also heavily projects to the substantia nigra compacta - and the previously reported results by Stamatakis et al. (2012) could occur independently of the VTA. Therefore, I used a RTPP with photoactivation of RMTg terminals within the VTA to determine if these GABAergic synapses regulate aversion.

5.1.2 Periaqueductal gray

The PAG is also known for its role in many aversive responses. In contrast to the RMTg, however, the GABAergic projection to the VTA has never been investigated *in vivo*. The PAG is organized into longitudinal columns that dictate connectivity and behavioral outputs to pain, stress, and threats: dorsal subdivisions (dPAG) are associated with the generation of both active and passive responses (including e.g. both freezing and flight) while ventral PAG subdivisions (vPAG) are generally associated only with coordination of passive behaviors (Bandler and Shipley, 1994, Bandler and Keay, 1996). Dorsal PAG activation results in acute avoidance and learned behaviors to avoid that stimulation (Deng et al., 2016). Optogenetic activation of ventromedial hypothalamus to the dorsolateral PAG induces immobility (Wang et al., 2015). Activating the ventrolateral PAG induces quiescence, i.e. reduced spontaneous activity (Depaulis et al., 1994, Keay and Bandler, 2001, Morgan and Carrive, 2001). The ventrolateral PAG is primarily composed of GABAergic

interneurons and projection cells, along with a population of dopaminergic and glutamatergic cells. The dopaminergic cells in the vIPAG and neighboring dorsal raphe are involved in fear learning (Groessl et al., 2018). The GABAergic cells in the vIPAG are involved in behavioral responses related to fear learning and anxiety; chemogenetic inhibition of vIPAG GABA cells using Designer Receptors Exclusively Activated by Designer Drugs (DREADDs) is anxiogenic in light-dark exploration and open field procedures (Lowery-Gionta et al., 2018). The vIPAG is also a major component of the descending pain pathway and is a major site of opioid analgesia. Inhibition of vIPAG GABA cells reduces pain behavioral responses (Samineni et al., 2017). Microinjections of lidocaine, MOR antagonists, or GABAA receptor agonists into the vIPAG all prevented capsaicin-induced antinociception, suggesting that this region is involved in the ascending pathway that triggers analgesia in the presence of painful stimuli (Tobaldini et al., 2018). Despite these intriguing properties, the functional relevance of $PAG_{GABA} \rightarrow VTA$ synapses is unknown.

5.2 RESULTS

5.2.1 Activating $RMTg_{GABA} \rightarrow VTA$ synapses is aversive

The RMTg has a high spontaneous firing rate, reportedly 3-9 Hz in vitro and 10-30 Hz in vivo (Lecca et al., 2011, Jalabert et al., 2011). Moreover, the firing rate can increase to 50 Hz or more during presentation of aversive stimuli, such as a strong footshock or mechanical stimulation (Lecca et al., 2011). The behavioral effect of activating GABAergic RMTg cells is similar to that of local interneurons in the VTA, where activation is aversive and disrupts reward consumption (Tan et al., 2012, Van Zessen et al., 2012) while interneuron silencing induces appetitive-related behaviors (Jennings et al., 2013). Optogenetic activation of lateral habenula excitatory inputs on RMTg cells at 60 Hz in vivo results in a robust place aversion (Stamatakis and Stuber, 2012). However, it is unknown if $RMTg_{GABA}$ terminal stimulation specifically in the VTA is by itself aversive. I measured place aversion to 60 Hz stimulation of $RMTg_{GABA}$ terminals in the VTA using

RTPP. I injected AAV-DIO-ChR2 unilaterally in the RMTg of a VGAT-IRES-Cre mouse and implanted a light fiber ipsilaterally above the VTA (Figure 1H). After allowing several weeks for viral expression, mice underwent a pretest on day 1; on day 2, one side of the chamber was paired in a counterbalanced manner with 60 Hz blue LED light stimulation, and on day 3 was a posttest (Figure 1A). With only unilateral stimulation of the RMTg-VTA pathway, mice with ChR2 expression spent significantly less time in the light-paired chamber compared to control mice expressing the fluorophore only (fluorophore 26.0 ± 20.8 s, $n = 6$ mice, ChR2 -67.1 ± 21.8 s, $n = 6$ mice; $t = 3.084$, $p = 0.012$; Figure 1B-C) and displayed a nonsignificant tendency to avoid the light-paired chamber in a posttest conducted 24 hours later in the absence of light stimulation (fluorophore -5.8 ± 24.8 s, $n = 6$ mice, ChR2 -95.5 ± 36.9 s, $n = 6$ mice; $t = 2.019$, $p = 0.071$; Figure 1D). The frequency of visits to the light-paired chamber also significantly decreased in fluorophore mice compared to ChR2 mice during the light test (fluorophore 1.2 ± 4.6 s, $n = 6$ mice, ChR2 -11.3 ± 2.8 , $n = 6$ mice, $t = 2.329$, $p = 0.042$; Figure 1E) with a similar trend in the posttest (fluorophore -0.7 ± 6.3 , $n = 6$ mice, ChR2 -14.5 ± 2.5 , $n = 6$ mice, $t = 2.049$, $p = 0.068$; Figure 1E). The mean velocity in the light-paired chamber, distance traveled, and performance on a rotarod test were not different between experimental and control groups (Figure 1F-G; Figure 6B).

5.2.2 Activating vPAG_{GABA}→VTA synapses induces a quiescent phenotype

The behavioral output of specifically activating vPAG_{GABA}→VTA synapses in vivo is unknown, despite a wealth of research about the behavioral role of the PAG. The vPAG is needed for fear learning (Johansen et al., 2010, McNally et al., 2011) and motivation related to prey hunting (Mota-Ortiz et al., 2012). Activating the vPAG induces quiescence or freezing (Depaulis et al., 1994, Keay and Bandler, 2001, Morgan and Carrive, 2001) and specifically activating GABAergic cells in the vPAG facilitates nociception (Samineni et al., 2017). It is possible that signaling in the vPAG_{GABA}→VTA projection mediates some or all these behaviors. Alternatively, the projection

could be involved in behaviors typically associated with the VTA, such as reward or aversion. Therefore, I decided to screen for a basic preference or aversion during in vivo light stimulation. To target vPAG_{GABA} cells selectively, I unilaterally expressed stop-floxed ChR2 in the vPAG of VGAT-cre mice (AAV-DIO-ChR2-mCherry) or a control fluorescent reporter only (AAV-DIO-EYFP or AAV-DIO-mCherry) and implanted a light fiber ipsilaterally in the VTA. I chose to use a frequency of light stimulation, 20 Hz, that exceeds the basal firing rate I recorded in vitro (8.1 ± 1.1 Hz) in a range similar to that reported in vivo (Tovote et al., 2016). A frequency of 20 Hz optogenetic stimulation of ventrolateral PAG cells increased freezing in rats when the light fiber was in the PAG itself (Assareh et al., 2017).

Mice were tested in a RTPP procedure lasting four days: day 1 consisted of a pretest to determine initial side bias, days 2 – 3 consisted of 20 Hz light stimulation on one side of the apparatus, and day 4 consisted of a posttest without light stimulation (Figure 2A). On either day 2 or 3, mice received in vivo stimulation with the protocol that potentiated synapses in vitro (oLFS: 1 Hz for 6 min) in an empty 30 cm x 30 cm home cage 15 min prior to the RTPP. Unilateral light-induced activation of vPAG_{GABA}→VTA synapses had little effect on overall time spent in the light-paired chamber compared to pretest values for either group during the 20 Hz test, LFS/20 Hz test or posttest ($F(1,15) = 0.47$, $p = 0.50$; $n = 7$ fluorophore mice, $n = 10$ opsin mice; Figure 2C). However, I noticed that mice in the opsin group frequently exhibited a freezing-like phenotype when receiving light stimulation (Figure 2C). I used the parameter of immobility to quantify this: calculated by averaging the velocity of the center point of the mouse every 10 samples and velocity less than 1.75 cm/s over this period was categorized as immobile. Indeed, there was an increased percentage of time spent immobile in the light-paired chamber compared to pretest values between experimental groups for both light tests ($F(1,15) = 9.72$, $p = 0.007$; Figure 2D). Immobility in the light-paired chamber during the 20 Hz (fluorophore $-0.8 \pm 5.0\%$, $n = 7$ mice, opsin $16.8 \pm 4.9\%$, $n = 10$ mice) and LFS/20 Hz light test (fluorophore $0.1 \pm 5.3\%$, $n = 7$ mice, opsin

19.1 ± 3.7%, n = 10 mice) was significantly different between fluorophore and opsin groups (Sidak's multiple comparisons, 20 Hz test: p = 0.026, LFS/20 Hz test: p = 0.013). The frequency of immobile bouts in the apparatus compared to pretest values differed between experimental groups for both light tests (F (1,15) = 8.49, p = 0.01; Figure 2E). Frequency of immobile bouts during the 20 Hz (fluorophore 0 ± 20, n = 7 mice, opsin 101 ± 25, n = 10 mice) and LFS/20 Hz light test (fluorophore 44 ± 29, n = 7 mice, opsin 135 ± 26, n = 10 mice) was significantly different between fluorophore and opsin groups (Sidak's multiple comparisons, 20 Hz test: p = 0.02, LFS/20 Hz test: p = 0.04). The distance traveled in the apparatus differed between experimental groups for both light tests (F (1,15) = 11.72, p = 0.004; Figure 2F). Distance traveled during the 20 Hz (fluorophore -38 ± 269 cm, n = 7 mice, opsin 1157 ± 245 cm, n = 10 mice) and LFS/20 Hz light test (fluorophore -289 ± 217 cm, n = 7 mice, opsin 1128 ± 137 cm, n = 10 mice) was decreased in the opsin mice vs. the fluorophore mice (Sidak's multiple comparisons, 20 Hz test: p = 0.002, LFS/20 Hz test: p = 0.023). The mean velocity in the light-paired chamber differed between experimental groups for both light tests (F (1,15) = 8.01, p = 0.013; Figure 2G). Mean velocity during the 20 Hz light test (fluorophore -0.37 ± 0.51 cm/s, n = 7 mice, opsin -2.03 ± 0.42 cm/s, n = 10 mice) and LFS/20 Hz light test (fluorophore -0.38 ± 0.64 cm/s, n = 7 mice, opsin -1.91 ± 0.24 cm/s, n = 10 mice) was significantly reduced in the opsin mice vs. the fluorophore mice (Sidak's multiple comparisons, 20 Hz test: p = 0.026, LFS/20 Hz test: p = 0.04).

For LFS preconditioning, I used a within-group experimental design to be able to compare values in individuals. With these mean values, the immobile phenotype was not potentiated by LFS preconditioning on any of the parameters tested. However, it is possible that order effects of testing resulted in a washing out any differences between the two conditions. When analyzing the data based on test order (Figure 3A), mice that received the LFS/20 Hz light condition on the first day were more immobile than mice that first received the 20 Hz alone condition (Figure 3B).

5.2.3 Morphine blocks vPAG_{GABA}→VTA stimulation-induced quiescent behavior

As noted in vitro (Chapter 4), GABAergic oIPSCs from the vPAG were robustly depressed by DAMGO, a MOR agonist. If an input is profoundly depressed by opioid exposure, the influence exerted by that projection on the VTA may be taken offline in vivo when morphine is present. Therefore, I hypothesized that in vivo morphine administration might prevent the immobility promoted by optogenetically driving vPAG_{GABA}→VTA synapses. A different cohort of mice was tested in a RTPP to determine the effect of light stimulation in the presence of morphine (Figure 4A). Three groups of mice were used: fluorophore + morphine, opsin + morphine, and opsin + saline. Mice were habituated to intraperitoneal (i.p.) injections prior to testing. Two days prior to testing, all mice were injected with saline in the animal care facility and returned to their homecage. One day prior to testing, mice were injected i.p. with saline in the behavior testing room, prior to being returned to the animal care facility. On Day 1, all mice received an i.p. injection of saline 30 minutes prior to being connected to an optic fiber and being placed in the 2-chamber apparatus for a 10 minute pretest. On Day 2, mice were given either saline or morphine (3 mg/kg i.p.) 30 minutes prior to the RTPP procedure where all groups received light stimulation upon entering the light-paired chamber. On Day 3, all mice received saline and the same procedure as the pretest was repeated for the posttest.

As with the original RTPP cohort, there was no effect on overall time spent in the light-paired chamber compared to pretest values for any group during the light test or the posttest ($F(2,18) = 0.17$; $p = 0.84$, $n = 6-8$ mice/group; Figure 4B-C). However, there was a significant effect of group for time immobile in the light-paired chamber compared to pretest values ($F(2,18) = 8.5$, $p = 0.003$; Figure 4D). Fitting with the prior results, only the opsin + saline group showed an increased percentage of time spent immobile compared to fluorophore + morphine group in the light test (fluorophore + MOR: $2.3 \pm 3.4\%$, $n = 8$ mice; opsin + MOR: $6.8 \pm 3.4\%$, $n = 6$ mice; opsin + SAL: $18.7 \pm 1.6\%$, $n = 7$ mice; Tukey's multiple comparisons, fluorophore + MOR vs. opsin + MOR: $p = 0.56$, fluorophore + MOR vs. opsin + SAL: $p = 0.002$). The frequency of immobile

bouts in the apparatus compared to pretest values, however, was not significantly different between groups ($F(2,18) = 1.40$, $p = 0.27$; fluorophore + MOR: 85.6 ± 20.0 , $n = 8$ mice; opsin + MOR: 84.2 ± 19.3 , $n = 6$ mice; opsin + SAL: 125.7 ± 19.7 , $n = 7$ mice; Figure 4E). The distance traveled in the apparatus differed between experimental groups in the light test ($F(2,18) = 6.5$, $p = 0.007$; Figure 4F), again with the opsin + saline group being significantly reduced compared to the control group (fluorophore + MOR: -299 ± 151 cm, $n = 8$ mice; opsin + MOR: -370 ± 171 cm, $n = 6$ mice; opsin + SAL: -1021 ± 149 cm, $n = 7$ mice; Tukey's multiple comparisons, fluorophore + MOR vs. opsin + MOR: $p = 0.95$, fluorophore + MOR vs. opsin + SAL: $p = 0.009$, opsin + MOR vs. opsin + SAL: $p = 0.029$). The mean velocity in the light-paired chamber differed between experimental groups in the light test ($F(2,18) = 9.8$, $p = 0.001$; Figure 4G). The opsin + saline group was significantly reduced compared to the control group (fluorophore + MOR: 0.1 ± 0.3 cm/s, $n = 8$ mice; opsin + MOR: -0.6 ± 0.3 cm/s, $n = 6$ mice; opsin + SAL: -0.7 ± 0.2 cm/s, $n = 7$ mice; Tukey's multiple comparisons, fluorophore + MOR vs. opsin + MOR: $p = 0.31$, fluorophore + MOR vs. opsin + SAL: $p = 0.001$, opsin + MOR vs. opsin + SAL: $p = 0.044$).

During RTPP 20 Hz light tests, the increase in light-induced immobility was most pronounced during the first half of the test (Figure 5A-B, D). In contrast, the 6 minutes of LFS preconditioning of 1 Hz photostimulation did not change the immobility of opsin mice compared to control fluorophore mice (Figure 5C). In the RTPP with drug injections, I used a morphine dosage that minimized any locomotion effects. This is evidenced by a lack of difference between total distance traveled in the arena normalized to pretest when comparing control fluorophore groups that did or did not receive an injection of morphine (Figure 5E). The only experimental groups that differed from the un-injected control fluorophore group were the un-injected opsin and opsin + saline groups (Figure 5E). Finally, I tested for the possibility that these results could be explained by a general motor deficit. A rotarod test can be used to gauge locomotor performance. Light-induced immobility in this or the original light tests is unlikely to be explained by motor suppression as

there were no deficits in motor performance in a rotarod test ($F(1,8) = 0.11$, $p = 0.75$; fluorophore: light OFF 1.2 ± 0.4 falls, ON 1.0 ± 0.5 falls, opsin: OFF 1.0 ± 0.5 falls, ON 0.8 ± 0.4 falls, $n = 5$ mice per group; Figure 6).

5.2.4 RMTg_{GABA}→VTA or vPAG_{GABA}→VTA does not disrupt consumption of palatable food

Inhibition of the RMTg can disrupt responses to conditioned aversive stimuli (Jhou et al., 2013) and direct activation of the RMTg can disrupt reward behaviors (Stamatakis and Stuber, 2012, Proulx et al., 2018). I used an adapted version of novelty-induced suppression of feeding task (NSF) to determine if RMTg→VTA or vPAG→VTA stimulation in vivo would disrupt motivation to consume a palatable substance. Mice were trained to consume sweetened condensed milk for two 30 minute training sessions in a clean home cage while tethered to an optic fiber. After these training sessions, mice underwent counterbalanced test sessions of either 60 Hz blue LED stimulation or no light (Figure 7A). I measured latency to approach and first lick of the milk spout, and if a mouse never approached or licked the spout, it received a score of 300 seconds (the total duration of the test). Although there was no significant difference in the latency to approach, latency to first lick, or distance traveled for light OFF vs. ON test sessions (Approach $F(1,10) = 0.09$, $p = 0.77$; Lick $F(1,10) = 3.69$, $p = 0.08$; Distance $F(1,10) = 1.6$, $p = 0.23$; Figure 7B-D), the percentage of mice in the opsin group that failed to lick for the duration of a session was higher than that of the control group (Figure 7H). I also tested whether the vPAG_{GABA}→VTA projection influences this motivated behavior using the same NSF test differing only in that the light stimulation frequency was 20 Hz. Latency to first approach of the milk spout, latency to first lick, and total distance traveled were all unaffected by 20 Hz light stimulation (Approach $F(1,15) = 0.21$, $p = 0.65$; Lick $F(1,15) = 2.1$, $p = 0.17$; Distance $F(1,15) = 1.1$, $p = 0.31$; Figure 5D-F). All mice in the vPAG group licked during the test sessions (Figure 5H). In conclusion, RMTg_{GABA}→VTA stimulation mildly disrupted performance on palatable food consumption, but PAG_{GABA}→VTA stimulation had no effect.

5.3 DISCUSSION

The RMTg has garnered attention for its robust projection to the VTA and role in aversion. As expected, selective activation of the RMTg projection to the VTA in vivo resulted in real time place aversion. Conversely, the PAG to VTA inhibitory projection has never been studied in vivo. Activating this input in vivo was sufficient to induce quiescent behavior, a phenotype associated with the ventrolateral PAG. Quiescence was not elicited by light stimulation after an animal had received morphine, perhaps because the release of GABA from vPAG inputs is almost completely blocked by opioids.

Afferent-specific regulation of the VTA

These findings raise the question of why two GABAergic afferents to the same target brain region may have such different effects on behavior. One possibility is that RMTg and vPAG afferents target different VTA subpopulations, such as medial vs. lateral VTA, and therefore participate in different circuits (Lammel et al., 2014). However, my in vitro recordings (Chapter 4) were all made from dopamine neurons in the lateral VTA and exhibited light-evoked IPSCs from both afferent regions. Instead, to account for the behavioral differences, distinct cell populations would have to exist within the same VTA subregion. Another possibility is that VTA cells that receive RMTg input themselves have projection targets distinct from those innervated by vPAG inputs (Beier et al., 2015). Alternatively, the differences in behavior I observed could be because the RMTg mainly innervates dopamine cells while the PAG targets both dopaminergic and GABAergic cells (Balcita-Pedicino et al., 2011, Ntamati et al., 2018). However, the viral genetic strategy does not eliminate the possibility that VGAT⁺ cells could produce distinct effects via co-release of neurotransmitters such as glutamate (Jonas et al., 1998, Fattorini et al., 2015, Granger et al., 2017) or neuropeptides (Omelchenko and Sesack, 2010) and our lab recently reported that RMTg afferents can co-release glycine, but the co-release of glycine and GABA is expected to inhibit postsynaptic cells similarly to GABA release alone (Polter et al., 2018). Finally, differences in

spontaneous activity and synaptic strength of RMTg vs. vPAG GABAergic inputs (Chapter 4, Figure 9) may contribute to different behavioral responses. Larger RMTg-originating IPSCs may occur because RMTg terminals tend to synapse on larger diameter dendrites of VTA neurons, suggesting that they may preferentially target proximal dendrites (Balcita-Pedicino et al., 2011); in contrast, average amplitudes of PAG-originating IPSCs are relatively small (Ntamati et al., 2018). Any of these differences might affect the way in which synaptic input modulates VTA cell activity and resulting behavioral output.

Activating RMTg inputs to the VTA is aversive

Although the projection to the VTA is one of the densest RMTg efferents, there are other projection targets, such as the dorsal raphe, PAG, and pedunculopontine nucleus (Lavezzi and Zahm, 2011) that also have been linked to emotional behavior. A 60 Hz frequency was selected because prior reports used this frequency of optogenetic stimulation within the RMTg (Stamatakis and Stuber, 2012), and because I wanted to stimulate at a frequency above the high spontaneous firing rate of RMTg cells. While the results are not particularly astonishing, to my knowledge this is the first report of a real time place aversion induced with selective activation of RMTg inhibitory synapses in the VTA. Furthermore, I observed that mice expressing ChR2 in the RMTg became increasingly more uncooperative during handling than other groups of mice as testing progressed after the RTPP, perhaps as the aversive nature of the stimulation became associated with the experimenter or the behavioral testing room.

Activating vPAG_{GABA} inputs to the VTA induces quiescence

The in vitro synaptic plasticity results with vPAG inputs to the VTA from Chapter 4 were interesting because of the unusual LTP, however, without understanding the role of the pathway this unusual LTP of PAG_{GABA}→VTA synapses is especially cryptic. Although the above experiments elucidated some relevance of the pathway, much remains unknown about the function of this projection. My

results raise questions about the significance of quiescent behavior; it could be part of a fear circuit, a decision-making circuit, or simply motor output. PAG-mediated behaviors often only require descending motor-related projections, for example, freezing behavior depends on a PAG projection to the magnocellular nucleus of the medulla (Tovote et al., 2016). However, there are exceptions in which behavior is regulated by ascending projections from the PAG (Rizvi et al., 1991, Vianna and Brandao, 2003) such as the vPAG dopaminergic input to the central amygdala that is integral for fear learning (Groessl et al., 2018). The VTA is active during pain and fear, in addition to reward (Kender et al., 2008, Li et al., 2016, Pezze and Feldon, 2004, Tan et al., 2012), and it is possible that the PAG→VTA afferents may contribute to fear-related circuits. For example, freezing elicited by a conditioned stimulus requires the dopaminergic connection from VTA to basolateral amygdala (de Oliveira et al., 2017), and vPAG inputs to the VTA could contribute to this effect. Future experiments characterizing the projection targets of VTA dopamine cells that receive vPAG input may help to clarify these circuit questions.

One technical consideration is that all behavioral experiments only used unilateral activation of the vPAG_{GABA}→VTA projection and this was sufficient to induce quiescence, a behavior that has also been reported during direct nonspecific activation of the vPAG (Depaulis et al., 1994). Moreover, this means that the vPAG_{GABA}→VTA pathway is sufficient to induce quiescence without involving excitatory cells in the vPAG, and other GABAergic vPAG projection neurons are not necessary for inducing quiescence. Preceding the RTPP with 1 Hz light stimulation may have weakly potentiated the effect of 20 Hz light stimulation, as seen by the effect of test order in Figure 5-3. In brain slices, oLFS potentiated oIPSCs to nearly 150% of their baseline amplitude, and as such, I expected a greater effect on behavior with oLFS. However, I did note in vitro (Chapter 4) that if the 1 Hz stimulation was unaccompanied by depolarization, LTP was not induced; it is possible that under the conditions of the in vivo test, these requirements were not always met, leading to inter-individual variability.

Potential role of VTA afferents originating in the vPAG for the acute actions of opioids

Like the VTA, the PAG plays an integral role in the response to opioids, for instance, morphine injections into the PAG result in tolerance perhaps contributing to increased opiate consumption (Siuciak and Advokat, 1987, Lane et al., 2004). In the VTA, many drugs of abuse block at least one form of LTP at inhibitory synapses (LTP_{GABA}) for over 24 hours (Nugent et al., 2007, Guan and Ye, 2010, Niehaus et al., 2010). Inhibitory synapse plasticity may thus represent an avenue for therapeutic intervention for addiction. I showed that $vPAG_{GABA} \rightarrow VTA$ synapses exhibit LTP after LFS and are profoundly depressed by MOR activation, and increased quiescence seen with $vPAG_{GABA} \rightarrow VTA$ activation is absent after morphine treatment in vivo. One caveat is that morphine given in vivo will affect multiple pathways, while my LED fiber will affect only the VTA region. While the immobility phenotype reported here may be one readout of activating $vPAG \rightarrow VTA$ afferents, further work is needed to fully appreciate the behavioral relevance of this pathway. The reversal of this phenotype by morphine does suggest that whatever the role of this GABAergic input is, opioid drugs are capable of removing its influence.

Motivated behavior is not disrupted by $vPAG_{GABA} \rightarrow VTA$ photostimulation

The slight disruption of consumption of a palatable substance with $RMT_{GABA} \rightarrow VTA$ photostimulation fits with the notion that this pathway is broadly involved with aversive processing (Li et al., 2019). With the PAG, however, I hypothesized that the quiescent phenotype could interrupt consumption, although activating the $vPAG_{GABA} \rightarrow VTA$ did not appear to disrupt motivation to approach a palatable substance. This finding is consistent with a recent report that chemogenetic inhibition of the GABAergic vPAG cells also had no effect in a similar hypophagia task (Lowery-Gionta et al., 2018). This could mean that the vPAG afferents are not involved in this type of motivated behavior. Also, this observation complements the rotarod finding that stimulation does not induce general motor deficits. Future studies on other aspects of motivation are an interesting avenue of research that should be explored.

FIGURE 5-1. In vivo stimulation of RMT_{GABA}→VTA synapses is aversive

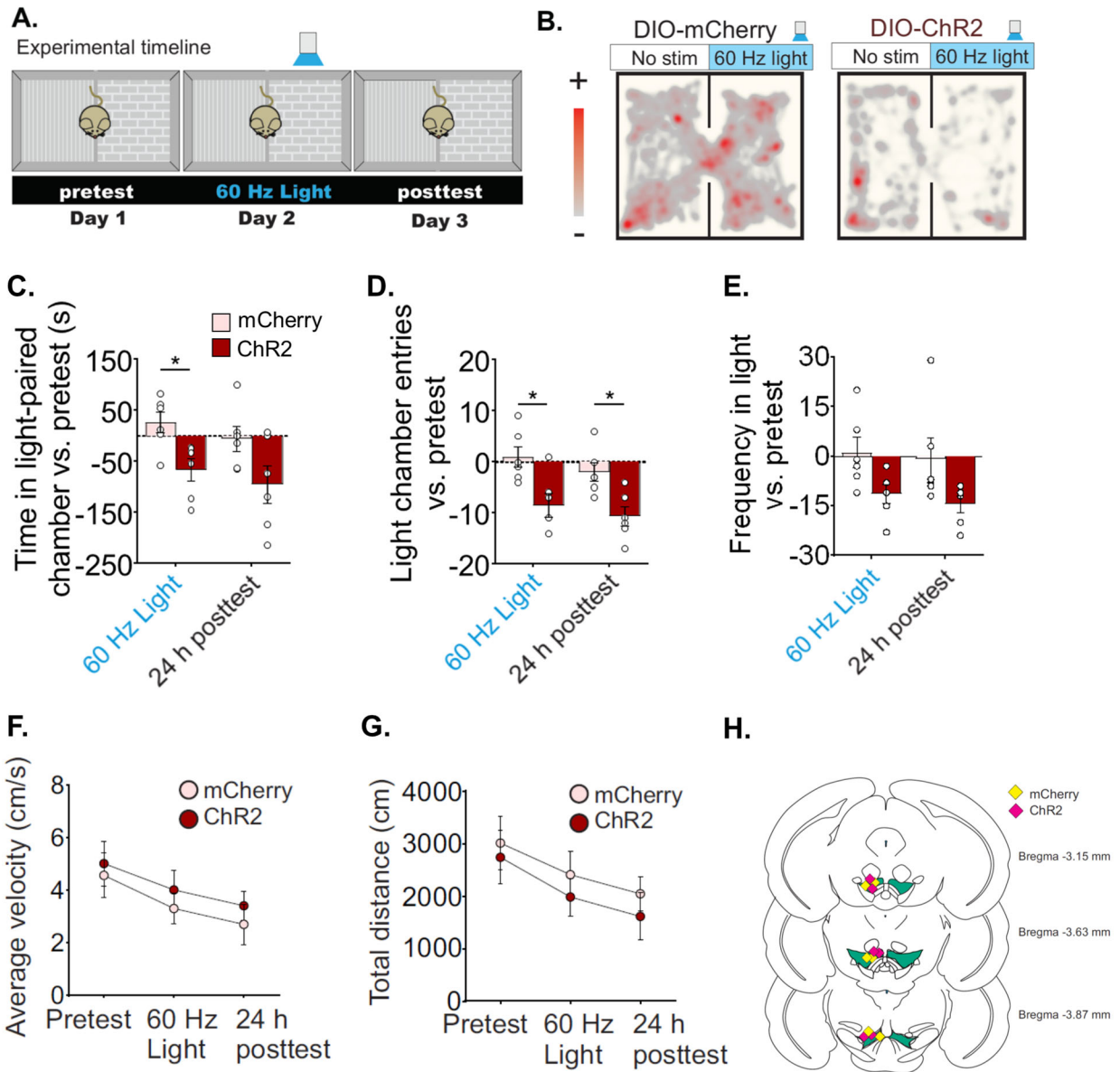


FIGURE 5-1. In vivo stimulation of RMTg_{GABA}→VTA synapses is aversive.

A. Real-time place preference (RTPP) experimental timeline. Day 1 and day 3, no light stimulation on either side. Day 2, blue light paired with one side. **B.** Representative location plot of a mCherry-expressing mouse (left) and ChR2-expressing mouse (right) over 10 minute RTPP test sessions. LED light was delivered constantly at 60 Hz whenever the mouse entered the light-paired chamber. **C.** ChR2 mice spend less time in the light-paired chamber during a 60 Hz RTPP compared to fluorophore controls (n = 6 mice per group). **D.** ChR2 mice make fewer visits to the light-paired chamber during a 60 Hz light test and 24h later in a posttest compared to fluorophore controls. **E.** ChR2 trend towards fewer overall instances of being in the light chamber compared to fluorophore controls **F.** Average velocity or **G.** distance traveled during the trials was not significantly different between experimental and control groups. **H.** Location of fiber implant tip in the VTA, coronal sections adapted from (Franklin, 2013).

Bars represent Mean ± SEM

Data analyzed using 2-way ANOVA, Sidak multiple comparisons of fluorophore vs. ChR2

**p < 0.05*

FIGURE 5-2. In vivo stimulation of vPAG_{GABA}→VTA synapses induces quiescence

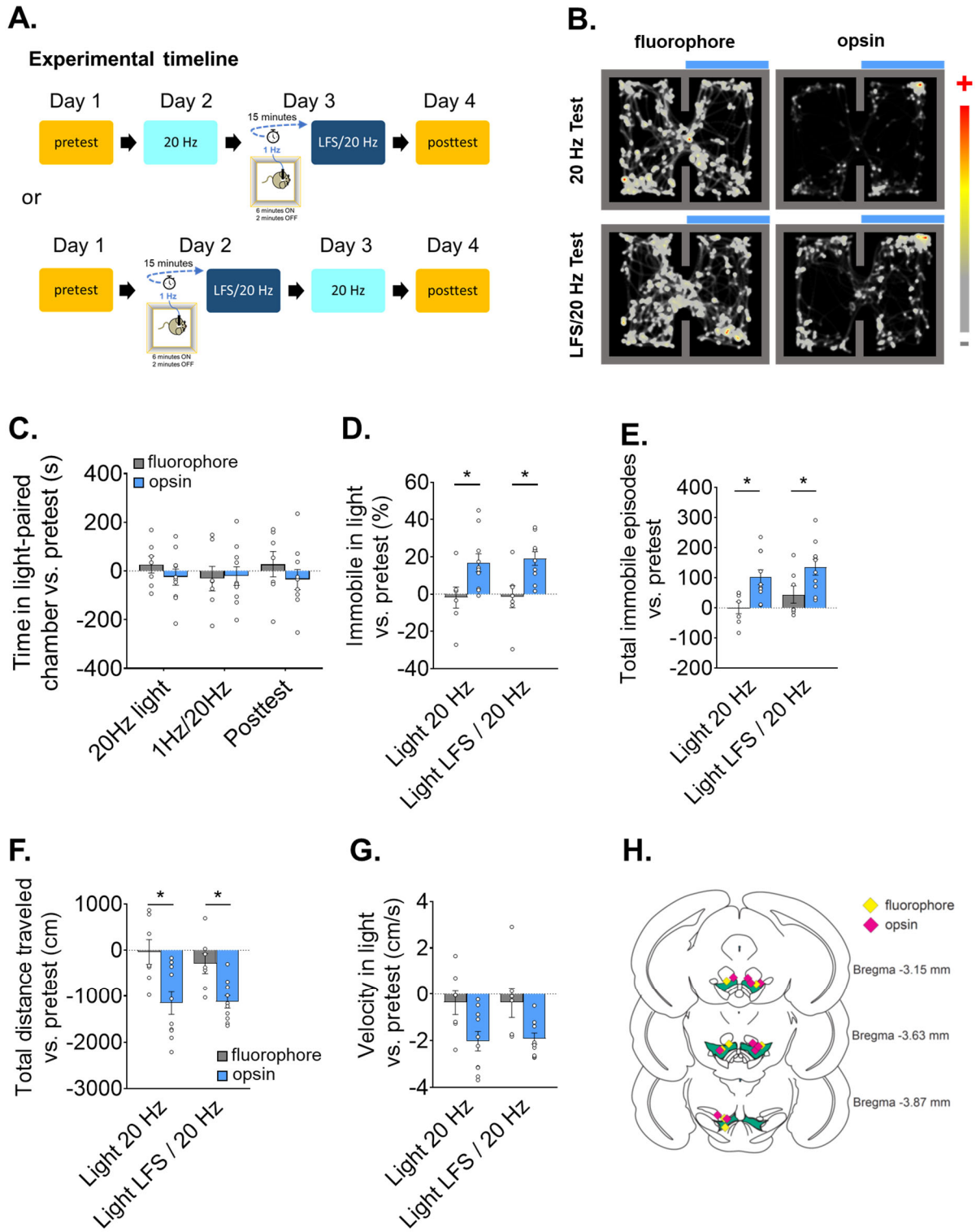


FIGURE 5-2. In vivo stimulation of vPAG_{GABA}→VTA synapses induces quiescence

A. Experimental timeline of real time place preference procedure. Days 1 and 4, no light either side. Days 2 and 3, light paired with one side. LFS: prior to the test on either Day 2 or Day 3, 1 Hz light trains were delivered for 6 min in a separate apparatus. **B.** Representative location plot of a control fluorophore-expressing mouse (left) and opsin-expressing mouse (right) over 10 minute RTPP test sessions. LED light was delivered constantly at 20 Hz if the mouse entered the light-paired chamber. **C.** Average time spent in light-paired chamber vs. pretest (n = 7 fluorophore mice, n = 9 opsin mice). **D.** Mice expressing opsin in the vPAG increased the percentage of time spent immobile on the light-paired side vs. pretest compared to fluorophore control mice. **E.** The frequency of immobility episodes in the arena vs. pretest. **F.** Total distance traveled in the arena vs. pretest. **G.** Mean velocity in light-paired chamber vs. pretest. **H.** Location of fiber implant tip in the VTA, coronal sections adapted from (Franklin, 2013).

Bars represent Mean ± SEM

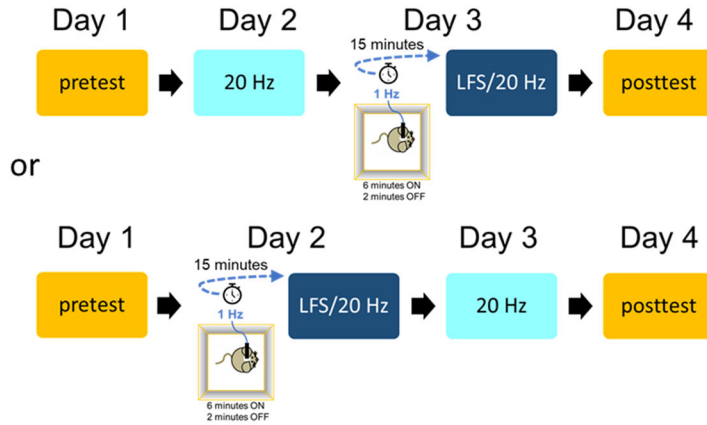
Data analyzed using 2-way ANOVA, Sidak multiple comparisons of fluorophore vs. opsin

**p < 0.05*

FIGURE 5-3. Effect of test order with LFS preconditioning before RTPP

A.

Experimental timeline



B.

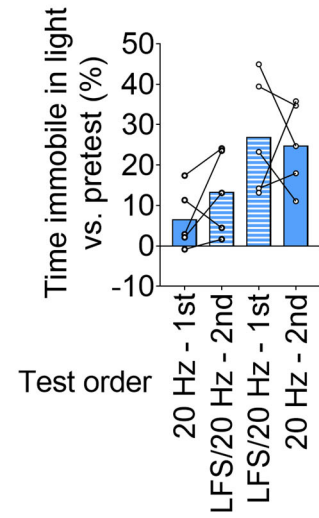


FIGURE 5-3. Test order with LFS preconditioning before RTPP affects quiescence

Comparison of time spent immobile versus pretest values separated by test order. **A.** Counterbalanced experimental design. **B.** Time immobile vs. pretest for vPAG opsin mice. Left two bars indicate that 20 Hz light test occurred on the Day 2 and LFS/20 Hz light test occurred on Day 3. Right two bars indicate the reverse scenario.

FIGURE 5-4. Optogenetically driven quiescent behavior is blocked by systemic morphine

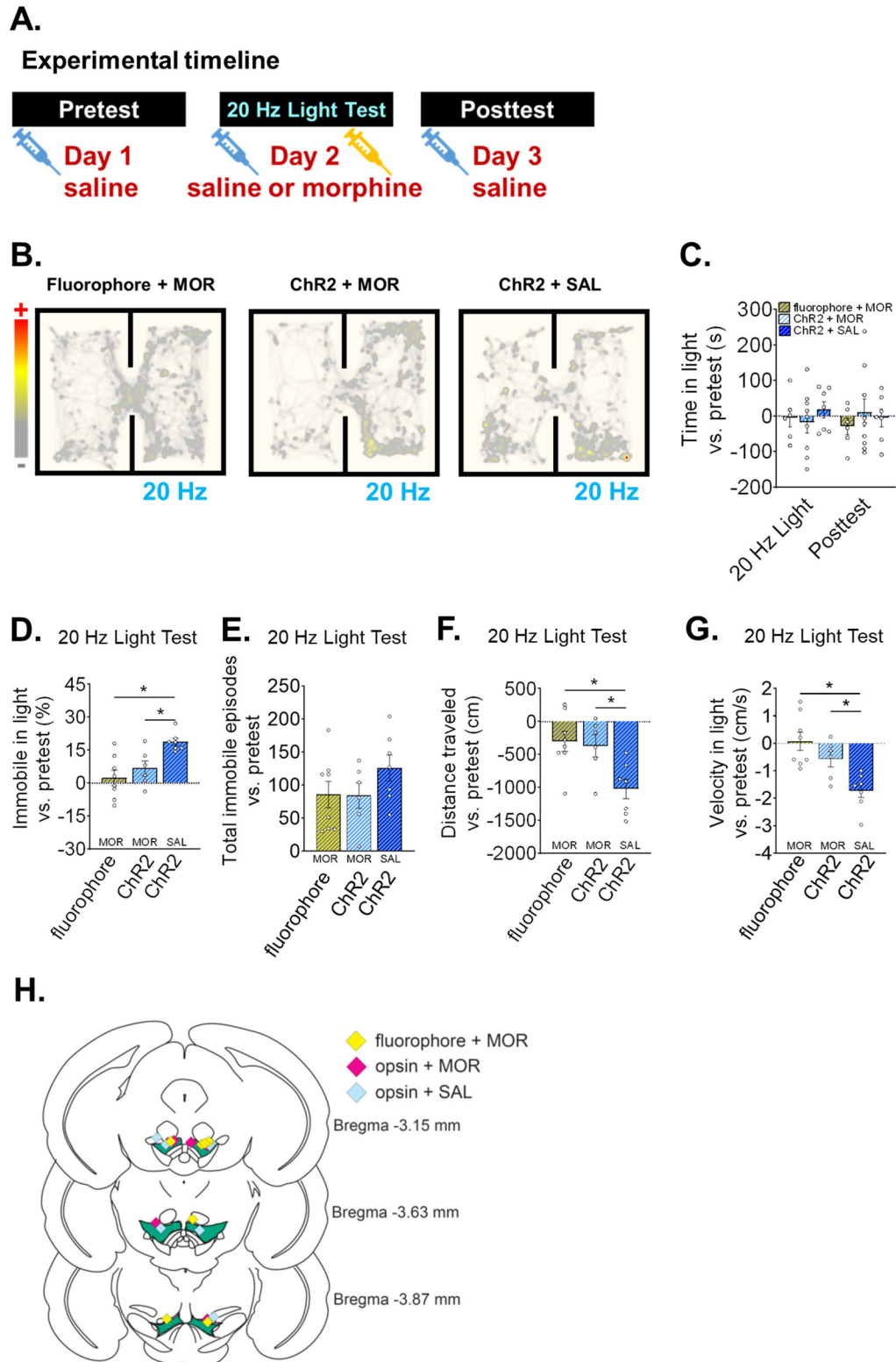


FIGURE 5-4. Optogenetically driven quiescent behavior is blocked by systemic morphine

A. Experimental timeline of real time place preference procedure with morphine. Injections were given 30 minutes prior to testing. **B.** Representative location plots for a 10 minute RTPP light test session. LED light was delivered constantly at 20 Hz if the mouse entered the light-paired chamber. **C.** Average time spent in light-paired chamber vs. pretest (n = 8 fluorophore + MOR, n = 6 opsin + MOR, n = 7 opsin + SAL). **D.** Opsin mice that received a saline injection increased the percentage of time spent immobile on the light-paired side compared to fluorophore or ChR2 mice that received 3 mg/kg morphine mice. **E.** The frequency of immobility episodes in the arena did not differ between groups. **F.** Total distance traveled in the arena vs. pretest was significantly different for the opsin group that received saline. **G.** Mean velocity in light-paired chamber vs. pretest was significantly different for the opsin group that received saline. **H.** Location of fiber implant tip in the VTA, coronal sections adapted from (Franklin, 2013).

Bars represent Mean \pm SEM

Data analyzed using 1-way ANOVA, Tukey's multiple comparisons of fluorophore-MOR, opsin-MOR, and opsin-SAL

**p < 0.05*

FIGURE 5-5. Time course of immobility during light tests

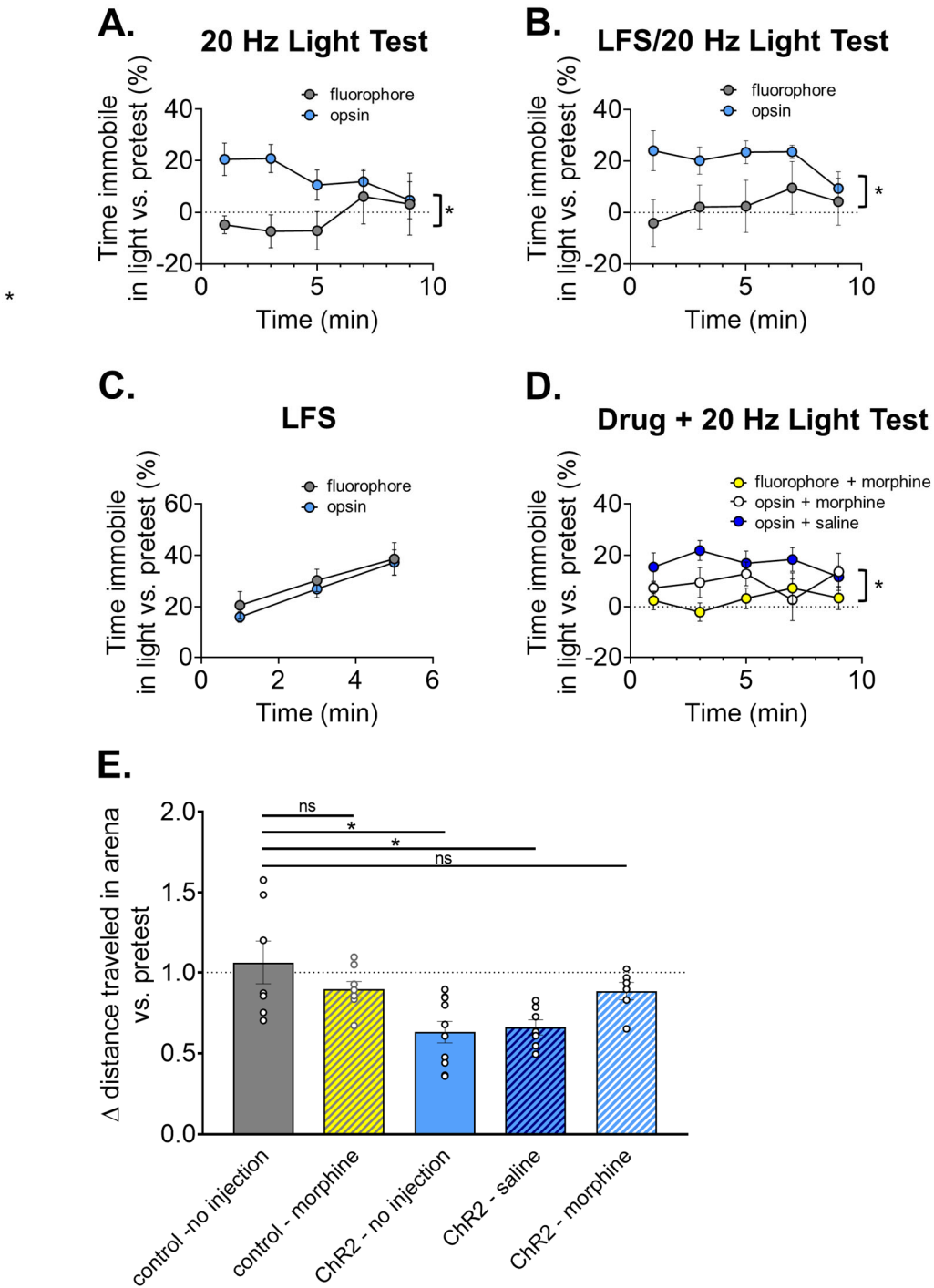


FIGURE 5-5. Time course of immobility during light tests

Time course of immobility during a 20 Hz light test for **A.** 20 Hz only and **B.** LFS/20 Hz light tests. **C.** Time course of immobility during the 6 minutes of LFS preconditioning. **D.** Time course of immobility for saline and morphine 20 Hz light tests. **E.** Distance traveled in the entire arena normalized to the pretest for all 20 Hz light tests.

Bars/circles represent Mean \pm SEM

(A-D) Data analyzed using a mixed model 2-way ANOVA

(E) Data analyzed using a 1-way ANOVA and Dunnett's multiple comparisons

**p < 0.05*

FIGURE 5-6. RMTg_{GABA}→VTA or vPAG_{GABA}→VTA does not disrupt rotarod performance

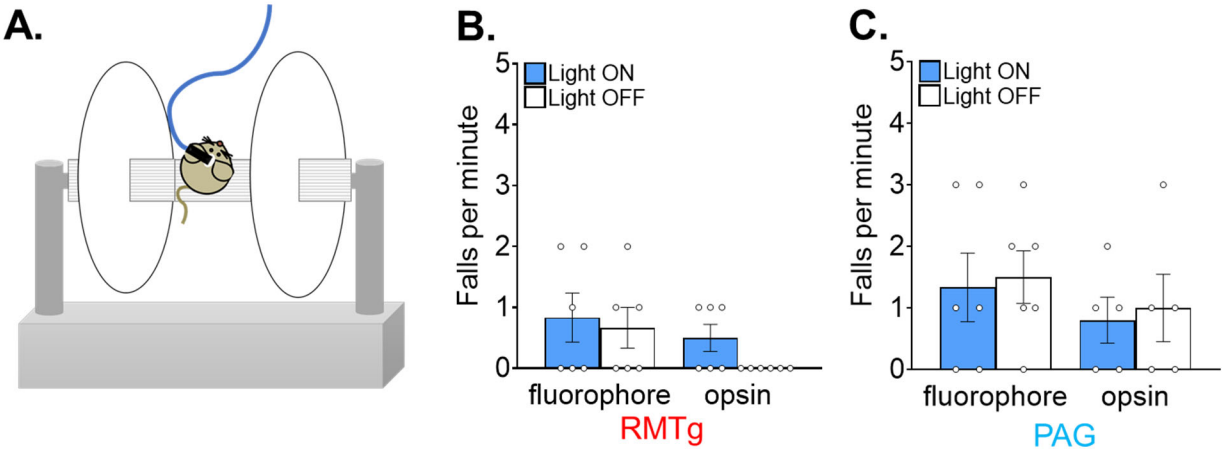


Figure 5-6. RMTg_{GABA}→VTA or vPAG_{GABA}→VTA does not disrupt rotarod performance

A. Diagram of rotarod setup. **B.** Performance on a rotarod test were not different between experimental and control groups in light ON and light OFF conditions for RMTg (60 Hz) or **C.** vPAG (20 Hz) mice.

Bars represent Mean ± SEM

Data analyzed using 2-way ANOVA, Sidak multiple comparisons of fluorophore vs. Chr2 for RMTg and PAG

**p < 0.05*

FIGURE 5-7. RMTg_{GABA}→VTA, but not vPAG_{GABA}→VTA, photoactivation slightly disrupts palatable food consumption

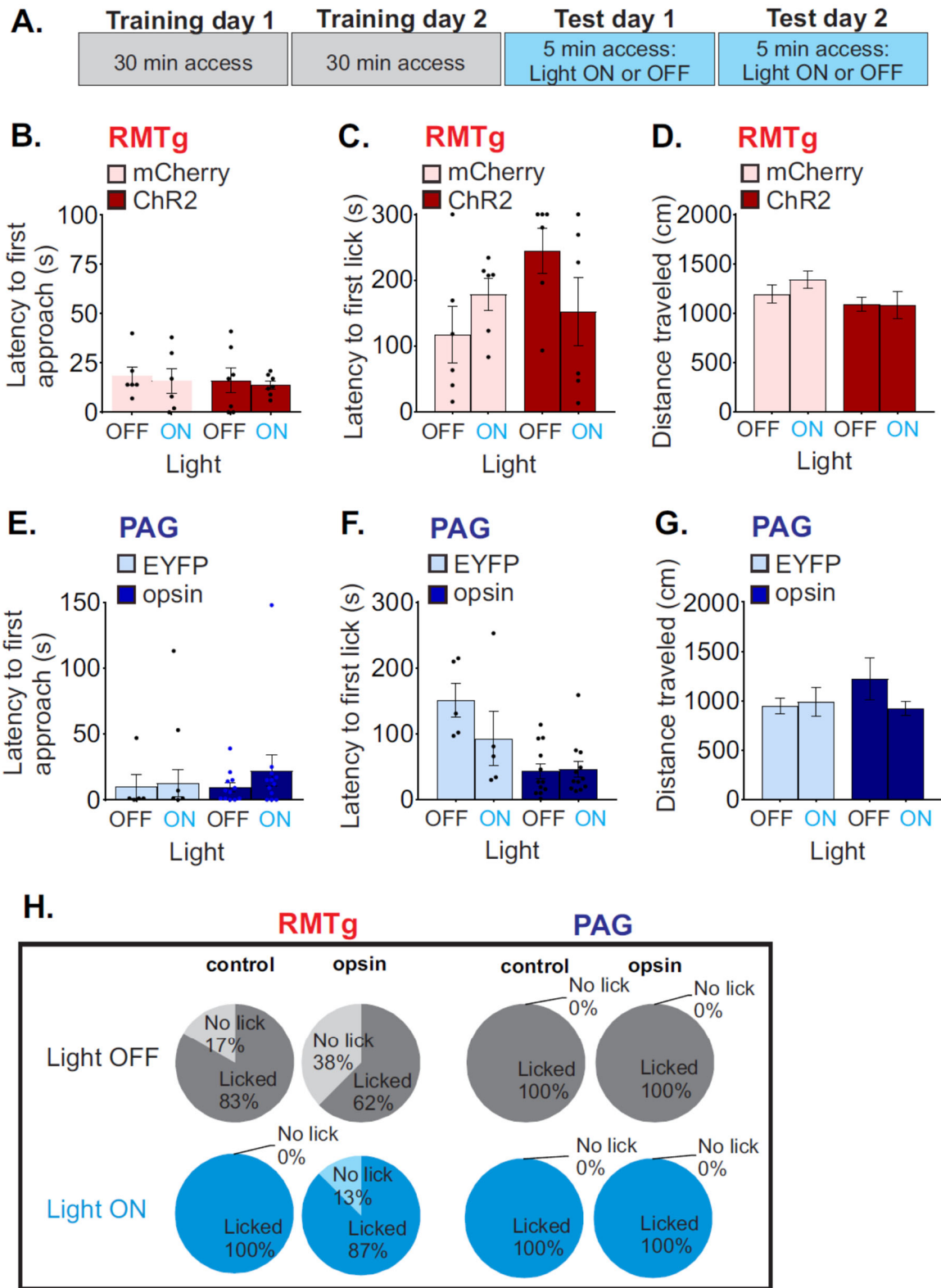


Figure 5-7. RMTg_{GABA}→VTA, but not vPAG_{GABA}→VTA, photoactivation slightly disrupts palatable food consumption

A. Experimental timeline of light-induced suppression of feeding test with sweetened condensed milk. **B.** Average latency to first approach a milk spout was not significantly different from RMTg ChR2 vs. fluorophore mice. **C.** Average latency to first lick a milk spout was not significantly different from RMTg ChR2 vs. fluorophore mice. **D.** Total distance traveled was not significantly different across test days. **E.** Average latency to first approach a milk spout was not significantly different from vPAG ChR2 vs. fluorophore mice. **F.** Average latency to first lick a milk spout was not significantly different from vPAG ChR2 vs. fluorophore mice. **G.** Total distance traveled was not significantly different across test days. **H.** A greater percentage of RMTg ChR2 mice never licked in 5 minute test session vs. RMTg fluorophore mice (left). All vPAG mice licked during all test sessions (right).

Bars represent Mean ± SEM

Data analyzed using 2-way ANOVA, Sidak multiple comparisons of fluorophore vs. ChR2

**p < 0.05*

CHAPTER 6

SUMMARY AND DISCUSSION

6.1 Summary

The dopamine cells in the VTA are a critical node for transmitting signals relating to rewarding and aversive information. While the VTA is heralded for its potential role in addiction, more recent work highlights the unique complexity of different subpopulations within the region. Some of this heterogeneity is determined by the different afferent projections converging onto dopamine cells comprised of excitatory, inhibitory, and neuromodulatory classes. Persistent changes in synaptic strength can fundamentally alter the output of VTA dopamine cells. There is a rich literature aimed at understanding alterations at excitatory synapses in the VTA and some studies have even informed effective therapeutic intervention in human drug addicts. However, inhibitory synaptic plasticity in the VTA is comparatively under-studied, despite inhibition being a crucial regulator of dopamine cells and a nearly ubiquitous component of circuits throughout the central nervous system. Removing the influence of even a single inhibitory afferent to the VTA can occlude the excitatory effect of opioids on dopamine cells (Jalabert et al., 2011). Opioids act mainly on inhibitory synapses in the VTA and block two known forms of plasticity at inhibitory synapses, LTP_{GABA} and LTD_{GABA} (Nugent et al., 2007, Dacher and Nugent, 2011). Recently, LTP_{GABA} was shown to not be ubiquitous at all GABA synapses. The original finding of LTP_{GABA} used electrical stimulation and the follow-up studies used optogenetic stimulation of VTA, RMTg, or NAc-originating afferents. It is likely that the discrepancy results from electrical stimulation biasing toward activating some synapses while excluding others. If this is true, it means that other prior reports of synaptic plasticity are likely to be afferent-specific, but also that there could be other forms that are yet to be discovered.

In Chapter 3 I use a location of a stimulation electrode that differs from the typical one – placed caudal to and outside of the VTA in a horizontal slice (Figure 3-1A). With this placement, I serendipitously discovered that the induction protocol used to induce LTD_{GABA} instead potentiated GABA inputs. Furthermore, this LTP occurred independently of NMDAR activation and was not

occluded by forskolin, indicating that it occurs via a mechanism distinct from LTP_{GABA} . In Chapter 4, I use optogenetic isolation of RMTg or PAG afferent inputs and found that $LFS-LTP_{GABA}$ is expressed at PAG synapses and conversely, RMTg inputs express the canonical LTD_{GABA} . The differences between these two inputs did not stop with synaptic plasticity; RMTg and PAG synapses differed in opioid sensitivity, basal amplitude, and behavioral output. In Chapter 4, I found that PAG inputs were depressed more than RMTg inputs that, prior to this report, were the most opioid-sensitive afferent input. In Chapter 5, $RMTg_{GABA} \rightarrow VTA$ photoactivation caused real time place aversion but PAG photoactivation did not cause aversion or preference. Instead, $PAG_{GABA} \rightarrow VTA$ photoactivation resulted in a quiescent phenotype characterized by bouts of immobility. Furthermore, quiescence evoked by $PAG_{GABA} \rightarrow VTA$ photostimulation was prevented by morphine administration.

6.2 Shared or unique mechanisms of electrical LFS-LTP and PAG LFS-LTP

The PAG was not the first region that I hypothesized was being stimulated by my caudal electrode. However, it is possible that the topographical organization of PAG projections matches with the stimulation location. Efferent projections from the PAG are organized into bundles based on projection regions. The ventral bundle innervates the VTA, substantia nigra, and retrorubral field (Cameron et al., 1995). The most likely conclusion is that the caudal electrical stimulation was biased towards PAG inputs, however, there are alternative explanations. Other caudal regions that I did not test, such as the dorsal raphe or LDT, may exhibit LFS-LTP too and could have been activated by the caudal electrode. Occlusion experiments with electrical and optogenetic stimulation are required to test they hypothesis that the two LTP results are both from PAG synapses. Another explanation of the optogenetic RMTg results is that the expression of the opsin interfered with the LFS-LTP induction mechanism, although this explanation is unlikely given that the PAG inputs were able to potentiate.

Based on the current results, it appears that presynaptic region determines plasticity outcome with LFS, however, postsynaptic cell identity – a variable not investigated here - can also dictate plasticity (Dacher et al., 2013). In other regions, such as the hippocampus, a single afferent input can have divergent synaptic plasticity outcomes separated solely on the postsynaptic cell target (Pelkey et al., 2005, Pelkey et al., 2006). In this case, mossy fiber to CA3 pyramidal cell synapses potentiated with HFS but mossy fiber to CA3 interneuron synapses depressed with HFS. However, when metabotropic glutamate receptor subtype 7 (mGluR7) activation preceded HFS in the mossy fiber to interneuron experiments, mGluR7 was internalized, and HFS-induced potentiation was unmasked (Pelkey et al., 2005). Similarly, at mossy fiber to stratum lacunosum-moleculare interneuron synapses, HFS resulted in LTD rather than LTP when mGluR α were blocked (Galvan et al., 2008). It is possible that plasticity of VTA inhibitory afferents could share a similar principle: under certain conditions, synapses may display LTD or LTP with the same plasticity induction protocol. However, there remains a lot of work to first understand the basis of the LFS-LTP at PAG synapses before investigating if this form of plasticity is latent at other afferent synapses.

A major remaining question about this newfound LTP is what the underlying mechanism is. For electrical LFS, NMDAR antagonism, postsynaptic calcium chelation, postsynaptic GPCR inhibition, and prior forskolin potentiation did not block or occlude LTP. For optogenetic PAG experiments, I tried several other mechanistic experiments. One hypothesis was based on the fact that PAG cells projecting to the VTA had evidence of dense core vesicles and therefore may release peptides in addition to classical neurotransmitter. However, the first peptide receptor antagonist that I chose, for neurotensin receptor 1, does not block LTP of light-evoked PAG inputs (Figure 4-5 A-C). Additional manipulations that did not block LTP of PAG inputs were NMDAR antagonism or genetic isolation of VGAT-defined presynaptic inputs. Another possible mechanism is that VGAT+ cells could co-release glutamate and activate mGluR on presynaptic

or postsynaptic terminals, setting off a signaling cascade that leads to increased GABA release. I did find that when depolarization to -40 mV during the optical LFS was omitted, LTP did not occur. Future experiments will be needed to investigate this perplexing result – perhaps explained by calcium entry or release of a signaling molecule that depends on postsynaptic depolarization.

6.3 Recognition of VTA inhibitory sources as a heterogeneous population

The results detailed in the previous data chapters show that not only are VTA dopamine cells themselves heterogeneous, but their afferent inputs are as well. It was surprising that caudal stimulation did not appear to be preferentially activating the RMTg mainly because it is located just caudal to the VTA, and initially the caudal placement was used to attempt to activate RMTg terminals specifically. Although, LFS did not always result in LTP with electrical stimulation, and those experiments could reasonably have included RMTg inputs. Additionally, with caudal stimulation I sometimes recorded excessively large amplitude currents, on the order of 1-2 nA, that I hypothesize may have originated in the RMTg. The physiological properties of these currents were quite interesting, in addition to the large amplitude, they often had an all-or-none quality to them (Figure 6-1). Due to technical limitations in effectively voltage-clamping such a large input, these experiments were excluded from analyses. However, it would be fascinating to determine if these inputs originated in the RMTg. The Jhou lab reports that RMTg synapses on VTA dopamine cells sometimes synapse on proximal dendrites and appear to contact the dendrite almost like a climbing fiber (personal communication).

6.4 Afferent-specific regulation of opioid responses

Not only did RMTg and PAG inputs differ in the amount of current generated by photostimulation, but they also differed in acute depression by a MOR agonist (DAMGO). It is well established that opioids hyperpolarize GABA neurons by activating a potassium current through GIRK channels

(Johnson and North, 1992, Chieng et al., 2011, Jalabert et al., 2011). However, the density of opioid receptors, coupling efficiency to G proteins, or heterogeneity of opioid receptor expression within an afferent population could explain differences in opioid responsivity. Furthermore, different downstream signaling pathways could also account for differences. For instance, DAMGO depresses GABAergic activity via different mechanisms in the VTA and PAG: DAMGO's effect on GABAergic inputs required Gi protein and potassium channels sensitive to 4-AP in VTA cells but required phospholipase 2 signaling in PAG cells (Zhang et al., 2015). One hypothesis is that PAG terminals in the VTA require phospholipase 2 signaling and RMTg terminals require potassium currents for opioid-induced depression of GABAergic inhibition, and somehow phospholipase 2 signaling causes more profound hyperpolarization. Furthermore, differences in downstream signaling during opioid exposure could lead to long-lasting changes that regulate different aspects of maladaptive outcomes with opioid abuse.

At the behavioral level, different afferent populations may regulate different facets of opioid responses. For instance, neural correlates of acute opioid actions, opioid tolerance, and opioid withdrawal are differently mediated by VTA→VTA, RMTg→VTA, and NAc→VTA synapses (Matsui et al., 2014). Future experiments should investigate the possibility that the PAG→VTA projection is involved in acute or chronic opioid responses. The PAG is implicated in many aspects of the opioid response, and it is possible that the VTA projection regulates one or several of these.

6.5 Further characterization of synaptic plasticity and other behaviors linked to the VTA

One of the main takeaway messages from my dissertation is that there is a lot of complexity in the VTA that can be attributed to subcircuit organization (Figure 2). I demonstrated that while some canonical forms of synaptic plasticity exist at inhibitory synapses in the VTA, there are also other less common and unidentified forms as well. Furthermore, I isolated two GABAergic afferents and showed that different forms of synaptic plasticity mapped differently onto RMTg and

PAG inputs. Synaptic plasticity was not the only property that differed between afferent regions: opioid responses and behavior also differed. While these results were very informative for understanding the afferent populations, this is just the tip of the iceberg. Future experiments should include further investigation of the full complement of synaptic plasticity forms that can be expressed at these two inputs and whether drugs of abuse block them. For instance, it is unknown if the $\text{PAG}_{\text{GABA}} \rightarrow \text{VTA}$ synapse expresses nitric oxide-dependent LTP_{GABA} or if morphine administration blocks LFS-LTP. Additionally, it is important to determine if certain stimuli, such as aversive, painful, or fear-related stimuli, can induce LFS-LTD or LFS-LTP in the RMTg and PAG, respectively. Future work is needed to determine what aspects of PAG-mediated behaviors rely on the GABAergic projection to the VTA.

FIGURE 6-1. Exceptionally large amplitude inhibitory currents

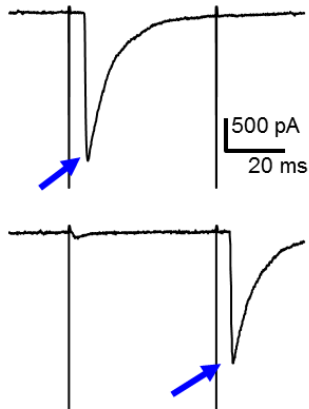
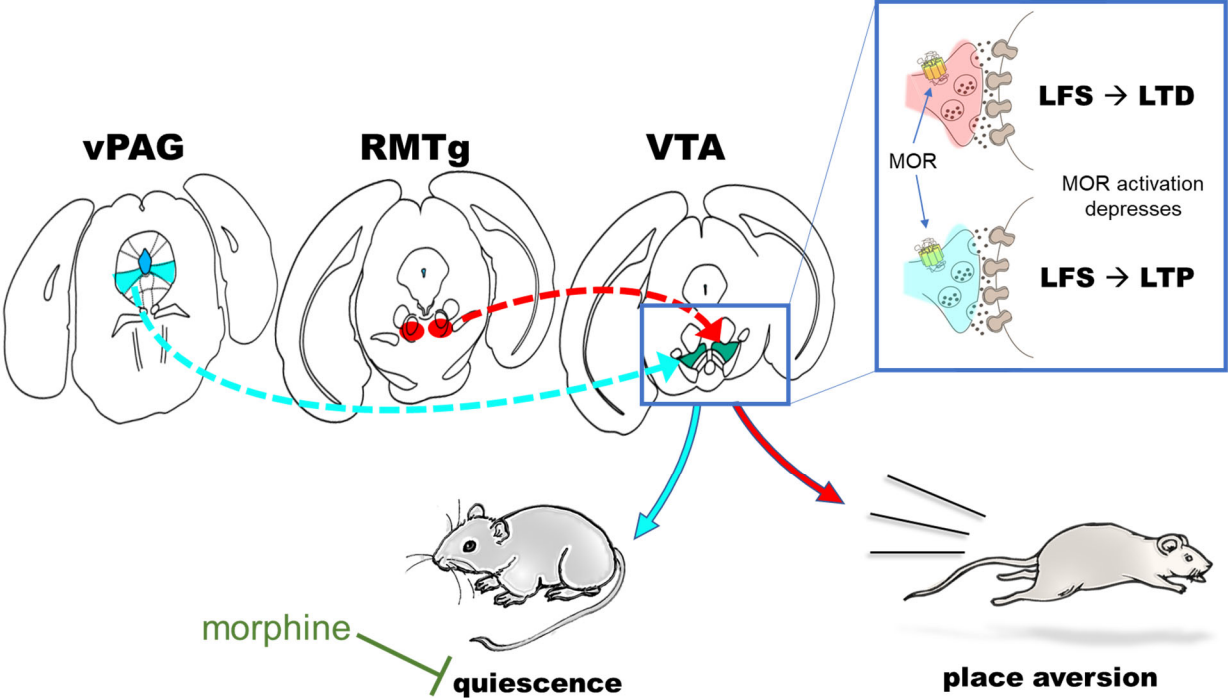


FIGURE 6-1. Exceptionally large amplitude inhibitory currents

Consecutive sweeps showing a large amplitude event (note scale bar) has all-or-none responses, only observed on one of two paired pulses at a time.

FIGURE 6-2. Summary



REFERENCES

- ADAMANTIDIS, A. R., TSAI, H.-C., BOUTREL, B., ZHANG, F., STUBER, G. D., BUDYGIN, E. A., TOURINO, C., BONCI, A., DEISSEROTH, K. & DE LECEA, L. 2011. Optogenetic interrogation of dopaminergic modulation of the multiple phases of reward-seeking behavior. *The Journal of neuroscience : the official journal of the Society for Neuroscience*, 31, 10829-35.
- ASSAREH, N., BAGLEY, E. E., CARRIVE, P. & MCNALLY, G. P. 2017. Brief optogenetic inhibition of rat lateral or ventrolateral periaqueductal gray augments the acquisition of Pavlovian fear conditioning. *Behav Neurosci*, 131, 454-459.
- BAIMEL, C., LAU, B. K., QIAO, M. & BORGLAND, S. L. 2017. Projection-Target-Defined Effects of Orexin and Dynorphin on VTA Dopamine Neurons. *Cell Rep*, 18, 1346-1355.
- BALCITA-PEDICINO, J. J., OMELCHENKO, N., BELL, R. & SESACK, S. R. 2011. The inhibitory influence of the lateral habenula on midbrain dopamine cells: Ultrastructural evidence for indirect mediation via the rostromedial mesopontine tegmental nucleus. *Journal of Comparative Neurology*, 519, 1143-1164.
- BANDLER, R. & KEAY, K. A. 1996. Columnar organization in the midbrain periaqueductal gray and the integration of emotional expression. *Prog Brain Res*, 107, 285-300.
- BANDLER, R. & SHIPLEY, M. T. 1994. Columnar organization in the midbrain periaqueductal gray: modules for emotional expression? *Trends Neurosci*, 17, 379-89.
- BARROT, M., SESACK, S. R., GEORGES, F., PISTIS, M., HONG, S. & JHOU, T. C. 2012. Braking Dopamine Systems: A New GABA Master Structure for Mesolimbic and Nigrostriatal Functions. *Journal of Neuroscience*, 32, 14094-14101.
- BEAR, M. F. & MALENKA, R. C. 1994. Synaptic plasticity: LTP and LTD. *Curr Opin Neurobiol*, 4, 389-99.
- BEIER, K. T., STEINBERG, E. E., DELOACH, K. E., XIE, S., MIYAMICHI, K., SCHWARZ, L., GAO, X. J., KREMER, E. J., MALENKA, R. C. & LUO, L. 2015. Circuit Architecture of VTA Dopamine Neurons Revealed by Systematic Input-Output Mapping. *Cell*, 162, 622-634.
- BEITZ, A. J., SHEPARD, R. D. & WELLS, W. E. 1983. The periaqueductal gray-raphé magnus projection contains somatostatin, neurotensin and serotonin but not cholecystokinin. *Brain Res*, 261, 132-7.
- BLACKMER, T., LARSEN, E. C., BARTLESON, C., KOWALCHYK, J. A., YOON, E.-J., PREININGER, A. M., ALFORD, S., HAMM, H. E. & MARTIN, T. F. J. 2005. G protein betagamma directly regulates SNARE protein fusion machinery for secretory granule exocytosis. *Nature neuroscience*, 8, 421-425.
- BOCKLISCH, C., PASCOLI, V., WONG, J. C. Y., HOUSE, D. R. C., YVON, C., DE ROO, M., TAN, K. R. & LÜSCHER, C. 2013. Cocaine disinhibits dopamine neurons by potentiation of GABA transmission in the ventral tegmental area. *Science (New York, N.Y.)*, 341, 1521-5.
- BONCI, A. & MALENKA, R. C. 1999. Properties and plasticity of excitatory synapses on dopaminergic and GABAergic cells in the ventral tegmental area. *The Journal of neuroscience : the official journal of the Society for Neuroscience*, 19, 3723-30.
- BONCI, A. & WILLIAMS, J. T. 1996. A common mechanism mediates long-term changes in synaptic transmission after chronic cocaine and morphine. *Neuron*, 16, 631-9.
- BONCI, A. & WILLIAMS, J. T. 1997. Increased probability of GABA release during withdrawal from morphine. *J Neurosci*, 17, 796-803.
- BOZARTH, M. A. & WISE, R. A. 1981. Intracranial self-administration of morphine into the ventral tegmental area in rats. *Life Sciences*, 28, 551-555.

- BRIGGS, C. A., MCAFEE, D. A. & MCCAMAN, R. E. 1988. Long-term regulation of synaptic acetylcholine release and nicotinic transmission: the role of cyclic AMP. *Br J Pharmacol*, 93, 399-411.
- CAMERON, A. A., KHAN, I. A., WESTLUND, K. N., CLIFFER, K. D. & WILLIS, W. D. 1995. The efferent projections of the periaqueductal gray in the rat: a Phaseolus vulgaris-leucoagglutinin study. I. Ascending projections. *J Comp Neurol*, 351, 568-84.
- CAMERON, D. L. & WILLIAMS, J. T. 1993. Dopamine D1 receptors facilitate transmitter release. *Nature*, 366, 344-7.
- CASTRO-ALAMANCOS, M. A. & CALCAGNOTTO, M. E. 1999. Presynaptic long-term potentiation in corticothalamic synapses. *J Neurosci*, 19, 9090-7.
- CHAVEZ-NORIEGA, L. E. & STEVENS, C. F. 1994. Increased transmitter release at excitatory synapses produced by direct activation of adenylate cyclase in rat hippocampal slices. *J Neurosci*, 14, 310-7.
- CHERGUI, K., CHARLETY, P. J., AKAOKA, H., SAUNIER, C. F., BRUNET, J. L., BUDA, M., SVENSSON, T. H. & CHOUVET, G. 1993. Tonic activation of NMDA receptors causes spontaneous burst discharge of rat midbrain dopamine neurons in vivo. *Eur J Neurosci*, 5, 137-44.
- CHIENG, B., AZRIEL, Y., MOHAMMADI, S. & CHRISTIE, M. J. 2011. Distinct cellular properties of identified dopaminergic and GABAergic neurons in the mouse ventral tegmental area. *J Physiol*, 589, 3775-87.
- CHU SIN CHUNG, P. & KIEFFER, B. L. 2013. Delta opioid receptors in brain function and diseases. *Pharmacology & therapeutics*, 140, 112-20.
- DACHER, M., GOUTY, S., DASH, S., COX, B. M. & NUGENT, F. S. 2013. A-Kinase Anchoring Protein-Calcineurin Signaling in Long-Term Depression of GABAergic Synapses. *Journal of Neuroscience*, 33, 2650-2660.
- DACHER, M. & NUGENT, F. S. 2011. Morphine-induced modulation of LTD at GABAergic synapses in the ventral tegmental area. *Neuropharmacology*, 61, 1166-1171.
- DE GUGLIELMO, G., MELIS, M., DE LUCA, M. A., KALLUPI, M., LI, H. W., NISWENDER, K., GIORDANO, A., SENZACQUA, M., SOMAINI, L., CIPPITELLI, A., GAITANARIS, G., DEMOPULOS, G., DAMADZIC, R., TAPOCIK, J., HEILIG, M. & CICCOCIOPPO, R. 2014. PPAR γ Activation Attenuates Opioid Consumption and Modulates Mesolimbic Dopamine Transmission. *Neuropsychopharmacology*, 40, 927-937.
- DE OLIVEIRA, A. R., REIMER, A. E., REIS, F. M. & BRANDAO, M. L. 2017. Dopamine D2-like receptors modulate freezing response, but not the activation of HPA axis, during the expression of conditioned fear. *Exp Brain Res*, 235, 429-436.
- DEISTER, C. A., TEAGARDEN, M. A., WILSON, C. J. & PALADINI, C. A. 2009. An intrinsic neuronal oscillator underlies dopaminergic neuron bursting. *J Neurosci*, 29, 15888-97.
- DENG, H., XIAO, X. & WANG, Z. 2016. Periaqueductal Gray Neuronal Activities Underlie Different Aspects of Defensive Behaviors. *J Neurosci*, 36, 7580-8.
- DEPAULIS, A., KEAY, K. A. & BANDLER, R. 1994. Quiescence and hyporeactivity evoked by activation of cell bodies in the ventrolateral midbrain periaqueductal gray of the rat. *Experimental Brain Research*.
- DI CHIARA, G. & IMPERATO, A. 1988. Drugs abused by humans preferentially increase synaptic dopamine concentrations in the mesolimbic system of freely moving rats. *Proceedings of the National Academy of Sciences of the United States of America*, 85, 5274-5278.
- EDWARDS, N. J., TEJEDA, H. A., PIGNATELLI, M., ZHANG, S., MCDEVITT, R. A., WU, J., BASS, C. E., BETTLER, B., MORALES, M. & BONCI, A. 2017. Circuit specificity in the inhibitory architecture of the VTA regulates cocaine-induced behavior. *Nat Neurosci*, 20, 438-448.

- EKSTRAND, M. I., NECTOW, A. R., KNIGHT, Z. A., LATCHA, K. N., POMERANZ, L. E. & FRIEDMAN, J. M. 2014. Molecular profiling of neurons based on connectivity. *Cell*, 157, 1230-1242.
- FAGET, L., OSAKADA, F., DUAN, J., RESSLER, R., JOHNSON, A. B., PROUDFOOT, J. A., YOO, J. H., CALLAWAY, E. M. & HNASKO, T. S. 2016. Afferent Inputs to Neurotransmitter-Defined Cell Types in the Ventral Tegmental Area. *Cell Reports*, 15, 2796-2808.
- FALEIRO, L. J., JONES, S. & KAUER, J. A. 2004. Rapid synaptic plasticity of glutamatergic synapses on dopamine neurons in the ventral tegmental area in response to acute amphetamine injection. *Neuropsychopharmacology : official publication of the American College of Neuropsychopharmacology*, 29, 2115-25.
- FATTORINI, G., ANTONUCCI, F., MENNA, E., MATTEOLI, M. & CONTI, F. 2015. Co-expression of VGLUT1 and VGAT sustains glutamate and GABA co-release and is regulated by activity in cortical neurons. *J Cell Sci*, 128, 1669-73.
- FLORESCO, S. B., WEST, A. R., ASH, B., MOORE, H. & GRACE, A. A. 2003. Afferent modulation of dopamine neuron firing differentially regulates tonic and phasic dopamine transmission. *Nature neuroscience*, 6, 968-73.
- FORD, C. P., MARK, G. P. & WILLIAMS, J. T. 2006. Properties and opioid inhibition of mesolimbic dopamine neurons vary according to target location. *The Journal of neuroscience : the official journal of the Society for Neuroscience*, 26, 2788-97.
- FORSTER, G. L. & BLAHA, C. D. 2000. Laterodorsal tegmental stimulation elicits dopamine efflux in the rat nucleus accumbens by activation of acetylcholine and glutamate receptors in the ventral tegmental area. *European Journal of Neuroscience*, 12, 3596-3604.
- FRANKLIN, G. P. K. B. J. 2013. *The Mouse Brain in stereotaxic coordinates, 4th edition*.
- GALVAN, E. J., CALIXTO, E. & BARRIONUEVO, G. 2008. Bidirectional Hebbian plasticity at hippocampal mossy fiber synapses on CA3 interneurons. *J Neurosci*, 28, 14042-55.
- GARIANO, R. F. & GROVES, P. M. 1988. Burst firing induced in midbrain dopamine neurons by stimulation of the medial prefrontal and anterior cingulate cortices. *Brain Research*, 462, 194-198.
- GEISLER, S. & ZAHM, D. S. 2005. Afferents of the ventral tegmental area in the rat-anatomical substratum for integrative functions. *Journal of Comparative Neurology*, 490, 270-294.
- GEORGES, F. & ASTON-JONES, G. 2001. Potent regulation of midbrain dopamine neurons by the bed nucleus of the stria terminalis. *The Journal of neuroscience : the official journal of the Society for Neuroscience*, 21, RC160.
- GEORGES, F. & ASTON-JONES, G. 2002. Activation of ventral tegmental area cells by the bed nucleus of the stria terminalis: a novel excitatory amino acid input to midbrain dopamine neurons. *J Neurosci*, 22, 5173-5187.
- GERACHSHENKO, T., BLACKMER, T., YOON, E.-J., BARTLESON, C., HAMM, H. E. & ALFORD, S. 2005. Gbetagamma acts at the C terminus of SNAP-25 to mediate presynaptic inhibition. *Nature neuroscience*, 8, 597-605.
- GLOVER, E. J., MCDUGGLE, M. J., SIEGEL, G. S., JHOU, T. C. & CHANDLER, L. J. 2016. Role for the Rostromedial Tegmental Nucleus in Signaling the Aversive Properties of Alcohol. *Alcohol Clin Exp Res*, 40, 1651-61.
- GONÇALVES, L., SEGO, C. & METZGER, M. 2012. Differential projections from the lateral habenula to the rostromedial tegmental nucleus and ventral tegmental area in the rat. *Journal of Comparative Neurology*, 520, 1278-1300.
- GONZALES, C. & CHESSELET, M. F. 1990. Amygdalonigral pathway: An anterograde study in the rat with Phaseolus vulgaris leucoagglutinin (PHA-L). *Journal of Comparative Neurology*, 297, 182-200.

- GONZALEZ, J., MORALES, I. S., VILLARREAL, D. M. & DERRICK, B. E. 2014. Low-frequency stimulation induces long-term depression and slow onset long-term potentiation at perforant path-dentate gyrus synapses in vivo. *J Neurophysiol*, 111, 1259-73.
- GRACE, A. A. & BUNNEY, B. S. 1984. The control of firing pattern in nigral dopamine neurons: burst firing. *J Neurosci*, 4, 2877-90.
- GRANGER, A. J., WALLACE, M. L. & SABATINI, B. L. 2017. Multi-transmitter neurons in the mammalian central nervous system. *Curr Opin Neurobiol*, 45, 85-91.
- GRAZIANE, N. M., POLTER, A. M., BRIAND, L. A., PIERCE, R. C. & KAUER, J. A. 2013. Kappa opioid receptors regulate stress-induced cocaine seeking and synaptic plasticity. *Neuron*, 77, 942-954.
- GREENGARD, P., JEN, J., NAIRN, A. C. & STEVENS, C. F. 1991. Enhancement of the glutamate response by cAMP-dependent protein kinase in hippocampal neurons. *Science*, 253, 1135-8.
- GROESSL, F., MUNSCH, T., MEIS, S., GRIESSNER, J., KACZANOWSKA, J., PLIOTA, P., KARGL, D., BADUREK, S., KRAITSY, K., RASSOULPOUR, A., ZUBER, J., LESSMANN, V. & HAUBENSAK, W. 2018. Dorsal tegmental dopamine neurons gate associative learning of fear. *Nat Neurosci*, 21, 952-962.
- GUAN, Y.-Z. & YE, J.-H. 2010. Ethanol blocks long-term potentiation of GABAergic synapses in the ventral tegmental area involving mu-opioid receptors. *Neuropsychopharmacology : official publication of the American College of Neuropsychopharmacology*, 35, 1841-1849.
- GUTLERNER, J. L., PENICK, E. C., SNYDER, E. M. & KAUER, J. A. 2002. Novel protein kinase A-dependent long-term depression of excitatory synapses. *Neuron*, 36, 921-31.
- GYSLING, K. & WANG, R. Y. 1983. Morphine-induced activation of A10 dopamine neurons in the rat. *Brain Res*, 277, 119-27.
- HNASKO, T. S., HJELMSTAD, G. O., FIELDS, H. L. & EDWARDS, R. H. 2012. Ventral tegmental area glutamate neurons: electrophysiological properties and projections. *J Neurosci*, 32, 15076-85.
- HOLLERMAN, J. R. & SCHULTZ, W. 1998. Dopamine neurons report an error in the temporal prediction of reward during learning. *Nat Neurosci*, 1, 304-9.
- HONG, S., JHOU, T. C., SMITH, M., SALEEM, K. S. & HIKOSAKA, O. 2011. Negative reward signals from the lateral habenula to dopamine neurons are mediated by rostromedial tegmental nucleus in primates. *The Journal of neuroscience : the official journal of the Society for Neuroscience*, 31, 11457-71.
- HUANG, Y. Y. & KANDEL, E. R. 1994. Recruitment of long-lasting and protein kinase A-dependent long-term potentiation in the CA1 region of hippocampus requires repeated tetanization. *Learn Mem*, 1, 74-82.
- HUANG, Y. Y. & KANDEL, E. R. 1998. Postsynaptic induction and PKA-dependent expression of LTP in the lateral amygdala. *Neuron*, 21, 169-78.
- HYLAND, B. I., REYNOLDS, J. N., HAY, J., PERK, C. G. & MILLER, R. 2002. Firing modes of midbrain dopamine cells in the freely moving rat. *Neuroscience*, 114, 475-92.
- HYMAN, S. E., MALENKA, R. C. & NESTLER, E. J. 2006. Neural mechanisms of addiction: the role of reward-related learning and memory. *Annu Rev Neurosci*, 29, 565-98.
- ILANGO, A., KESNER, A. J., KELLER, K. L., STUBER, G. D., BONCI, A. & IKEMOTO, S. 2014. Similar roles of substantia nigra and ventral tegmental dopamine neurons in reward and aversion. *J Neurosci*, 34, 817-822.
- JALABERT, M., BOURDY, R., COURTIN, J., VEINANTE, P., MANZONI, O. J., BARROT, M. & GEORGES, F. 2011. Neuronal circuits underlying acute morphine action on dopamine neurons. *Proc. Natl. Acad. Sci. U. S. A.*, 108, 16446-16450.

- JENNINGS, J. H., SPARTA, D. R., STAMATAKIS, A. M., UNG, R. L., PLEIL, K. E., KASH, T. L. & STUBER, G. D. 2013. Distinct extended amygdala circuits for divergent motivational states. *Nature*, 496, 224-228.
- JENSEN, T. S. & YAKSH, T. L. 1989. Comparison of the antinociceptive effect of morphine and glutamate at coincidental sites in the periaqueductal gray and medial medulla in rats. *Brain Res*, 476, 1-9.
- JHOU, T. C., FIELDS, H. L., BAXTER, M. G., SAPER, C. B. & HOLLAND, P. C. 2009a. The Rostromedial Tegmental Nucleus (RMTg), a GABAergic Afferent to Midbrain Dopamine Neurons, Encodes Aversive Stimuli and Inhibits Motor Responses. *Neuron*, 61, 786-800.
- JHOU, T. C., GEISLER, S., MARINELLI, M., DEGARMO, B. A. & ZAHM, D. S. 2009b. The mesopontine rostromedial tegmental nucleus: A structure targeted by the lateral habenula that projects to the ventral tegmental area of Tsai and substantia nigra compacta. *Journal of Comparative Neurology*, 513, 566-596.
- JHOU, T. C., GOOD, C. H., ROWLEY, C. S., XU, S.-P., WANG, H., BURNHAM, N. W., HOFFMAN, A. F., LUPICA, C. R. & IKEMOTO, S. 2013. Cocaine drives aversive conditioning via delayed activation of dopamine-responsive habenular and midbrain pathways. *The Journal of neuroscience : the official journal of the Society for Neuroscience*, 33, 7501-12.
- JOHANSEN, J. P., TARPLEY, J. W., LEDOUX, J. E. & BLAIR, H. T. 2010. Neural substrates for expectation-modulated fear learning in the amygdala and periaqueductal gray. *Nat Neurosci*, 13, 979-86.
- JOHNSON, S. W. & NORTH, R. A. 1992. Opioids excite dopamine neurons by hyperpolarization of local interneurons. *The Journal of neuroscience : the official journal of the Society for Neuroscience*, 12, 483-488.
- JONAS, P., BISCHOFBERGER, J. & SANDKUHLER, J. 1998. Corelease of two fast neurotransmitters at a central synapse. *Science*, 281, 419-24.
- JONES, S. & BONCI, A. 2005. Synaptic plasticity and drug addiction. *Curr Opin Pharmacol*, 5, 20-5.
- KAUER, J. A. 2004. Learning mechanisms in addiction: synaptic plasticity in the ventral tegmental area as a result of exposure to drugs of abuse. *Annu Rev Physiol*, 66, 447-475.
- KAUFLING, J., WALTISPERGER, E., BOURDY, R., VALERA, A., VEINANTE, P., FREUND-MERCIER, M. J. & BARROT, M. 2010. Pharmacological recruitment of the GABAergic tail of the ventral tegmental area by acute drug exposure. *British Journal of Pharmacology*, 161, 1677-1691.
- KEAY, K. A. & BANDLER, R. 2001. Parallel circuits mediating distinct emotional coping reactions to different types of stress. *Neuroscience and Biobehavioral Reviews*, 25, 669-678.
- KEITH, D. E., MURRAY, S. R., ZAKI, P. A., CHU, P. C., LISSIN, D. V., KANG, L., EVANS, C. J. & VON ZASTROW, M. 1996. Morphine activates opioid receptors without causing their rapid internalization. *Journal of Biological Chemistry*, 271, 19021-19024.
- KENDER, R. G., HARTE, S. E., MUNN, E. M. & BORSZCZ, G. S. 2008. Affective analgesia following muscarinic activation of the ventral tegmental area in rats. *J Pain*, 9, 597-605.
- KHALIQ, Z. M. & BEAN, B. P. 2008. Dynamic, nonlinear feedback regulation of slow pacemaking by A-type potassium current in ventral tegmental area neurons. *The Journal of neuroscience : the official journal of the Society for Neuroscience*, 28, 10905-17.
- KHALIQ, Z. M. & BEAN, B. P. 2010. Pacemaking in dopaminergic ventral tegmental area neurons: depolarizing drive from background and voltage-dependent sodium conductances. *J Neurosci*, 30, 7401-7413.

- KODANGATTIL, J. N., DACHER, M., AUTHEMENT, M. E. & NUGENT, F. S. 2013. Spike timing-dependent plasticity at GABAergic synapses in the ventral tegmental area. *J Physiol*, 591, 4699-710.
- KUDO, T., KONNO, K., UCHIGASHIMA, M., YANAGAWA, Y., SORA, I., MINAMI, M. & WATANABE, M. 2014. GABAergic neurons in the ventral tegmental area receive dual GABA/enkephalin-mediated inhibitory inputs from the bed nucleus of the stria terminalis. *European Journal of Neuroscience*, 39, 1796-1809.
- KUDO, T., UCHIGASHIMA, M., MIYAZAKI, T., KONNO, K., YAMASAKI, M., YANAGAWA, Y., MINAMI, M. & WATANABE, M. 2012. Three Types of Neurochemical Projection from the Bed Nucleus of the Stria Terminalis to the Ventral Tegmental Area in Adult Mice. *Journal of Neuroscience*, 32, 18035-18046.
- LAHTI, L., HAUGAS, M., TIKKER, L., AIRAVAARA, M., VOUTILAINEN, M. H., ANTTILA, J., KUMAR, S., INKINEN, C., SALMINEN, M. & PARTANEN, J. 2016. Differentiation and molecular heterogeneity of inhibitory and excitatory neurons associated with midbrain dopaminergic nuclei. *Development*, 143, 516-29.
- LAMMEL, S., HETZEL, A., HÄCKEL, O., JONES, I., LISS, B. & ROEPER, J. 2008. Unique Properties of Mesoprefrontal Neurons within a Dual Mesocorticolimbic Dopamine System. *Neuron*, 57, 760-773.
- LAMMEL, S., ION, D. I., ROEPER, J. & MALENKA, R. C. 2011. Projection-Specific Modulation of Dopamine Neuron Synapses by Aversive and Rewarding Stimuli. *Neuron*, 70, 855-862.
- LAMMEL, S., LIM, B. K. & MALENKA, R. C. 2014. Reward and aversion in a heterogeneous midbrain dopamine system. *Neuropharmacology*.
- LAMMEL, S., LIM, B. K., RAN, C., HUANG, K. W. & BETLEY, M. J. 2012. Input-specific control of reward and aversion in the ventral tegmental area. 491, 212-217.
- LAND, B. B., BRUCHAS, M. R., LEMOS, J. C., XU, M., MELIEF, E. J. & CHAVKIN, C. 2008. The Dysphoric Component of Stress Is Encoded by Activation of the Dynorphin κ -Opioid System. *The Journal of neuroscience : the official journal of the Society for Neuroscience*, 28, 407-414.
- LANE, D. A., TORTORICI, V. & MORGAN, M. M. 2004. Behavioral and electrophysiological evidence for tolerance to continuous morphine administration into the ventrolateral periaqueductal gray. *Neuroscience*.
- LANGLOIS, L. D., DACHER, M. & NUGENT, F. S. 2018. Dopamine Receptor Activation Is Required for GABAergic Spike Timing-Dependent Plasticity in Response to Complex Spike Pairing in the Ventral Tegmental Area. *Front Synaptic Neurosci*, 10, 32.
- LANTE, F., CAVALIER, M., COHEN-SOLAL, C., GUIRAMAND, J. & VIGNES, M. 2006. Developmental switch from LTD to LTP in low frequency-induced plasticity. *Hippocampus*, 16, 981-9.
- LASCHKA, E. & HERZ, A. 1977. Sites of action of morphine involved in the development of physical dependence in rats. III. Autoradiographic studies. *Psychopharmacology (Berl)*, 53, 33-7.
- LAVEZZI, H. N. & ZAHM, D. S. 2011. The mesopontine rostromedial tegmental nucleus: an integrative modulator of the reward system. *Basal Ganglia*, 1, 191-200.
- LAVIOLETTE, S. R., GALLEGOS, R. A., HENRIKSEN, S. J. & VAN DER KOOY, D. 2004. Opiate state controls bi-directional reward signaling via GABAA receptors in the ventral tegmental area. *Nature neuroscience*, 7, 160-169.
- LECCA, S., MELIS, M., LUCHICCHI, A., ENNAS, M. G., CASTELLI, M. P., MUNTONI, A. L. & PISTIS, M. 2011. Effects of drugs of abuse on putative rostromedial tegmental neurons, inhibitory afferents to midbrain dopamine cells. *Neuropsychopharmacology : official publication of the American College of Neuropsychopharmacology*, 36, 589-602.

- LECCA, S., MELIS, M., LUCHICCHI, A., MUNTONI, A. L. & PISTIS, M. 2012a. Inhibitory Inputs from Rostromedial Tegmental Neurons Regulate Spontaneous Activity of Midbrain Dopamine Cells and Their Responses to Drugs of Abuse. *Neuropsychopharmacology*, 37, 1164-1176.
- LECCA, S., MELIS, M., LUCHICCHI, A., MUNTONI, A. L. & PISTIS, M. 2012b. Inhibitory inputs from rostromedial tegmental neurons regulate spontaneous activity of midbrain dopamine cells and their responses to drugs of abuse. *Neuropsychopharmacology*, 37, 1164-76.
- LEONE, P., POCOCCO, D. & WISE, R. A. 1991. Morphine-dopamine interaction: Ventral tegmental morphine increases nucleus accumbens dopamine release. *Pharmacology, Biochemistry and Behavior*, 39, 469-472.
- LEWIS, V. A. & GEBHART, G. F. 1977. Evaluation of the periaqueductal central gray (PAG) as a morphine-specific locus of action and examination of morphine-induced and stimulation-produced analgesia at coincident PAG loci. *Brain Res*, 124, 283-303.
- LI, A. L., SIBI, J. E., YANG, X., CHIAO, J. C. & PENG, Y. B. 2016. Stimulation of the ventral tegmental area increased nociceptive thresholds and decreased spinal dorsal horn neuronal activity in rat. *Exp Brain Res*, 234, 1505-14.
- LI, H., PULLMANN, D., CHO, J. Y., EID, M. & JHOU, T. C. 2019. Generality and opponency of rostromedial tegmental (RMTg) roles in valence processing. *Elife*, 8.
- LI, Y., YU, L., ZHAO, L., ZENG, F. & LIU, Q. S. 2017. Resveratrol modulates cocaine-induced inhibitory synaptic plasticity in VTA dopamine neurons by inhibiting phosphodiesterases (PDEs). *Sci Rep*, 7, 15657.
- LINDEN, D. J. & AHN, S. 1999. Activation of presynaptic cAMP-dependent protein kinase is required for induction of cerebellar long-term potentiation. *J Neurosci*, 19, 10221-7.
- LODGE, D. J. & GRACE, A. A. 2006. The laterodorsal tegmentum is essential for burst firing of ventral tegmental area dopamine neurons. *Proceedings of the National Academy of Sciences of the United States of America*, 103, 5167-5172.
- LOWERY-GIONTA, E. G., DIBERTO, J., MAZZONE, C. M. & KASH, T. L. 2018. GABA neurons of the ventral periaqueductal gray area modulate behaviors associated with anxiety and conditioned fear. *Brain Struct Funct*.
- MADHAVAN, A., BONCI, A. & WHISTLER, J. L. 2010. Opioid-Induced GABA potentiation after chronic morphine attenuates the rewarding effects of opioids in the ventral tegmental area. *J Neurosci*, 30, 14029-35.
- MARGOLIS, E. B., HJELMSTAD, G. O., FUJITA, W. & FIELDS, H. L. 2014. Direct bidirectional μ -opioid control of midbrain dopamine neurons. *The Journal of neuroscience : the official journal of the Society for Neuroscience*, 34, 14707-16.
- MARGOLIS, E. B., LOCK, H., CHEFER, V. I., SHIPPENBERG, T. S., HJELMSTAD, G. O. & FIELDS, H. L. 2006a. Kappa opioids selectively control dopaminergic neurons projecting to the prefrontal cortex. *Proc. Natl. Acad. Sci. U. S. A.*, 103, 2938-2942.
- MARGOLIS, E. B., LOCK, H., HJELMSTAD, G. O. & FIELDS, H. L. 2006b. The ventral tegmental area revisited: is there an electrophysiological marker for dopaminergic neurons? *The Journal of physiology*, 577, 907-924.
- MARGOLIS, E. B., MITCHELL, J. M., ISHIKAWA, J., HJELMSTAD, G. O. & FIELDS, H. L. 2008. Midbrain dopamine neurons: projection target determines action potential duration and dopamine D(2) receptor inhibition. *The Journal of neuroscience*, 28, 8908-13.
- MARGOLIS, E. B., TOY, B., HIMMELS, P., MORALES, M. & FIELDS, H. L. 2012. Identification of rat ventral tegmental area GABAergic neurons. *PLoS One*, 7, e42365.
- MATSUI, A., JARVIE, B. C., ROBINSON, B. G., HENTGES, S. T. & WILLIAMS, J. T. 2014. Separate GABA afferents to dopamine neurons mediate acute action of opioids, development of tolerance, and expression of withdrawal. *Neuron*, 82, 1346-1356.

- MATSUI, A. & WILLIAMS, J. T. 2011. Opioid-Sensitive GABA Inputs from Rostromedial Tegmental Nucleus Synapse onto Midbrain Dopamine Neurons. *Journal of Neuroscience*, 31, 17729-17735.
- MAYER, D. J., WOLFLE, T. L., AKIL, H., CARDER, B. & LIEBESKIND, J. C. 1971. Analgesia from electrical stimulation in the brainstem of the rat. *Science*, 174, 1351-4.
- MAZEI-ROBISON, M. S. & NESTLER, E. J. 2012. Opiate-induced molecular and cellular plasticity of ventral tegmental area and locus coeruleus catecholamine neurons. *Cold Spring Harb Perspect Med*, 2, a012070.
- MCNALLY, G. P., JOHANSEN, J. P. & BLAIR, H. T. 2011. Placing prediction into the fear circuit. *Trends Neurosci*, 34, 283-92.
- MELIS, M., CAMARINI, R., UNGLESS, M. A. & BONCI, A. 2002. Long-lasting potentiation of GABAergic synapses in dopamine neurons after a single in vivo ethanol exposure. *J Neurosci*, 22, 2074-2082.
- MELLOR, J., NICOLL, R. A. & SCHMITZ, D. 2002. Mediation of hippocampal mossy fiber long-term potentiation by presynaptic Ih channels. *Science*, 295, 143-7.
- MORGAN, M. M. & CARRIVE, P. 2001. Activation of the ventrolateral periaqueductal gray reduces locomotion but not mean arterial pressure in awake, freely moving rats. *Neuroscience*, 102, 905-10.
- MOTA-ORTIZ, S. R., SUKIKARA, M. H., BITTENCOURT, J. C., BALDO, M. V., ELIAS, C. F., FELICIO, L. F. & CANTERAS, N. S. 2012. The periaqueductal gray as a critical site to mediate reward seeking during predatory hunting. *Behav Brain Res*, 226, 32-40.
- NESTLER, E. J. 2004. Historical review: Molecular and cellular mechanisms of opiate and cocaine addiction. *Trends Pharmacol Sci*, 25, 210-8.
- NICOLL, R. A. 2017. Review A Brief History of Long-Term Potentiation. *Neuron*, 93, 281-290.
- NIEHAUS, J. L., MURALI, M. & KAUER, J. A. 2010. Drugs of abuse and stress impair LTP at inhibitory synapses in the ventral tegmental area. *European Journal of Neuroscience*, 32, 108-117.
- NTAMATI, N. R., CREED, M., ACHARGUI, R. & LUSCHER, C. 2018. Periaqueductal efferents to dopamine and GABA neurons of the VTA. *PLoS One*, 13, e0190297.
- NUGENT, F. S., NIEHAUS, J. L. & KAUER, J. A. 2009. PKG and PKA Signaling in LTP at GABAergic Synapses. *Neuropsychopharmacology*, 34, 1829-1842.
- NUGENT, F. S., PENICK, E. C. & KAUER, J. A. 2007. Opioids block long-term potentiation of inhibitory synapses. *Nature*, 446, 1086-1090.
- OAKMAN, S. A., FARIS, P. L., KERR, P. E., COZZARI, C. & HARTMAN, B. K. 1995. Distribution of pontomesencephalic cholinergic neurons projecting to substantia nigra differs significantly from those projecting to ventral tegmental area. *The Journal of neuroscience : the official journal of the Society for Neuroscience*, 15, 5859-5869.
- OLMSTEAD, M. C. & FRANKLIN, K. B. 1997. The development of a conditioned place preference to morphine: effects of microinjections into various CNS sites. *Behavioral neuroscience*, 111, 1324-1334.
- OMELCHENKO, N. & SESACK, S. R. 2005. Laterodorsal tegmental projections to identified cell populations in the rat ventral tegmental area. *Journal of Comparative Neurology*, 483, 217-235.
- OMELCHENKO, N. & SESACK, S. R. 2010. Periaqueductal gray afferents synapse onto dopamine and GABA neurons in the rat ventral tegmental area. *J Neurosci Res*, 88, 981-91.
- OVERTON, P. & CLARK, D. 1992. Ionophoretically administered drugs acting at the N-methyl-D-aspartate receptor modulate burst firing in A9 dopamine neurons in the rat. *Synapse*, 10, 131-40.

- PAN, B., HILLARD, C. J. & LIU, Q. S. 2008. Endocannabinoid signaling mediates cocaine-induced inhibitory synaptic plasticity in midbrain dopamine neurons. *J Neurosci*, 28, 1385-97.
- PASCOLI, V., TERRIER, J., HIVER, A. S. & L??SCHER, C. 2015. Sufficiency of Mesolimbic Dopamine Neuron Stimulation for the Progression to Addiction. *Neuron*, 88, 1054-1066.
- PATHAN, H. & WILLIAMS, J. 2012. Basic opioid pharmacology: an update. *Br J Pain*, 6, 11-6.
- PELKEY, K. A., LAVEZZARI, G., RACCA, C., ROCHE, K. W. & MCBAIN, C. J. 2005. mGluR7 is a metaplastic switch controlling bidirectional plasticity of feedforward inhibition. *Neuron*, 46, 89-102.
- PELKEY, K. A., TOPOLNIK, L., LACAILLE, J. C. & MCBAIN, C. J. 2006. Compartmentalized Ca(2+) channel regulation at divergent mossy-fiber release sites underlies target cell-dependent plasticity. *Neuron*, 52, 497-510.
- PEZZE, M. A. & FELDON, J. 2004. Mesolimbic dopaminergic pathways in fear conditioning. *Prog Neurobiol*, 74, 301-20.
- POLTER, A. M., BARCOMB, K., TSUDA, A. C. & KAUER, J. A. 2018. Synaptic function and plasticity in identified inhibitory inputs onto VTA dopamine neurons. *Eur J Neurosci*, 47, 1208-1218.
- POLTER, A. M., BISHOP, R. A., BRIAND, L. A., GRAZIANE, N. M., PIERCE, R. C. & KAUER, J. A. 2014. Poststress block of kappa opioid receptors rescues long-term potentiation of inhibitory synapses and prevents reinstatement of cocaine seeking. *Biological Psychiatry*, 76, 785-793.
- PROULX, C. D., ARONSON, S., MILIVOJEVIC, D., MOLINA, C., LOI, A., MONK, B., SHABEL, S. J. & MALINOW, R. 2018. A neural pathway controlling motivation to exert effort. *Proc Natl Acad Sci U S A*, 115, 5792-5797.
- RAHMAN, S. & MCBRIDE, W. J. 2000. Feedback control of mesolimbic somatodendritic dopamine release in rat brain. *J Neurochem*, 74, 684-92.
- RAYNOR, K., KONG, H., CHEN, Y., YASUDA, K., YU, L., BELL, G. I. & REISINE, T. 1994. Pharmacological characterization of the cloned kappa-, delta-, and mu-opioid receptors. *Molecular pharmacology*, 45, 330-4.
- RIZVI, T. A., ENNIS, M., BEHBEHANI, M. M. & SHIPLEY, M. T. 1991. Connections between the central nucleus of the amygdala and the midbrain periaqueductal gray: Topography and reciprocity. *Journal of Comparative Neurology*.
- SAAL, D., DONG, Y., BONCI, A. & MALENKA, R. C. 2003. Drugs of abuse and stress trigger a common synaptic adaptation in dopamine neurons. *Neuron*, 37, 577-582.
- SALIN, P. A., MALENKA, R. C. & NICOLL, R. A. 1996. Cyclic AMP mediates a presynaptic form of LTP at cerebellar parallel fiber synapses. *Neuron*, 16, 797-803.
- SAMINENI, V. K., GRAJALES-REYES, J. G., COPITS, B. A., O'BRIEN, D. E., TRIGG, S. L., GOMEZ, A. M., BRUCHAS, M. R. & GEREAU, R. W. 2017. Divergent Modulation of Nociception by Glutamatergic and GABAergic Neuronal Subpopulations in the Periaqueductal Gray. *eneuro*, 4, ENEURO.0129-16.2017.
- SCHULTZ, W. 1986. Responses of midbrain dopamine neurons to behavioral trigger stimuli in the monkey. *J Neurophysiol*, 56, 1439-61.
- SCHULTZ, W. 1997. Dopamine neurons and their role in reward mechanisms. *Curr Opin Neurobiol*, 7, 191-7.
- SIMMONS, D. V., PETKO, A. K. & PALADINI, C. A. 2017. Differential expression of long-term potentiation among identified inhibitory inputs to dopamine neurons. *J Neurophysiol*, 118, 1998-2008.
- SIUCIAK, J. A. & ADVOKAT, C. 1987. Tolerance to morphine microinjections in the periaqueductal gray (PAG) induces tolerance to systemic, but not intrathecal morphine. *Brain Research*.

- STAMATAKIS, A. M. & STUBER, G. D. 2012. Activation of lateral habenula inputs to the ventral midbrain promotes behavioral avoidance. *Nature neuroscience*, 15, 1105-7.
- STEFANIK, M. T., KUPCHIK, Y. M., BROWN, R. M. & KALIVAS, P. W. 2013. Optogenetic evidence that pallidal projections, not nigral projections, from the nucleus accumbens core are necessary for reinstating cocaine seeking. *Journal of Neuroscience*, 33, 13654-13662.
- STEFFENSEN, S. C., STOBBS, S. H., COLAGO, E. E. O., LEE, R. S., KOOB, G. F., GALLEGOS, R. A. & HENRIKSEN, S. J. 2006. Contingent and non-contingent effects of heroin on mu-opioid receptor-containing ventral tegmental area GABA neurons. *Experimental Neurology*, 202, 139-151.
- TAN, K. R., YVON, C., TURIAULT, M., MIRZABEKOV, J. J., DOEHNER, J., LABOUEBE, G., DEISSEROTH, K., TYE, K. M. & LUSCHER, C. 2012. GABA neurons of the VTA drive conditioned place aversion. *Neuron*, 73, 1173-83.
- TERRANEO, A., LEGGIO, L., SALADINI, M., ERMANI, M., BONCI, A. & GALLIMBERTI, L. 2016. Transcranial magnetic stimulation of dorsolateral prefrontal cortex reduces cocaine use: A pilot study. *European Neuropsychopharmacology*, 26, 37-44.
- TOBALDINI, G., SARDI, N. F., GUILHEN, V. A. & FISCHER, L. 2018. Pain Inhibits Pain: an Ascending-Descending Pain Modulation Pathway Linking Mesolimbic and Classical Descending Mechanisms. *Mol Neurobiol*.
- TOVOTE, P., ESPOSITO, M. S., BOTTA, P., CHAUDUN, F., FADOK, J. P., MARKOVIC, M., WOLFF, S. B., RAMAKRISHNAN, C., FENNO, L., DEISSEROTH, K., HERRY, C., ARBER, S. & LUTHI, A. 2016. Midbrain circuits for defensive behaviour. *Nature*, 534, 206-12.
- TSAI, H.-C., ZHANG, F., ADAMANTIDIS, A., STUBER, G. D., BONCI, A., DE LECEA, L. & DEISSEROTH, K. 2009. Phasic firing in dopaminergic neurons is sufficient for behavioral conditioning. *Science*, 324, 1080-4.
- TSCHUMI, C. W. & BECKSTEAD, M. J. 2018. Neurotensin speeds inhibition of dopamine neurons through temporal modulation of GABAA and GABAB receptor-mediated synaptic input. *Neuropharmacology*, 131, 414-423.
- UNGLESS, M. A. & GRACE, A. A. 2012. Are you or aren't you? Challenges associated with physiologically identifying dopamine neurons. *Trends Neurosci*, 35, 422-30.
- UNGLESS, M. A., WHISTLER, J. L., MALENKA, R. C. & BONCI, A. 2001. Single cocaine exposure in vivo induces long-term potentiation in dopamine neurons. *Nature*, 411, 583-7.
- VAN ZESSEN, R., PHILLIPS, J. L., BUDYGIN, E. A. & STUBER, G. D. 2012. Activation of VTA GABA Neurons Disrupts Reward Consumption. *Neuron*, 73, 1184-1194.
- VAUGHAN, C. W., BAGLEY, E. E., DREW, G. M., SCHULLER, A., PINTAR, J. E., HACK, S. P. & CHRISTIE, M. J. 2003. Cellular actions of opioids on periaqueductal grey neurons from C57B16/J mice and mutant mice lacking MOR-1. *Br J Pharmacol*, 139, 362-7.
- VEZINA, P. & STEWART, J. 1987. Conditioned locomotion and place preference elicited by tactile cues paired exclusively with morphine in an open field. *Psychopharmacology*, 91, 375-380.
- VIANNA, D. M. & BRANDAO, M. L. 2003. Anatomical connections of the periaqueductal gray: specific neural substrates for different kinds of fear. *Braz J Med Biol Res*, 36, 557-66.
- WANG, L., CHEN, I. Z. & LIN, D. 2015. Collateral pathways from the ventromedial hypothalamus mediate defensive behaviors. *Neuron*, 85, 1344-58.
- WATABE-UCHIDA, M., ZHU, L., OGAWA, S. K., VAMANRAO, A. & UCHIDA, N. 2012. Whole-Brain Mapping of Direct Inputs to Midbrain Dopamine Neurons. *Neuron*, 74, 858-873.
- WEISSKOPF, M. G., CASTILLO, P. E., ZALUTSKY, R. A. & NICOLL, R. A. 1994. Mediation of hippocampal mossy fiber long-term potentiation by cyclic AMP. *Science*, 265, 1878-82.

- WHISTLER, J. L. & VON ZASTROW, M. 1998. Morphine-activated opioid receptors elude desensitization by beta-arrestin. *Proceedings of the National Academy of Sciences of the United States of America*, 95, 9914-9.
- WILLIAMS, J. T. & GRUDT, T. J. 1995. Opioid Receptors and the Regulation of Ion Conductances. *Reviews in the Neurosciences*.
- WITTEN, I. B., STEINBERG, E. E., LEE, S. Y., DAVIDSON, T. J., ZALOCUSKY, K. A., BRODSKY, M., YIZHAR, O., CHO, S. L., RAMAKRISHNAN, C., STUBER, G. D., TYE, K. M. & JANAK, P. H. 2012. Recombinase-driver rat lines: tools, techniques, and optogenetic application to dopamine-mediated reinforcement. *72*, 721-733.
- YAKSH, T. L., YEUNG, J. C. & RUDY, T. A. 1976. Systematic examination in the rat of brain sites sensitive to the direct application of morphine: observation of differential effects within the periaqueductal gray. *Brain Res*, 114, 83-103.
- YANG, H., DE JONG, J. W., TAK, Y., PECK, J., BATEUP, H. S. & LAMMEL, S. 2018. Nucleus Accumbens Subnuclei Regulate Motivated Behavior via Direct Inhibition and Disinhibition of VTA Dopamine Subpopulations. *Neuron*, 97, 434-449 e4.
- YOO, J. H., ZELL, V., GUTIERREZ-REED, N., WU, J., RESSLER, R., SHENASA, M. A., JOHNSON, A. B., FIFE, K. H., FAGET, L. & HNASKO, T. S. 2016. Ventral tegmental area glutamate neurons co-release GABA and promote positive reinforcement. *Nat Commun*, 7, 13697.
- ZANGEN, A., IKEMOTO, S., ZADINA, J. E. & WISE, R. A. 2002a. Rewarding and psychomotor stimulant effects of endomorphin-1: anteroposterior differences within the ventral tegmental area and lack of effect in nucleus accumbens. *J Neurosci*, 22, 7225-7233.
- ZANGEN, A., IKEMOTO, S., ZADINA, J. E. & WISE, R. A. 2002b. Rewarding and psychomotor stimulant effects of endomorphin-1: anteroposterior differences within the ventral tegmental area and lack of effect in nucleus accumbens. *J Neurosci*, 22, 7225-33.
- ZHANG, W., YANG, H. L., SONG, J. J., CHEN, M., DONG, Y., LAI, B., YU, Y. G., MA, L. & ZHENG, P. 2015. DAMGO depresses inhibitory synaptic transmission via different downstream pathways of μ opioid receptors in ventral tegmental area and periaqueductal gray. *Neuroscience*, 301, 144-154.
- ZHAO, S., TING, J. T., ATALLAH, H. E., QIU, L., TAN, J., GLOSS, B., AUGUSTINE, G. J., DEISSEROTH, K., LUO, M., GRAYBIEL, A. M. & FENG, G. 2011. Cell type-specific channelrhodopsin-2 transgenic mice for optogenetic dissection of neural circuitry function. *Nat Methods*, 8, 745-52.
- ZHUANG, X., MASSON, J., GINGRICH, J. A., RAYPORT, S. & HEN, R. 2005. Targeted gene expression in dopamine and serotonin neurons of the mouse brain. *J Neurosci Methods*, 143, 27-32.